HEAT PIPE

DESIGN HANDBOOK

VOLUME I

PREPARED FOR
NATIONAL AERONAUTICS AND SPACE ADMINISTRATION
GODDARD SPACE FLIGHT CENTER
GREENBELT, MARYLAND 20771

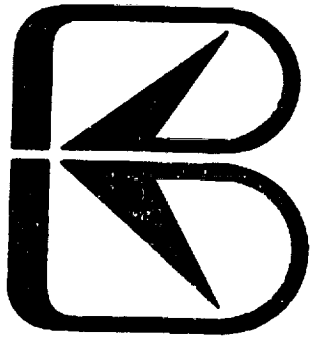

B&K ENGINEERING, INC.
SUITE 825, ONE INVESTMENT PLACE
TOWSON, MARYLAND 21204

HEAT PIPE DESIGN HANDBOOK

June 1979

Prepared for

National Aeronautics and Space Administration
Goddard Space Flight Center
Greenbelt, Maryland 20771

Under

Contract No. NAS5-23406

Prepared by

B & K ENGINEERING, INC.
Suite 825, One Investment Place
Towson, Maryland 21204

Co-Authored By: Patrick J. Brennan
and Edward J. Kroliczek

FORWARD

This Handbook was prepared under NASA Contract NAS5-23406, "Updating of a Heat Pipe Design and Applications Handbook." The work was administered by the Goddard Space Flight Center, Greenbelt, Maryland, and Mr. Roy McIntosh was the NASA Technical Monitor.

The program was conducted by B & K Engineering, Inc., Towson, Maryland, with Mr. Patrick J. Brennan serving as Program Manager and Mr. Edward J. Kroliczek as Principal Investigator.

Special thanks are due Mrs. Dolores M. Vassallo, who typed the entire manuscript; Mr. Nam Nguyen who developed the Heat Pipe Fluid Properties Program; and Mr. Hans U. Mair, who prepared many of the figures and coordinated the final preparation of the Manual. Thanks also go to Mr. Michael R. Huber who helped prepare the first draft.

TABLE OF CONTENTS

VOLUME I — PAGE

TABLE OF CONTENTS (CONTINUED)

VOLUME I

PAGE

TABLE OF CONTENTS (CONTINUED)

VOLUME I

TABLE OF CONTENTS (CONTINUED)

VOLUME I

VOLUME I

VOLUME II

ILLUSTRATIONS

VOLUME I

VOLUME II

TABLES

VOLUME I

VOLUME II

INTRODUCTION

1.1 HISTORY

In 1944, Gaugler (1) patented a lightweight heat transfer device which was essentially the present heat pipe. However, the technology of that period presented no clear need for such a device and it lay dormant for two decades. The idea was resurrected in connection with the space program, first as a suggestion by Trefethen (2) in 1962 and then in the form of a patent application by Wyatt in 1963. It was not until Grover and his co-workers (3) of the Los Alamos Scientific Laboratory independently invented the concept in 1963 and built prototypes that the impetus was provided to this technology. Grover also coined the name "heat pipe" and stated, "With certain limitations on the manner of use, a heat pipe may be regarded as a synergistic engineering structure which is equivalent to a material having a thermal conductivity greatly exceeding that of any known metal."

The first heat pipe which Grover built used water as the working fluid and was followed shortly by a sodium heat pipe which operated at 1100^{o}K. Both the high temperature and ambient temperature regimes were soon explored by many workers in the field. It was not until 1966 that the first cryogenic heat pipe was developed by Haskin (4) of the Air Force Flight Dynamic Laboratory at Wright-Patterson Air Force Base.

The concept of a Variable Conductance or Temperature Controlled Heat Pipe was first described by Hall of RCA in a patent application dated October 1964. However, although the effect of a non-condensing gas was shown in Grover's original publication, its significance for achieving variable conductance was not immediatly recognized. In subsequent years the theory and technology of gas controlled variable conductance heat pipes was greatly advanced, notably by Bienert and Brennan at Dynatherm (5) and Marcus at TRW (6).

On April 5, 1967, the first "0-g" demonstration of a heat pipe was conducted by a group of engineers of the Los Alamos Scientific Laboratory. This first successful flight experiment overcame the initial hesitation that many spacecraft designers had for using this new technology to solve the ever-present temperature control problems on spacecraft. Subsequently, more and more spacecraft have relied on heat pipes either to control the temperature of individual components or of the entire structure. Past examples of this trend are the OAO-C (7) and ATS-6 (8) spacecraft. Current applications include heat pipe isothermalizers for the I.U.E. (9) and gas-controlled heat pipes on the CTS (10).

A number of different types of fixed conductance and variable conductance heat pipes are being developed or proposed for various shuttle missions including thermal canister (11), LDEF (12), and the Atmospheric Cloud Physics Lab (13), to mention a few. The Galileo Mission will use copper/water heat pipes to cool the radiator fins of the Selenide Isotope Generators (SIG) (14) which provide power for the Jupiter probe. In short, heat pipes have received broad acceptance throughout the aerospace industry.

The early development of terrestrial applications of heat pipes progressed at a much slower pace. In 1968, RCA developed a heat pipe heat sink for transistors used in aircraft transmitters. This probably represented the first commercial application of heat pipes. The early use of heat pipes for electronic cooling was prohibited by cost and the improvements were minimal because of the relatively low power densities of many of the electronic components that were available. Since that time, however, the "Energy Crisis" was experienced and the production of low cost "gravity-assist" heat pipes followed. The most notable single application is the stabilization of the permafrost in the Alyeska Pipeline (15). Heat pipe heat recovery systems also represent a substantial market which is continually growing. The demand for alternate energy sources had led to the development of innovative intermediate and high temperature heat pipes for solar collection (16, 17) and coal gasification (18). In addition, considerable development has also been conducted to utilize heat pipes for the deicing of highways (19), bridges (20), and airport runways (21).

In addition to the advancements realized from the various applications, basic research and development has also continued. Improved geometries have been developed or proposed for axially grooved heat pipes (22, 23). Graded porosity wicks have also been fabricated (24). Several priming techniques for arterial wick designs including venting foils (25), Clausius-Claperon priming (26), and jet-pump assist (27), have evolved. Control techniques including the blocking orifice diode (28), liquid trap diodes and thermal switches (29), vapor modulated variable conductance (30), and soluble gas absorption reservoirs (31), have also been developed. Finally, analytical techniques and computer programs have been developed to predict performance and establish heat pipe designs for many of the systems noted above.

Regarding the literature, the first Heat Pipe Design Handbook (32) was published for NASA Manned Spacecraft Center, Houston in August 1972. Since that time, three International Heat Pipe Conferences have been conducted, two books on heat pipes have been authored, and numerous papers have been written on the subject.

This Design Manual represents an update of the original Design HandBook. The principal reference sources that were used are listed in Table 1-1. A brief discussion of heat pipe operation is given in the next sections and then the arrangement of the Manual is defined.

TABLE 1-1. MAJOR REFERENCES

AUTHOR	TITLE	PUBLICATION DATE	REFERENCE NO.
B. D. Marcus	Theory and Design of Variable Conductance Heat Pipes	April 1972	6
W. B. Bienert and E. A. Skrabek	Heat Pipe Design Handbook	August 1972	32
F. Edelstein and Haslett	Heat Pipe Manufacturing Study	August 1974	33
P. D. Dunn and D. A. Reay	Heat Pipes	1976	34
S. W. Chi	Heat Pipe Theory and Practice	1976	35

1.2 PRINCIPLES OF OPERATION

The basic heat pipe is a closed container which contains a capillary wick structure and a small amount of working fluid which is saturated at operating conditions. The heat pipe employs a boiling-condensing cycle and the capillary wick pumps the condensate to the evaporator. This is shown schematically in Fig. 1-1.

The vapor pressure drop between the evaporator and the condenser is very small; and, therefore, the boiling-condensing cycle is essentially an isothermal process. Furthermore, the temperature losses between the heat source and the vapor and between the vapor and the heat sink can be made small by proper design. Therefore, one feature of the heat pipe is that it can be designed to transport heat between the heat source and the heat sink with very small temperature drop.

The amount of heat that can be transported as latent heat of vaporization is usually several orders of magnitude larger than can be transported as sensible heat in a conventional convective system with an equivalent temperature difference. Therefore, a second feature of the heat pipe is that relatively large amounts of heat can be transported with small lightweight structures.

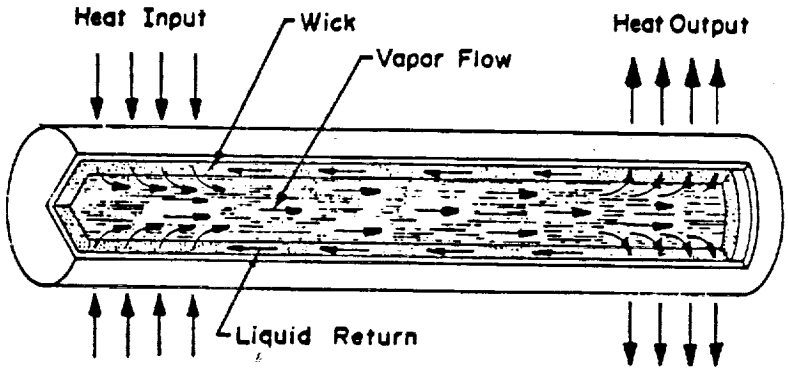

Fig. 1-1. Schematic representation of heat pipe operation

The capillary pumping head is derived from a difference in the radii of curvature of the fluid surfaces in the capillary pores in the evaporator and condenser wick sections. In order for the available capillary pumping head to be able to provide adequate circulation of the working fluid, it must be sufficient to overcome the viscous and dynamic losses of the system and it must compensate for adverse gravity effects. Capillary pumping heads are normally small when compared to the pumping heads available in dynamic systems. Therefore, certain restrictions must be imposed on the application of heat pipes in gravity environments.

1.3 TYPES OF HEAT PIPES

Heat pipes are classified into two general types--"Fixed Conductance" and "Variable Conductance." A fixed conductance heat pipe is a device of very high thermal conductance with no fixed operating temperature. Its temperature rises or falls according to variations in the heat source or heat sink.

It was recognized rather early in the history of the heat pipe research (36) that techniques could be developed which would provide for control of the effective thermal conductance of the heat pipe. This was first envisioned as blocking a portion of the condenser by a non-condensible gas. More recently several other types of control have been developed including liquid blockage and liquid and vapor modulation. Such techniques enable the device to be operated at a fixed temperature independent of source and sink conditions.

1.4 HEAT PIPE OPERATING TEMPERATURE RANGES

In this manual, the operating temperature ranges of the heat pipes are referred to as "cryogenic" (0^{o} to $150^{o}K$) (-459^{o} to $-189^{o}F$), "low temperature (150^{o} to $750^{o}K$) (-189^{o} to $+890^{o}F$), and "high temperature" (750^{o} to $3000^{o}K$) (890^{o} to $5432^{o}F$). These ranges have been defined somewhat arbitrarily such that the currently known working fluids are generally of the same type within each range, and each range is roughly four times as large as the preceding one. Working fluids are usually elemental or simple organic compounds in the cryogenic range, mainly polar molecules or halocarbons in the low temperature range, and liquid metals in the high temperature range.

1.5 ARRANGEMENT OF THE MANUAL

The new manual consists of two volumes as defined by the Table of Contents. Volume I contains ten chapters which are numbered consecutively and progress from analysis through design fabrication, test and the application of both fixed conductance and variable conductance heat pipes. Chapters 6 and 8 on Manufacturing and Testing are major new additions. Each of the chapters are independent and are arranged to permit the addition of new material as it becomes available.

Volume II contains tabulated property data for most common working fluids and summarizes the available heat pipe computer codes. It is intended to be used as a separate reference for working data.

REFERENCES

1. Gaugler, R. S., "Heat Transfer Device," U. S. Patent 2,350,348, June 6, 1944.

2. Trefethen, L., "On the Surface Tension Pumping of Liquids or a Possible Role of the Candlewick in Space Exploration," G.E. Tech. Info., Serial No. 615 D114, February 1962.

3. Grover, G. M., Cotter, T. P., and Erikson, G. E., "Structures of Very High Thermal Conductivity," J. Applied Physics, 35, 1990 (1964)

4. Haskin, W. L., "Cryogenic Heat Pipe," Technical Report AFFOL-TR-66-228, June 1967.

5. Bienert, W. B., Brennan, P. J., and Kirkpatrick J. P., "Feedback Controlled Variable Conductance Heat Pipes," AIAA Paper No. 71-42, 6th Thermophysics Conf., Tullahoma, TN., April 1971.

6. Marcus, B. D., "Theory and Design of Variable Conductance Heat Pipes," NASA CR 2018, TRW Systems Group, Redondo Beach, California, April 1972.

7. Bienert, W., and Kroliczek, E. J., "Experimental High Performance Heat Pipes for the OAO-C Spacecraft," NAS 5-11271, ASME Paper No. 71-AV-26, Dynatherm Corp., Cockeysville, MD., 1971.

8. Berger, M. E., and Kelly, W. H., "Application of Heat Pipes to the ATS F Spacecraft," ASME Paper No. 73-ENAs-46, Fairchild Space and Electronics Co., Germantown, MD., 1973.

9. "Technical Summary Report for I.U.E. Heat Pipe Test," NAS 5-24063, Dynatherm Corp., Cockeysville, MD., August 15, 1974.

10. Tower, L. K., and Kaufman, W. B., "Accelerated Life Tests of Specimen Heat Pipes from Communication Technology Satellite (CTS)" NASA TM-73846, 1977.

11. Harwell, W., and Canaras, T., "Transient Thermal Response of a Thermal Control Canister," NAS5-22570, Grumman Aerospace Corporation, Bethpage, New York, 1976.

12. Edelstien, F., "Transverse Flat Plate Heat Pipe Experiment," presented at 3rd International Heat Pipe Confernece, May 1978.

13. "Final Definition and Preliminary Design Study for the Initial Atmospheric Cloud Physics Laboratory," Final Report for NAS8-3143, General Electric Space Division, January 1977.

14. Strazza, N. P., Brennan, P. J., and Nguyen, N. H., "Copper/Water Axially-Grooved Heat Pipes for RTG Applications," 13th Intersociety Energy Conversion Engineering Conference, August 1978.

15. Waters, E. D., Johnson, C. L., and Wheeler, J. A., "The Application of Heat Pipes to the Trans-Alaska Pipeline," 10th Intersociety Energy Conversion Engineering Conference, August 1975, p. 1496.

16. Bienert, W. B., and Wolf, D. A., "Heat Pipe Applied to Flat-Plate Solar Collectors," Final Report, Dynatherm Corp., Cockeysville, MD., Energy Research and Development Administration, May 1976.

17. Kroliczek, E. J., Yuan S. W., and Bloom, A. M., "Application of Heat Pipes to Ground Storage of Solar Energy," AIAA 12th Thermophysics Conf., Albuquerque, New Mexico, July 27-29, 1977.

18. Ranken, W. A., "Potential of the Heat Pipe in Coal Gasification Processes," Los Alamos Scientific Lab., New Mexico, 1976.

19. Bienert, W. B., "Snow and Ice Removal from Pavements Using Stored Earth Energy," Final Report, Report No. FHWA-RD-75-6, Dynatherm Corp., Cockeysville, MD., May 1974.

20. Ferrara, A. A., and Haslett, R., "Prevention of Preferential Bridge Icing Using Heat Pipes," Report No. FHWA-RD-75-111, Grumman Aerospace Corp., Bethpage, New York, July 1975.

21. Pravda, M. F., "Heating Systems for Airport Pavement Snow, Slush, and Ice Control," Final Report, Report No. FAA-RD-75-139, Dynatherm Corp., Cockeysville, MD., July 1975.

22. Harwell, W., "Analysis and Tests of NASA Covert Groove Heat Pipe," NASA CR-135156, Grumman Aerospace Corp., December 1976.

23. Kroliczek, E. J., and Jen, H., "Summary Report for Axially Grooved Heat Pipe Study," NAS5-22562, B & K Engineering, Inc., May 1977.

24. Eninger, J. E., "Graded Porosity Heat Pipe Wicks," NAS2-8310, TRW Systems Group, Redondo Beach, California, August 1974.

25. Eninger, J. E., "Menisci Coalescence as a Mechanism for Venting Non-condensible Gas from Heat Pipe Arteries," TRW Systems Group, Redondo Beach, California, 1974.

References - Continued

26. Kosson, R., et.al., "Development of a High Capacity Variable Conductance Heat Pipe," AIAA Paper No. 73-728, July 1973.

27. Bienert, W., "Development of a Jet Pump-Assisted Arterial Heat Pipe," Final Report, Dynatherm Corp., Cockeysville, MD., May 6, 1977.

28. Kosson, R., Quadrini, J., and Kirkpatrick, J., "Development of a Blocking Orifice Thermal Diode Heat Pipe," AIAA Paper No. 74-754, 1974.

29. Brennan, P. J., and Groll, M., "Application of Axial Grooves to Cryogenic Variable Conductance Heat Pipe Technology," 2nd International Heat Pipe Conference, April 1976.

30. Eninger, J. E., Fleischman, G. L., and Luedke, E. E., "Vapor-Modulated Heat Pipe Report. Flight Data Analysis and Further Development of Variable-Conductance Heat Pipes," TRW Systems Group, Redondo Beach, California, Materials Technology Dept., June 30, 1975.

31. Saaski, E. W., "Heat Pipe Temperature Control Utilizing a Soluble Gas Absorption Reservoir," NASA CR-137,792, NASA Ames Research Center, February 1976.

32. Skrabek, E. A., "Heat Pipe Design Handbook," Dynatherm Corp., NAS 9-11927, August 1972.

33. Edelstein, F., "Heat Pipe Manufacturing Study," Final Report, NAS5-23156, Grumman Aerospace Corp., August 1974.

34. Dunn, P., and Reay, D. A., "Heat Pipes," University of Reading, England and International Research and Development Co., Ltd., Newcastle-Upon-Tyne, England, 1976.

35. Chi, S. Q., "Heat Pipe Theory and Practice," The George Washington University, McGraw-Hill Book Company, New York, 1976.

36. Cotter, T. P., "Theory of Heat Pipes," Los Alamos Scientific Laboratory Report LA-3246-MS, February 1965.

NOMENCLATURE

The following pages contain a listing of the symbols used throughout this Manual. The units for each quantity are given in both the SI system and the English Engineering Units.

Symbol		SI Unit	English Units
A	Area	m^2	ft^2
A, A_o B, B_o	Constants for Beattie-Bridgman Equation	--	--
C	Molal Density	kg moles m^{-3}	lb mole ft^{-3}
C_p	Heat Capacity	J $kg^{-1}K^{-1}$	Btu lbm^{-1} F^{-1}
D	Diameter	m	ft (in)
D_i	Inside Diameter of Tube	m	ft (in)
D_o	Outside Diameter of Tube	m	ft (in)
F	Body Force	N	lbf
F_ℓ	Pressure Drop Ratio	--	--
C	Thermal Conductance	W K^{-1}	Btu hr^{-1} F^{-1}
G	Gibbs Free Energy	J kg^{-1}	Btu lbm^{-1}
H	Wicking Height Factor	m^2	ft^2
K	Permeability	m^2	ft^2
L	Length	m	ft (in)
MW	Molecular Weight	kg $kmole^{-1}$	lbm $mole^{-1}$
N	Number of Grooves	--	--
N_ℓ	Liquid Transport Factor	W m^{-2}	W in^{-2}
Q	Axial Heat Flow Rate	W	Btu hr^{-1}
QL	Heat Transport Factor	W m	W in
R	Principal Radius of Curvature	m	ft (in)
R	Thermal Impedance	KW^{-1}	F W^{-1}
Re	Reynolds Number	--	--
R_g	Gas Constant (R_o/M)	J $kg^{-1}K^{-1}$	ft lbf lbm^{-1} F^{-1}
R_o	Universal Gas Constant	J $kmole^{-1}K^{-1}$	Btu $mole^{-1}$ F^{-1}
$\bar{S}$	Average Land Thickness	m	in
S	Crimping Factor	--	--
T	Temperature	K	F
V	Velocity	m s^{-1}	ft s^{-1}

Symbol		SI Unit	English Unit
V	Volume	m^3	ft^3
We	Weber Number	--	--
a	Area Per Unit Length	m	ft
a,b,c	Constants for Beattie-Bridgman Equation	--	--
b	Tortuosity Factor	--	--
d	Wire Diameter	m	in
g	Acceleration	$m\ s^{-2}$	$ft\ s^{-2}$
h	Heat Transfer Coefficient	$W\ cm^{-2}K^{-1}$	$Btu\ ft\ hr^{-1}\ F^{-1}$
h	Elevation	m	ft
k	Thermal Conductivity	$W\ cm^{-1}K^{-1}$	$Btu\ ft\ hr^{-1}ft^{-2}\ F^{-1}$
k	Spring Constant of Bellows	$N\ m^{-1}$	$lbf\ ft^{-1}$
m	Mass Flow Rate	$kg\ s^{-1}$	$lbm\ hr^{-1}$
p	Pressure	$N\ m^{-2}$	$(psia)\ lbf\ in^{-2}$
q	Radial Heat Flu /Unit Length	$W\ m^{-2}$	$W\ in^{-2}$
r	Radius	m	ft
t	Thickness	m	ft
v_n	Molal Specific Volume	$m^3\ mole^{-1}$	$ft^3\ mole^{-1}$
w	Groove Width	m	in
x	Axial Coordinate	m	ft
y	Perpendicular Coordinate	m	ft
z	Characteristic Dimension (in We)	m	in
α	Aspect Ratio	--	--
α	Fraction of Impinging Molecules Sticking to Surface	--	--
α	Groove Half Angle	rad	deg
α	Ostwald Coefficient	--	--
β	Heat Pipe Orientation with Respect to Gravity	rad	deg
γ	Ratio of Specific Heats	--	--
δ	Depth of Grooves	m	in

Symbol		SI Unit	English Unit
ε	Porosity	--	--
η	Gravity Factor	--	--
η	Liquid Void Fraction in Gas Absorption Reservoir	--	--
θ	Contact Angle	rad	deg
λ	Heat of Vaporization	J kg^{-1}	Btu lbm^{-1}
μ	Viscosity (dynamic)	N s m^{-2}	lbf s ft^{-2}
μ	Mesh Number (of screens)	m^{-1}	in^{-1}
ν	Kinematic Viscosity	m^2 s^{-1}	ft^2 s^{-1}
ρ	Density	kg m^{-3}	lbm ft^{-3}
σ	Surface Tension	N m^{-1}	lbf ft^{-1}
τ			
ω	Angular Velocity	rad s^{-1}	deg s^{-1}

Symbol	
Δ	Incremental
∇	Del Operator

Subscripts

a	Active Section of VCHP
a	Adiabatic
b	Bellows
c	Condenser
cond	Condensation
e	Evaporator
en	Envelope
ev	Evaporation
ex	Excess
ext	External
h	Hydraulic
i	Inactive Section of VCHP
int	Internal
j	Counter Index
ℓ	Liquid
max	Maximum
min	Minimum
n	Nucleation Cavity
o	Sink
p	Pore
r	Radial
r	Reservoir
s	Source
st	Storage
t	Total
v	Vapor
vap	Vaporization
w	Wick
$\parallel$	Parallel
$\perp$	Perpendicular

FIXED CONDUCTANCE HEAT PIPE THEORY

The basic heat pipe theory as first presented by Cotter (1) has remained unchanged. This Chapter presents the theory associated with the hydrodynamic and heat transfer characteristics of fixed conductance heat pipes. The hydrodynamics determines the heat transport limits of heat pipes and the heat transfer theory relates to their temperature control behavior. Basic operating principles are discussed in Section 2.1. The theory that defines a heat pipe's transport capability within the capillary pumping limit is presented in Section 2.2 through 2.6. Other heat transport limitations including sonic, entrainment, and heat flux limits are discussed in Section 2.7. The heat transfer characteristics of a heat pipe which is operating within the heat transport limits are given in Section 2.8.

2.1 HEAT PIPE OPERATION

The principle of operation of a heat pipe is best described by using the simple cylindrical geometry shown in Fig. 2-1. The essential components of a heat pipe are the sealed container, a wick and a suitable working fluid which is in equilibrium with its own vapor. When heat is applied along one section of the pipe (evaporator), the local temperature is raised slightly and part of the working fluid evaporates. Because of the saturation condition this temperature difference results in a difference in vapor pressure which, in turn, causes vapor to flow from the heated section to a cooler part of the pipe (condenser). The rate of vaporization is commensurate with heat absorbed in the form of latent heat of evaporation. The excess vapor condenses at the cooler end and releases its latent heat. During steady-state operation, conservation of energy requires that the amount of heat absorbed is identical to the heat released. Return of the liquid condensate occurs through the wick. The wick provides a flow path for the liquid and is also responsible for the pumping. During evaporation the liquid recedes somewhat into the pores of the wick thus forming menisci at the liquid-vapor interface which are highly curved. On the other hand, condensation occurs mainly on the surface of the wick with corresponding flat menisci. A pressure difference which is related to the radius of curvature exists across any curved liquid-vapor interface in thermodynamic equilibrium. Since the curvature is different at the evaporator from that at the condenser, a net pressure difference exists within the system. This capillary pumping pressure maintains circulation of the fluid against the liquid and vapor flow losses and sometimes against adverse body forces.

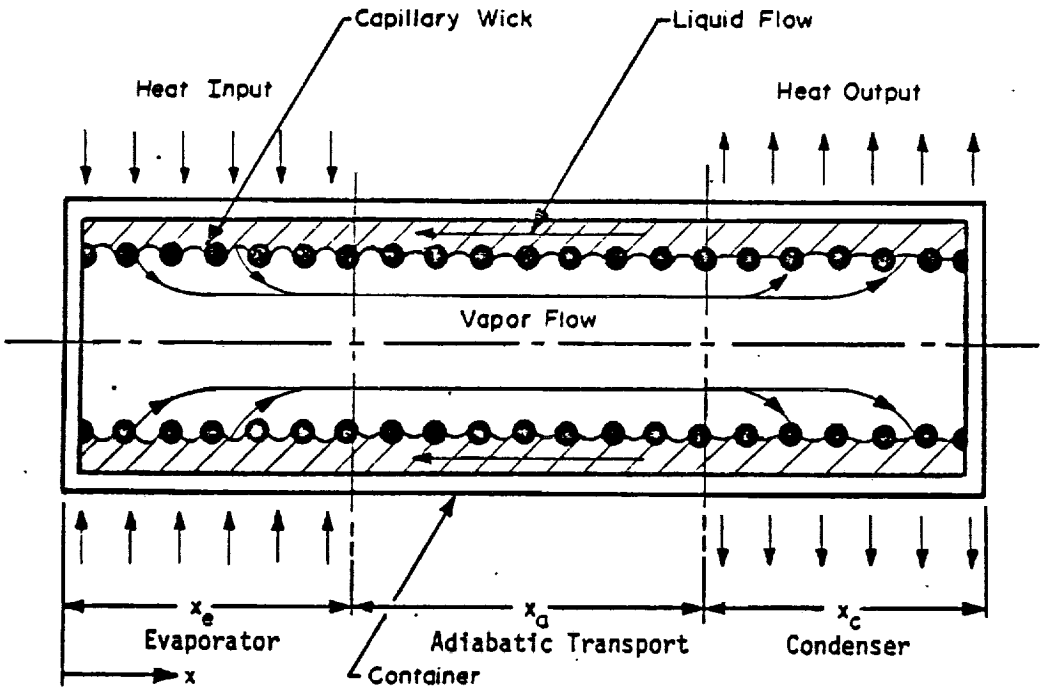

Fig. 2-1. Schematic diagram of the principle of operation of a heat pipe

In addition to an evaporator and condenser, the heat pipe frequently also has an "adiabatic" section. It is characterized by zero heat exchange with the environment. It should also be noted that the heat pipe is not limited to having only one evaporator and condenser but may have several heat input and output areas interdispersed along its length.

As generally conceived, heat pipe theory consists of the description of concurrent hydrodynamic and heat transfer processes. Hydrodynamic theory is used to describe the circulation process. Its most important function is to establish the maximum circulation and, therefore, the maximum heat transport capability of the heat pipe. It also defines and sets bounds upon various factors affecting maximum circulation.

Heat transfer theory deals essentially with the transfer of heat into and out of the heat pipe. It is used primarily to predict overall conductance. Since the heat pipe utilizes evaporation and condensation, it is subject to limitations, such as boiling, which do not apply to solid conductors. Heat transfer theory is used to investigate these limitations and also to provide a model for the overall conductance.

Fundamentally, the internal heat transport process of a heat pipe is a thermodynamic cycle subject to the First and Second Laws. A quantity of heat is applied to the system at a temperature T_1, and the same quantity of heat is rejected at a lower temperature T_2. "Work" is generated internally but it is completely consumed in overcoming the hydrodynamic losses of the system. The energy conversion process occurs in the phase change across the curved liquid-vapor interface, where thermal energy is converted to mechanical energy with the appearance of a pressure head. The curvature of this interface adjusts automatically, such that the capillary pumping (the "work" of the system) is just adequate to meet the flow requirement. As with every thermodynamic cycle a finite temperature difference must exist between the heat source and heat sink; that is, heat rejection must occur at a lower temperature than heat addition. In most heat pipes this ΔT associated with the circulation of the working fluid is small compared to other conductive temperature gradients. Nevertheless, even an ideal heat pipe can never be completely isothermal because this would violate the Second Law of Thermodynamics.

Although its performance does have definite limits, the heat pipe generally has very high heat transport capability. The limitations include maximum capillary pumping ability, choking of the vapor flow when it approaches sonic velocity, entrainment of liquid droplets in the vapor stream, and disruption of the liquid flow by the occurrence of boiling in the wick.

2.2 FUNDAMENTAL CONSIDERATIONS

The liquid and the vapor phases of the working fluid are in close contact with each other along the entire length of the heat pipe. Because of the circulation, the pressures in the liquid and vapor are not constant, but vary along the length of the pipe. Furthermore, the pressure difference between the liquid and the vapor is also a function of the location. In order to maintain the pressure balance between liquid and vapor, the interface separating them must be curved. Any curved liquid-vapor interface creates a pressure difference which can be expressed in terms of the surface tension and the principal radii of curvature R_1 and R_2 of the interface as given in Eqs. 2-1 and 2-2 (2). The principal radii of the surface are shown in Fig. 2-2.

$$\Delta p_i (x) = p_v (x) - p_\ell (x) \qquad (2\text{-}1)$$

$$\Delta p_i (x) = \sigma \left(\frac{1}{R_1 (x)} + \frac{1}{R_2 (x)} \right) \qquad (2\text{-}2)$$

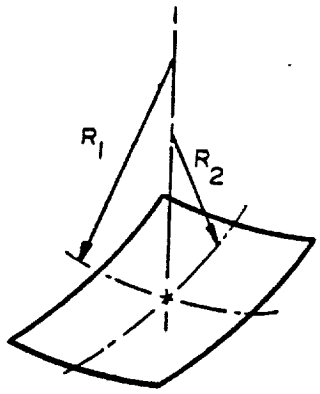

Fig. 2-2. Principal radii of curvature of liquid-vapor interface

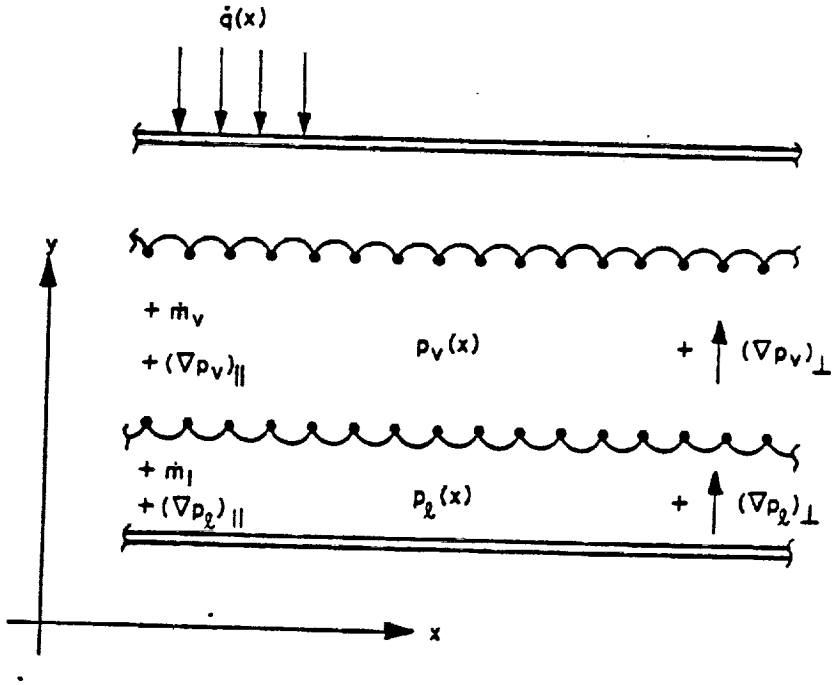

Fig. 2-3. Model of heat pipe hydrodynamics

This interfacial pressure difference Δp_i maintains the pressure balance between vapor and liquid at any point along the length of the heat pipe. Since the interfacial pressure difference varies with location, the radii of curvature of the menisci also vary along the heat pipe. If the interface is concave with respect to the vapor, the pressure in the liquid will be lower than the pressure in the vapor.

The function of the wick in a heat pipe is to provide a medium for establishing curved interfaces between liquid and vapor. It must be emphasized that the interfacial pressure difference Δp_i is independent of the wick properties and is only determined by the curvature of the interfacial surface. Wick properties such as pore size and contact angle only determine the upper bound of the interfacial pressure difference. This upper limit is frequently referred to as "capillary pressure."

In addition to pressure differences between liquid and vapor, there exist pressure gradients within both phases of the working fluid. These gradients are the result of viscous, momentum and body forces. It is convenient to group the gradients according to their origin; that is, whether they are associated with the flow or due to independent body forces.

$$\nabla p = (\nabla p)_{flow} + \frac{\vec{dF}}{dV} \qquad (2\text{-}3)$$

The vector Eq. 2-3 applies to both liquid and vapor phases.

For a heat pipe with one-dimensional liquid and vapor flow, the gradients are given in Eqs. 2-4 and 2-5 in terms of their axial and perpendicular components.

$$(\nabla p)_{\parallel} = \frac{\partial p}{\partial x} = \left(\frac{\partial p}{\partial x}\right)_{flow} + \left(\frac{dF}{dV}\right)_{\parallel} \quad \text{(Axial)} \qquad (2\text{-}4)$$

$$(\nabla p)_{\perp} = \frac{\partial p}{\partial y} = \left(\frac{dF}{dV}\right)_{\perp} \quad \text{(Perpendicular)} \qquad (2\text{-}5)$$

The components of the pressure gradients are shown schematically in Fig. 2-3. This figure also establishes the sign convention adopted throughout this Handbook. The "x" coordinate is parallel to the heat pipe axis, and the "y" coordinate is perpendicular to the axis. The origin of the coordinate system is located at the bottom and at the evaporator end. All vector components, such as pressure gradients, mass flow rates and body forces shall have a positive sign if they are directed in the positive "x" or "y" direction.

In some cases, a different coordinate system may be more convenient. For example, in a heat pipe with multiple evaporators and/or condensers, one might arbitrarily choose one end of the pipe as the origin of the coordinate system. All hydrodynamic equations are actually independent of the choice of the coordinate system. Care must be exercised, however, in selecting the proper sign for all vector components if a different system is selected.

Obviously the assumption of one-dimensional fluid flow does not hold in the areas where evaporation and condensation occur, or in two-or-three dimensional heat pipes such as flat plates, cavities, etc. But for most conventional heat pipes, the one-dimensional model represents a very close approximation.

The body force term in Eqs. 2-3, 2-4, and 2-5 consists of those mass action forces which are independent of flow; e.g., gravity, acceleration, and electrostatic effects. This form of the equation does not include flow dependent body forces such as arise due to magnetic effects which are generally not applicable to heat pipes.

The pressure gradients give rise to mass transfer along the heat pipe. The two axial mass-flow rates, $\dot{m}_v$ and $\dot{m}_\ell$ are related through the Continuity Eq.

$$\dot{m}_v (x) + \dot{m}_\ell (x) = 0 \qquad (2\text{-}6)$$

Eq. 2-6 simply states that during steady-state operation mass accumulation does not occur and vapor and liquid flow rates must be equal in magnitude but opposite in direction.

Finally, the mass flow rates are related to the local heat exchange through the Energy equation:

$$\frac{d\dot{m}(x)}{dx} = \frac{1}{\lambda} \dot{q}(x) \qquad (2\text{-}7)$$

Eq. 2-7 is a simplified form of the First Law of Thermodynamics where $\dot{q}(x)$ is the rate of heat addition (or removal) per unit length of the heat pipe. It is defined as positive in the case of heat addition (evaporator) and negative for heat removal (condenser). In Eq. 2-7 the effects of conduction in the axial direction are neglected. It is also assumed that sensible heat transport is negligible. In the following sections the various terms used in describing the performance of heat pipes are examined in more detail.

2.3 CAPILLARY PRESSURE

The capillary pressure is defined as the maximum interfacial pressure difference which a given wick/fluid combination can develop, or:

$$\Delta p_{cap} \equiv (\Delta p_i)_{max} \tag{2-8}$$

The capillary pressure is related to the surface tension of the liquid, the contact angle between liquid and vapor, and the effective pumping radius through (3):

$$\Delta p_{cap} = \frac{2\ \sigma \cos \theta_c}{r_p} \tag{2-9}$$

With few exceptions, the wicks employed in most heat pipes very often do not have a well defined pore geometry. Therefore, it is common practice to define an effective pumping radius which is determined experimentally and which satisfies Eq. 2-9.

For some well defined wick systems analytical expressions for the effective pumping radius can be found. For a circular pore the meniscus is spherical and the two principal radii of curvature of the surface are equal. Referring to Fig. 2-4 we have:

$$(R_1)_{min} = (R_2)_{min} = \frac{r_p}{\cos \theta_c} \tag{2-10}$$

According to Eq. 2-2, the maximum interfacial pressure difference which the capillary forces are capable of handling is:

$$(\Delta p_i)_{max} = \sigma \left(\frac{1}{R_{1,min}} + \frac{1}{R_{2,min}} \right) = \left[\frac{2\ \sigma \cos \theta_c}{r_p} \right] \tag{2-11}$$

A comparison of Eqs. 2-9 and 2-11, along with the identity 2-8, yields the results that for circular pores the effective pumping radius r_p is equal to the physical pore radius.

In long, open channels one of the principal radii is infinite. Using Fig. 2-5 the minimum radii can readily be calculated:

$$R_1 = \infty\ ,\ (R_2)_{min} = \frac{W/2}{\cos\ (\alpha + \theta_c)} \tag{2-12}$$

The maximum interfacial pressure difference becomes:

$$(\Delta p_i)_{max} = \frac{\sigma \cos\ (\alpha + \theta_c)}{W/2} \tag{2-13}$$

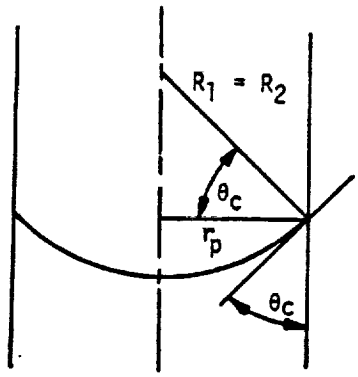

Fig. 2-4. Effective pumping radii in a circular capillary

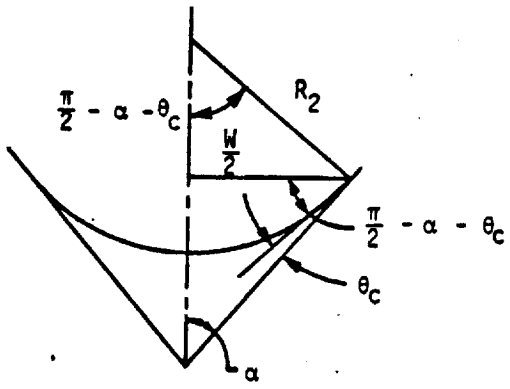

θ_c Contact Angle

α Half Angle of Groove

W Groove Width

R_2 Minimum Radius of Curvature (Filled Groove)

Fig. 2-5. Effective pumping radii in an open triangular groove

In the limit of grooves with parallel walls ($\alpha = 0$) Eq. 2-13 reduces to:

$$(\Delta p_i)_{max} = \frac{2 \sigma \cos \theta_c}{W} \qquad (2\text{-}14)$$

If we compare Eqs. 2-14 with 2-9 along with the Identity 2-8, we see that the effective pumping radius of a rectangular groove is equal to the groove width while for circular pores it is equal to half the pore diameter. The reason for this difference is, of course, the absence of curvature in the direction of the groove length. Several methods for determining the effective radius of various wick geometries are discussed in the Design Section.

A volume of literature exists on the contact angle, and many inconsistencies in experimental results are reported. However, it has been well established now that much of the "inconsistent" behavior of the contact angle is due to very low level impurities in the liquid or on the surface being wetted. Thus, combinations of scrupulously clean surfaces and very pure liquids will exhibit no difference in advancing and receding contact angles; and water and other liquids with low surface tensions should exhibit a contact angle of approximately zero (2) on all clean metal surfaces with which they do not react chemically. The fact that much larger contact angles are often observed usually indicates the presence of absorbed impurities on the surface, which is generally more difficult to clean than the working fluid.

The capillary pressure, as defined in this section, refers to the maximum interfacial pressure difference which a given wick/liquid combination can sustain; but, as pointed out earlier, the interfacial pressure varies along the heat pipe. The upper and lower limit of the interfacial pressure difference must be known in order to determine the maximum heat transport capability. The lower limit corresponds to the maximum value of the radius of curvature of the meniscus. It can be determined that for wetting liquids the pressure in the liquid cannot exceed that of the vapor. Equal pressures in liquid and vapor correspond to an infinite radius of curvature which is equivalent to a flat meniscus. For nonwetting liquids the pressure in the liquid always exceeds that of the vapor.

The point of pressure equality in liquid and vapor represents a well-defined boundary condition for the integration of the flow equations. Frequently it is located at the end of the condenser of the heat pipe. In the presence of body forces and with complicated

heat pipe geometries or distributed heat loads, this will not necessarily be the case and a careful analysis is required to determine its location. This subject will be discussed in more detail in conjunction with the integration of the flow equations.

2.4 PRESSURE GRADIENTS IN THE LIQUID

The liquid is subjected to a number of different forces, such as the shearing forces associated with viscous flow, the forces associated with momentum in a dynamic system, and the body force effects arising from external force fields. The actions of these forces upon the liquid result in pressure gradients along the heat pipe as was indicated in Eq. 2-3.

The ratio of the dynamic-to-viscous flow pressure gradients in a capillary passage is on the order of magnitude of the Reynold's number determined using the average flow in a pore (4). Since this number will be small with respect to unity for heat pipes, the inertial (dynamic) forces in the liquid will be neglected.

2.4.1 Viscous Pressure Gradients in the Liquid

The pressure gradient resulting from viscous shear forces in an incompressible liquid with laminar flow through a porous media is given directly by Darcy's Law (5):

$$\frac{dp_\ell}{dx} = \frac{-\mu_\ell \dot{m}_\ell (x)}{K A_w \rho_\ell} \qquad (2\text{-}15)$$

For some geometries where the physical dimensions of the pores are known and are well defined the permeability K may be expressed in terms of a hydraulic diameter D_h and the porosity of the wick ε (6):

$$K = \frac{\varepsilon D_h^2}{32} \qquad (2\text{-}16)$$

The hydraulic diameter D_h is defined as:

$$D_h = \frac{4A}{WP} \qquad (2\text{-}17)$$

The above definition represents a good approximation for many geometries. More refined expressions for permeability are given in Chapter 4.

For cylindrical passages with diameter D, Eq. 2-17 yields for the hydraulic diameter:

$$D_h = D \qquad (2\text{-}18)$$

and Eq. 2-15 reduces to a form of Poiseuille's Law:

$$\frac{dp_\ell}{dx} = \frac{-32\ \mu_\ell\ \dot{m}_\ell\ (x)}{\varepsilon\ A_w\ \rho_\ell\ D_{h,\ell}^2} \tag{2-19}$$

For many wick geometries the hydraulic diameter cannot be calculated, particularly for those which involve porous materials. In these cases it is best to resort to experimental measures to obtain a value for the permeability.

When the wicking system consists of uncovered channels as in the case of axially grooved heat pipes there is a shearing effect on the liquid which results from the counterflow of the vapor. This induced liquid loss can be significant particularly at low vapor pressures or at high axial heat loads (e.g. commercial applications). Hufschmidt, et.al. (7) determined an empirical expression for a rectangular groove whose depth is greater than the groove width, which accounts for this loss.

$$\frac{dp_\ell}{dx} = -\frac{\mu_\ell\ \dot{m}_\ell\ (x)}{K(x)A_\ell(x)\ \rho_\ell}\left(1+\frac{\phi^2\ \psi}{3}\right) \tag{2-20}$$

This is basically the Hagon-Poiseuille Eq. modified by the term $(\frac{\phi^2}{3}\ \psi)$ to account for the liquid-vapor shear loss, where ϕ is the groove aspect ratio.

$$\phi \equiv \frac{\text{Groove width at the liquid-vapor interface}}{2\ (\text{Groove depth})}$$

For the groove geometry shown in Fig. 2-6

$$\phi = \frac{(R_v + R_t)\ \text{Sin}\ \frac{\pi}{N} - R_t}{R_i - R_v} \tag{2-21}$$

The parameter ψ is dependent on whether the vapor flow is laminar or turbulent (8).

For laminar vapor flow ($Re_v < 2000$)

$$\psi = \frac{4\ (R_i - R_v)}{R_v}\ \frac{\nu_v}{\nu_\ell}\ \frac{A_\ell}{A_v} \tag{2-22}$$

For turbulent vapor flow ($Re_v > 2000$)

$$\psi = 0.0328\ \frac{R_i - R_v}{R_v^{0.25}}\ \frac{A_\ell}{A_v^{1.75}}\ \frac{\mu_v^{0.25}}{\rho_v\ \nu_v}\ \dot{m}_v^{0.75} \tag{2-23}$$

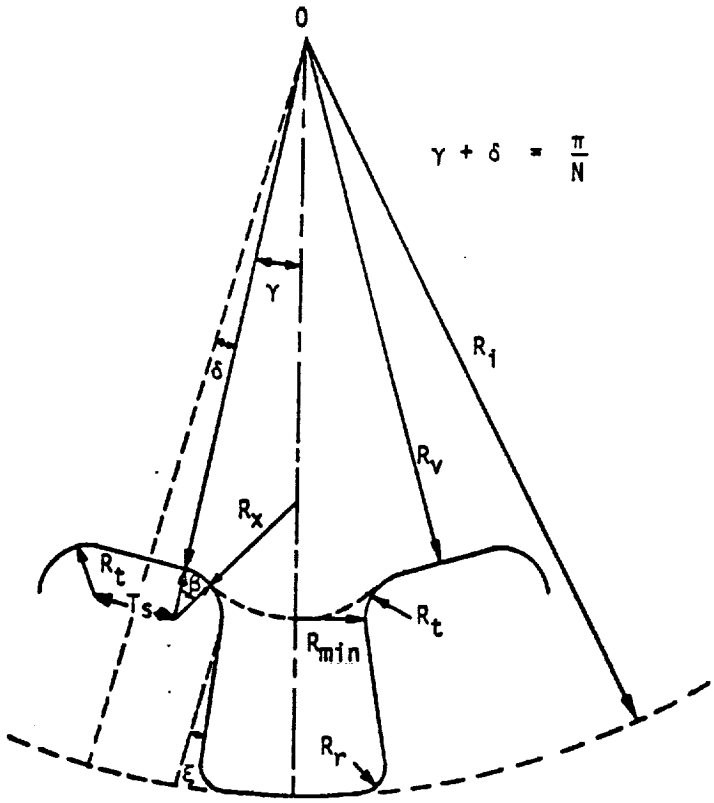

Fig. 2-6. Trapezoidal groove geometry

2.4.2 Body Forces in the Liquid

The pressure gradients in the liquid resulting from body forces can either augment or diminish the gradients associated with viscous flow. The body forces result from external fields which can be applied in any direction with respect to the heat pipe's axis. The body force can be expressed as:

$$\left(\frac{\vec{dF}}{dV}\right) = \rho_\ell \vec{g} \qquad (2\text{-}24)$$

In a gravity field the heat pipe will experience two components of body force. The obvious body force component is the axial component which is parallel to the mass flow along the heat pipe:

$$\left(\frac{dF}{dV}\right)_{\parallel} = \rho_\ell g = -\rho_\ell g \sin \beta \qquad (2\text{-}25)$$

Depending on whether the condenser ($\beta > 0$) or the evaporator ($\beta < 0$) is elevated, the axial body force component of gravity will either augment or impede the liquid flow. Wherever possible in terrestrial applications, the heat pipe or heat pipe system is oriented to take advantage of the gravity assist to the liquid return. This mode of operation is often referred to as "refluxing." On the other hand as discussed in Chapter 8, heat pipes for aerospace applications are generally tested at a slight adverse elevation to demonstrate performance without any possible gravity assist.

Less frequently considered is the perpendicular body force component:

$$\left(\frac{dF}{dV}\right)_{\perp} = \rho_{\ell} g_{\perp} = - \rho_{\ell} \, g \cos \beta \qquad (2\text{-}26)$$

Unlike the axial body force component, this component will always act to the detriment of heat pipe operation. It generates a pressure gradient which is perpendicular to the liquid flow (Eq. 2-5). When integrating the flow equations, it is found that this perpendicular gradient always detracts from the capillary pumping (Section 2.6).

Body forces originate not only from gravity but from any acceleration vector, $\vec{g}$. A typical, and frequently encountered non-gravitational body force is that resulting from acceleration due to rotation. Its vector is directed in a radial direction from the axis of rotation and its magnitude is:

$$g_{rot} = \tau \omega^2 \qquad (2\text{-}27)$$

where τ is the distance between the axis of rotation and the point where the body force is encountered.

2.5 PRESSURE GRADIENTS IN THE VAPOR

The pressure gradients in the vapor will also result from a combination of flow dependent (viscous and dynamic) effects, and flow independent external force fields or body forces. However, the effects on heat pipe performance of the various pressure gradients in the vapor phase are not as easily determined as those of the liquid. Much of this difficulty is attributable to the higher flow velocities in the vapor which make it more susceptible to the effects of mass addition and removal along the length of the heat pipe, to the frequently non-negligible dynamic effects, to the existence of turbulent

flow, and to the compressibility of the vapor. All of these factors combine to produce a condition which does not permit simple, all encompassing, analytical expressions for the vapor pressure losses.

2.5.1 Viscous Pressure Gradients in the Vapor

Under conditions of low axial heat flow and high vapor density, the vapor velocity will be low and viscous forces will predominate. If laminar, non-compressible flow occurs the vapor pressure gradient can also be expressed by Darcy's Law:

$$\frac{dp_v}{dx} = \frac{-\mu_v \dot{m}_v (x)}{K A_v \rho_v} \qquad (2\text{-}28)$$

Since the vapor passages are generally of a relatively simple geometry compared to those of the liquid, the concept of the "hydraulic diameter" is especially useful. Substituting the hydraulic diameter for the permeability in Eq. 2-16 the pressure gradient in the vapor becomes:

$$\frac{dp_v}{dx} = - \frac{32 \mu_v \dot{m}_v (x)}{\rho_v A_v D_{h,v}^2} \qquad (2\text{-}29)$$

By the definition of the porosity ε--i.e., the ratio of void volume to total volume, the vapor space porosity is unity.

2.5.2 Dynamic Pressure Gradients in the Vapor

Separation of viscous and dynamic effects in the vapor flow is not really possible. If the dynamic effects cannot be neglected, Eq. 2-29 should be replaced by Eq. 2-30 (1):

$$\frac{dp_v}{dx} = - \frac{32 \mu_v \dot{m}_v}{\rho_v A_v D_{h,v}^2} \left[1 + \frac{3}{4} Re_r - \frac{11}{270} Re_r^2 + \ldots .\right] \qquad (2\text{-}30)$$

where the radial Reynolds number, Re_r, is defined by:

$$Re_r = \frac{1}{2 \pi \mu_v} \frac{d\dot{m}_v}{dx} \qquad (2\text{-}31)$$

The expansion in Eq. 2-30 accounts for momentum changes due to evaporation or condensation. It obviously holds only for small rates of evaporation and condensation, i.e., for $Re_r << 1$. The momentum effects cause the pressure gradient in the evaporator to be higher than for viscous shear alone and the pressure gradient in the condenser to be lower due to decelera-

tion of the vapor flow. In the absence of mass addition or subtraction, as for example in the adiabatic section of a heat pipe, Eq. 2-30 reduces to that of purely viscous flow.

For high evaporation and condensation rates the pressure distribution in the vapor is considerably more complex. Analytical solutions exist only for the limiting case, where the radial Reynolds number approaches infinity. For this limit the pressure gradient is given in (9)

$$\frac{dp_v}{dx} = -\frac{S \pi \dot{m}_v}{\rho_v A_v D_{h,v}^2} \frac{d\dot{m}_v}{dx} \qquad (2\text{-}32)$$

The value for the numerical constant S is 1 for evaporation and $4/\pi^2$ for condensation. Eq. 2-32 predicts approximately 40% recovery of the dynamic head in the condenser.

2.5.3 Turbulent Flow and Compressibility Effects

Little is known about the onset of turbulence in vapor flow with high radial Reynolds numbers. In the adiabatic section, where the radial Reynolds number is zero, fully developed turbulent flow will occur if the axial Reynolds number exceeds 2000. The axial Reynolds number is defined in the usual manner as:

$$Re_v = \left(\frac{D_h \dot{m}}{A \mu}\right)_v \qquad (2\text{-}33)$$

For turbulent flow the viscous pressure gradient is given by the empirical Blasius Law (5)

$$\frac{dp_v}{dx} = \frac{0.156\ \mu_v^2}{\rho_v D_{h,v}^3} Re_v^{7/4} \qquad (2\text{-}34)$$

In the transition region, i.e., at an axial Reynolds number of approximately 2000, Blasius' Equation holds only approximately and gives slightly different numerical values than the expression for laminar flow.

Compressibility effects can normally be ignored if the Mach number of the flow is less than approximately 0.2. This criterion applies for most heat pipes with the notable exception of liquid metal heat pipes during start-up. If compressibility effects are taken into account, the pressure recovery for high axial fluxes may be as high as 90% (10) instead of the 40% predicted by Eq. 2-32. Compressibility can certainly not be neglected when the vapor flow approaches sonic conditions. This has been considered by Levy (11) (12) and is discussed in Section 2.7.

2.5.4 Body Forces in the Vapor

The theory of body forces acting upon the vapor is identical to that of the liquid. However, because of the large difference in density between liquid and vapor (usually on the order of 10^3) the effect of body forces in the vapor is generally negligible.

2.6 CAPILLARY HEAT TRANSPORT LIMIT

2.6.1 General Approach

The rate of circulation of the working fluid is determined by a balance of capillary pumping, body forces, and viscous and dynamic flow losses. During normal operation the pumping adjusts itself to meet the circulation requirements. But since capillary pumping is limited to a maximum capillary pressure (see Section 2.3) a limit also exists for the rate of circulation and therefore for the heat transport capability.

The capillary limit is the most commonly encountered limit and it relates to the hydrodynamics previously discussed. When the required interfacial pressure exceeds the capillary pressure that the wick can sustain, the pumping rate is no longer sufficient to supply enough liquid to the evaporation sites. Consequently, more liquid is evaporated than replenished and local dryout of the wick occurs.

For high velocity vapor flows, other hydrodynamic limits may restrict the heat transport even before the capillary limit is reached. The sonic limit occurs when the vapor velocity reaches the sonic point. A further increase in the mass flow is not possible without raising the saturation vapor pressure and therefore the vapor temperature. High velocity vapor flow may also interfere with the recirculating liquid causing liquid droplets to be entrained in the vapor and preventing sufficient liquid from returning to the evaporator (entrainment limit). Finally, high local heat fluxes can lead to nucleation within the liquid and result in with dryout (boiling limit). Each one of these limitations will be discussed separately in subsequent sections.

In the preceding sections the pressures and forces affecting the circulation of the working fluid of a one-dimensional heat pipe have been presented in differential form. No restriction has been placed on the distribution of heat fluxes into and out of the heat pipe, its orientation with respect to body forces, and the geometry of the wick. In order to arrive at the capillary limit, i.e., the maximum heat transport capability of a heat

pipe, the hydrodynamic equations must be integrated. In the general case, numerical methods have to be employed and the integration constants must be chosen judiciously, particularly when body forces and more than one evaporator and condenser are involved. The following approach will always lead to the correct capillary limit and can readily be reduced to a closed form solution for uniform geometries.

The pressure distribution in liquid and vapor is obtained by integrating the axial pressure gradients.

$$p_v(x) = \int_o^x (\nabla p_v)_{II} dx + p_v(0) \qquad (2\text{-}35)$$

$$p_\ell(x) = \int_o^x (\nabla p_\ell)_{II} dx + p_\ell(0) \qquad (2\text{-}36)$$

The integration is extended from one end of the heat pipe ($x = 0$) to the specific location x. The two integration constants must be determined before the absolute values of each pressure can be calculated. The two pressures are related at every point x through the interface Eq. 2-1.

$$\Delta p_i(x) = p_v(x) - p_\ell(x) \qquad (2\text{-}1)$$

Inserting the values for $p_v(x)$ and $p_\ell(x)$ from Eqs. 2-35 and 2-36 yields:

$$\Delta p_i(x) = \int_o^x \left[(\nabla p_v)_{II} - (\nabla p_\ell)_{II}\right] dx + p_v(0) - p_\ell(0) \qquad (2\text{-}37)$$

Equation 2-37 gives the required interfacial pressure difference Δp_i at any axial location x to within the additive constant $[p_v(0) - p_\ell(0)]$.

In general, Δp_i will vary along the length of the heat pipe and at some point x' will reach its lowest, or minimum value. It is generally assumed that this minimum interfacial pressure difference is zero (equal pressure in liquid and vapor, corresponding to a "flat" meniscus). The integration constant in Eq. 2-37 may then be evaluated as follows:

$$\Delta p_i(x') = 0 \qquad (2\text{-}38)$$

$$p_v(0) - p_\ell(0) = -\int_0^{x''} \left[(\nabla p_v)_{||} - (\nabla p_\ell)_{||} \right] dx \qquad (2\text{-}39)$$

The interfacial pressure difference becomes:

$$\Delta p_i(x) = \int_{x'}^{x} \left[(\nabla p_v)_{||} - (\nabla p_\ell)_{||} \right] dx \qquad (2\text{-}40)$$

This last equation describes the interfacial pressure difference at any location, x, of the heat pipe with respect to the reference value at x' which, conveniently, is equal to zero.

There always exists at least one axial location x" at which the interfacial pressure difference $\Delta p_i(x)$ reaches a highest, or maximum value. Once this point has been found (either by numerical or closed form solution) the maximum interfacial pressure difference can be expressed as:

$$(\Delta p_i)_{max} = \Delta p_i(x'') = \int_{x'}^{x''} \left[(\nabla p_v)_{||} - (\nabla p_\ell)_{||} \right] dx \qquad (2\text{-}41)$$

In the hydrodynamic limit the pumping requirement $(\Delta p_i)_{max}$ is equal to the maximum capillary pressure, Δp_{cap}, which the wick can develop. Proper circulation of the working fluid is assured if the pumping requirement is less than the maximum capillary pressure difference:

$$(\Delta p_i)_{max} \leq \Delta p_{cap} \qquad (2\text{-}42)$$

For a specified wick geometry and heat flux distribution, the above equation will in general be an inequality. In the course of a numerical analysis it establishes the criterion for a selected heat pipe and wick geometry to satisfy the heat transport requirement. Alternately, Eq. 2-42 may be used as an equality to determine the capillary pumping requirement. For most wicks, capillary pumping (pore size) and hydrodynamic pressure gradients are closely related. The approach is therefore to select a particular wick, compute the hydrodynamic requirements according to Eq. 2-41 and then compare the resulting $(\Delta p_i)_{max}$ with the capillary pumping capability Δp_{cap}. If the inequality is met, the selected wick will be adequate for the given heat transport requirement.

The preceding equations express the capillary pumping requirement in terms of integrated pressure gradients within liquid and vapor. These pressure gradients are related to the corresponding mass flow rates and the body forces. The mass flow rates, in turn, are determined by the heat transport requirement.

For a specified distribution of heat input and output, $\dot{q}(x)$, the mass flow rates of vapor and liquid are obtained by integrating Eq. 2-7.

$$\frac{d\dot{m}(x)}{dx} = \frac{1}{\lambda}\,\dot{q}(x) \tag{2-7}$$

Integration yields:

$$\dot{m}_v(x) = \int_0^x \frac{1}{\lambda}\,\dot{q}(x)\,dx + \dot{m}_v(0) \tag{2-43}$$

The above equation gives the mass flow rate of the vapor for every axial location, x, when the integration is extended from one end of the heat pipe, (x = 0), to the point x. Conservation of mass requires that the integration constant, $\dot{m}_v(0)$, goes identically to zero since no vapor enters or leaves the heat pipe. Thus:

$$\dot{m}_v(0) = 0 \tag{2-44}$$

The mass flow rate of the vapor is thus uniquely determined by the heat exchange with the environment. Because of the requirement of mass continuity (Eq. 2-6), the mass flow rate of the liquid is equal in magnitude and opposite in direction to the mass flow rate of the vapor.

$$\dot{m}_\ell(x) = -\dot{m}_v(x) \tag{2-45}$$

The net axial heat flow rate, $\dot{Q}$, is related to $\dot{m}_v$ and $\dot{m}_\ell$ through

$$\dot{Q}(x) = \lambda\,\dot{m}_v(x) = -\lambda\,\dot{m}_\ell(x) \tag{2-46}$$

The theory as presented so far does not include the effects of perpendicular components of the body forces. Since the hydrodynamic model is one-dimensional, perpendicular body forces do not affect the axial pressure gradient. The perpendicular body forces, however, create a pressure gradient within the liquid which is perpendicular

to the flow direction. Referring to Eq. 2-26, this pressure gradient is

$$\left(\frac{dF}{dV}\right)_{\perp} = \rho_{\ell}\, g_{\perp} = -\rho_{\ell}\, g \cos\beta \qquad (2\text{-}26)$$

The total pressure difference in the liquid across the heat pipe becomes:

$$(\Delta p_{\ell})_{\perp} = \int_{o}^{D_w} \frac{\partial p_{\ell}}{\partial y}\, dy = -\rho_{\ell} g D_w \cos\beta \qquad (2\text{-}47)$$

where the integration is extended from the bottom ($y = 0$) to the top ($y = D_w$) of the wick. Equation 2-47 holds for any axial location x. This pressure difference creates an additional capillary pumping requirement. The wick must be capable of supporting the interfacial pressure difference between any two locations within the heat pipe (including those at different vertical positions). The datum point of equal pressure in liquid and vapor will always be located at the lower liquid/vapor interface of the heat pipe ($x = x'$, $y = 0 + t_w$). Conservatively, we locate it at the bottom of the heat pipe ($y = 0$). The point of maximum interfacial pressure difference exists at $x = x''$, $y = D_w$. The additional interfacial pressure difference $p_{i_{\perp}}$ due to the perpendicular pressure gradient is given by:

$$\Delta p_{i_{\perp}} = (p_{\ell})_{top} - (p_{\ell})_{bottom} = \rho_{\ell}\, g\, D_w \cos\beta \qquad (2\text{-}48)$$

The amount of capillary pumping available for axial flow is therefore reduced and Eq. 2-42 must be modified as follows:

$$\begin{aligned}(\Delta p_i)_{max} &\leq \Delta p_{cap} - \Delta p_i' \\ &\leq \Delta p_{cap} - \rho_{\ell}\, g\, D_w \cos\beta\end{aligned} \qquad (2\text{-}49)$$

Most aerospace heat pipes are operated very nearly in the horizontal position. In this case the value of the cosine is close to unity and the additional pumping requirement is approximately

$$\Delta p_{i_{\perp}} \sim \rho_{\ell}\, g\, D_w \qquad (2\text{-}50)$$

Although this term can be significant when operation at an adverse elevation is required, in commercial applications where a gravity assist is employed this term will generally have a negligible effect.

2.6.2 Heat Transport Requirement and Heat Transport Capability

Two very useful parameters in heat pipe design are the "Heat Transport Requirement" $(\dot{Q}L)_R$, and the "Heat Transport Capability" $(\dot{Q}L)_{max}$. A meaningful definition of these parameters requires that:

(1) Both liquid and vapor regimes are laminar and momentum effects are negligible.

(2) All geometric properties of the wick and heat pipe and the fluid properties are constant along its length.

(3) At least one of the following conditions are met:

(a) Body forces are absent, and/or

(b) The location of minimum (x') and maximum (x") interfacial pressure are independent of $\dot{Q}$ (x).

The Heat Transport Requirement and the Heat Transport Capability shall be defined by referring to the pressure balance (Eq. 2-42) within the heat pipe. Using the applicable expressions (Eqs. 2-4, 2-20, 2-25, and 2-29) for the pressure gradients in liquid and vapor and Eq. 2-41 for the maximum interfacial pressure difference, the pressure balance (Eq. 2-42) can be written as follows:

$$\Delta p_{cap} \geq \int_{x'}^{x''} \left[\left\{ -\left(\frac{32\,\mu}{\rho\, AD_h^{\,2}} \right)_v - \left(\frac{\mu}{K(x)\, A(x)\, \rho} \right)_\ell \left(1 + \frac{\phi^2}{3}\psi \right) \right\} \frac{Q(x)}{\lambda} + \rho_\ell\, g \sin\beta \right] dx \qquad (2\text{-}51)$$

Using the above assumptions, Eq. 2-51 can then be rearranged to the following simplified form:

$$\Delta p_{cap} \geq -C \int_{x'}^{x''} \dot{Q}\, dx + \int_{x'}^{x''} \rho_\ell\, g \sin\beta\, dx \qquad (2\text{-}52)$$

where the constant C combines the wick and working fluid properties and is given by:

$$C = \frac{1}{\lambda}\left[\left(\frac{32\,\mu}{\rho\, A\, D_h^2}\right)_v + \left(\frac{\mu}{K\, A\, \rho}\right)_\ell \left(1 + \frac{\phi^2}{3}\psi\right)\right] \qquad (2\text{-}53)$$

In both Eqs. 2-51 and 2-52, the integration is extended from the point of minimum (x') to maximum (x") interfacial pressure difference. Further rearrangement of Eq. 2-52 yields:

$$\int_{x''}^{x'} \dot{Q}\,(x)\,dx \leq \frac{\Delta p_{cap}}{C} + \int_{x}^{x} \frac{\rho_\ell\, g \sin\beta}{C}\,dx \qquad (2\text{-}54)$$

The left side of Eq. 2-54 represents the heat transport requirement; i.e., the heat transport that is determined by the axial distribution of heat flow rates. The right side of Eq. 2-54 describes the capability of the heat pipe to meet these requirements for a specified orientation.

The Heat Transport Requirement is defined as the integral on the left side of Eq. 2-54:

$$(\dot{QL})_R \equiv \int_{x''}^{x'} \dot{Q}\,(x)\,dx \qquad (2\text{-}55)$$

It is completely described by the distribution of heat flow rates which is a function of the application only; it is independent of the heat pipe parameters and its orientation.

If Eq. 2-54 is examined, it is seen that the right side is independent of the heat transport requirement. It contains only physical heat pipe properties; i.e., wick vapor space and fluid properties and the orientation with respect to gravity. This term sets the upper limit for the Heat Transport Factor. It is therefore convenient to define the capability of the heat pipe in a form that permits a direct comparison with the requirements, namely, the heat pipes Heat Transport Capability is defined as:

$$(\dot{QL})_{max} \equiv \frac{\Delta p_{cap}}{C} + \int_{x''}^{x'} \frac{\rho_\ell\, g \sin\beta}{C} \qquad (2\text{-}56)$$

From the definition of $(\dot{QL})_{max}$, it is observed that it is necessary to impose the restriction that either body forces are absent or x' and x" are independent of $\dot{Q}\,(x)$. If at least one of these conditions is not met, $(\dot{QL})_{max}$ will be dependent on the heat transport requirement, and Eq. 2-56 will not describe the capability of the heat pipe.

Using the two definitions, Eqs. 2-55 and 2-56, the pressure balance assumes a simple form:

$$(\dot{QL})_R \leq (\dot{QL})_{max} \tag{2-57}$$

It must be emphasized again that $(\dot{QL})_R$ represents the heat transport requirement as prescribed by the application and $(\dot{QL})_{max}$ represents the heat pipe's transport capability to meet these requirements. The symbol $\dot{QL}$ for both parameters has not been chosen arbitrarily, both $(\dot{QL})_R$ and $(\dot{QL})_{max}$ are given in watt-meter or, more commonly, in watt-inches.

The significance of the Heat Transport Requirement and the Heat Transport Capability can best be realized by examining two special but very important cases.

(1) The first case involves a heat pipe operating in a 0-g environment. No restrictions shall be placed on the shape of the heat pipe* or the distribution of evaporators and condensers. Once this distribution has been specified, the net axial heat flow rate $\dot{Q}(x)$ can be obtained from Eqs. 2-43 and 2-46. Because of the assumption of uniform wick properties and the absence of dynamic effects and body forces, the interfacial pressure difference $\Delta p_i(x)$ is proportional to $\dot{Q}(x)$. Thus the locations x' and x" of the lowest and highest value of Δp_i are completely determined by the distribution of $\dot{Q}(x)$ and are independent of the heat pipe's geometry. The Heat Transport Requirement $(\dot{QL})_R$ is found from Eq. 2-55 and is also specified by the distribution of heat loads.

The Heat Transport Capability $(\dot{QL})_{max}$ is given by:

$$(\dot{QL})_{max} = \frac{\Delta p_{cap}}{C} \tag{2-58}$$

*As long as the one-dimensional flow model applies.

Closed form solutions for $(\dot{Q}L)_{max}$ which apply to this special case may be found in Chapter 4. Any distribution of heat input and output which results in a $(\dot{Q}L)_R$ that is less than $(\dot{Q}L)_{max}$ for a given heat pipe will be compatible with that heat pipe design.

(2) Another special, but frequently encountered case is that of a straight heat pipe which is operating in a gravity field and in the "heat pipe mode." The latter shall be defined by the following two conditions:

(a) The angle between the positive x axis and the horizontal is less than zero, i.e., evaporator above the condenser ($\beta < 0$).

(b) The net axial heat flow rate $\dot{Q}$ is positive (or zero) at all axial locations x.

The above conditions state that the net axial heat flow rate should everywhere have a component in the direction of gravity. For this special case it can be shown that the points of maximum and minimum interfacial pressure are always located at the ends of the heat pipe, i.e.,

$$x'' = 0,\ x' = L \tag{2-59}$$

For this case, the Heat Transport Requirement becomes

$$(\dot{Q}L)_R = \int_0^L \dot{Q}\,(x)\,dx \tag{2-60}$$

The Heat Transport Capability Factor $(\dot{Q}L)_{max}$ can be found by carrying out the integration in Eq. 2-56:

$$(\dot{Q}L)_{max} = \frac{1}{C}\,(\Delta p_{cap} + \rho_\ell\, g\, L \sin\beta) \tag{2-61}$$

The first term on the right side of Eq. 2-61 represents the Heat Transport Capability Factor in the absence of gravity. Eq. 2-61 can therefore be expressed as:

$$(\dot{Q}L)_{max} = (\dot{Q}L)_{max,0\text{-}g} + \frac{\rho_\ell\, g\, L}{C} \sin\beta \tag{2-62}$$

As expected, operation at an adverse elevation reduces the heat transport capability in 1-g. Equation 2-62 describes the reduction of the "0-g" Heat Transport Capability Factor due to a gravitational hydrostatic head.

2.6.3 Closed Form Solution

Closed form solutions of the hydrodynamic transport equations may be found for several heat pipe cases. One of the most useful is for the conventional heat pipe shown in Fig. 2-7 which has uniform heat addition and removal near the two ends, uniform wick properties along the length, and is operated in the "heat pipe mode" ($\beta < 0$, evaporator above condenser). Additional requirements necessary to obtain explicit closed form solutions are laminar flow in the liquid and the vapor and negligible momentum pressure gradients. Although the requirements of laminar flow and the absence of momentum effects appear restrictive, good design practices usually avoid these regimes altogether. Special modes of operation such as the start-up transients of liquid metal heat pipes are exceptions.

The Heat Transport Capability for this conventional heat pipe is given by Eq. 2-61. Using the appropriate expressions for the constant C (Eq. 2-53) and for Δp_{cap} (Eq. 2-9 in conjunction with Eq. 2-49), $(\dot{Q}L)_{max}$ becomes:

$$(\dot{Q}L)_{max} = \frac{2 K A_w (1 + \eta) \cos \theta_c F_\ell}{r_p} N_\ell \qquad (2\text{-}63)$$

The following abbreviations have been used in Eq. 2-63

(1) The parameter η is defined as the ratio of the sum of all pressure differences resulting from body forces to the available capillary pressure, i.e.,

$$\eta = -\left[\frac{r_p D \cos \beta}{2 H_\ell \cos \theta} + \frac{r_p L \sin \beta}{2 H_\ell \cos \theta}\right] \qquad (2\text{-}64)$$

where H_ℓ is the Wicking Height Factor, and is a property of the working fluid only:

$$H_\ell \equiv \frac{\sigma}{\rho_\ell g} \qquad (2\text{-}65)$$

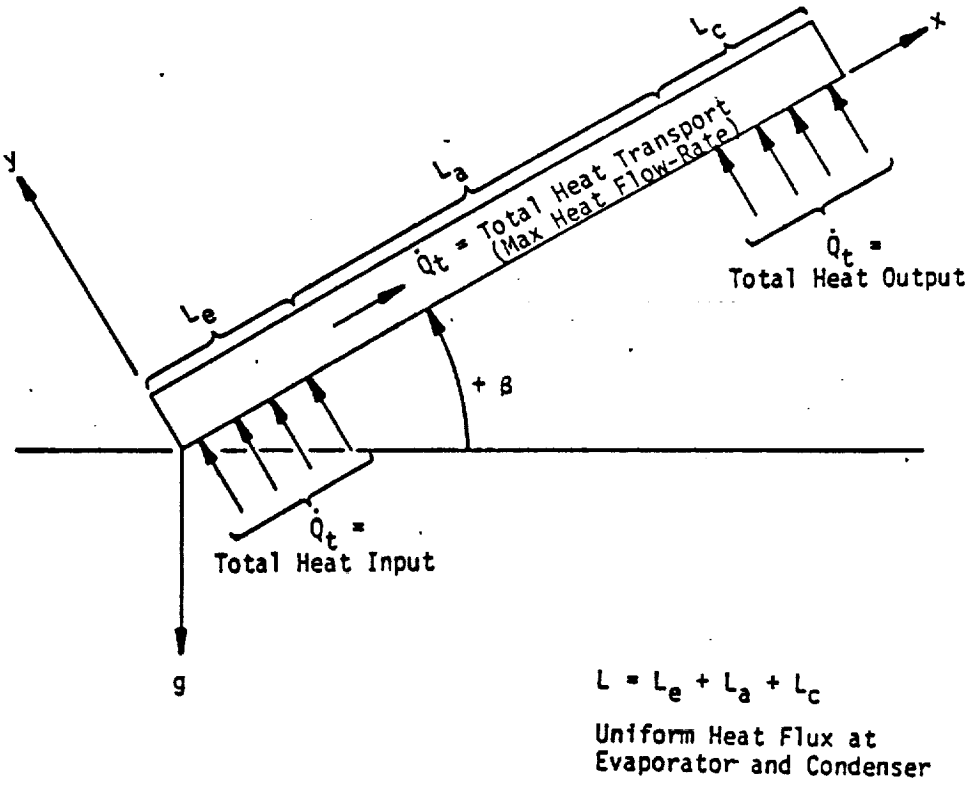

Fig. 2-7. Conventional heat pipe with uniform heat loads

(2) The parameter F_ℓ represents the ratio of the viscous pressure drop in the liquid to the sum of all the pressure drops in the liquid and vapor.

$$F_\ell = \frac{\Delta p_\ell}{\Delta p_\ell + \Delta p_{\ell v} + \Delta p_v} \tag{2-66}$$

$$F_\ell = \frac{1}{1 + \frac{\phi^2}{3}\Psi + \frac{\nu_v}{\nu_\ell}\frac{32\,K}{D^2_{h,v}}\frac{A_w}{A_v}} \tag{2-67}$$

As mentioned previously, Eqs. 2-63 and 2-67 assume uniform wick properties. In the case of the axially grooved geometry the effect of meniscus recession can have a significant impact on the magnitude of the permeability K and the wick area A_w. However, as shown in Ref. 8 a closed form approximation of these parameters can be obtained. Hence the values of K, A_w, ϕ and Ψ in Eqs. 2-63 and 2-67 can be taken as average values. Specific relations which define the value for a given groove geometry are presented in Chapter 4.

(3) The Liquid Transport Factor N_ℓ is a property of the working fluid and is defined as:

$$N_\ell = \left(\frac{\rho_\ell \lambda \sigma}{\mu_\ell} \right) \tag{2-68}$$

Equation 2-63 defines the maximum heat transport capability of a conventional heat pipe provided that capillary pumping is the limiting factor. Since in most applications the capillary limit is the controlling one, Eq. 2-63 is one of the most useful expressions for the design of heat pipes.

In order to obtain an expression for the maximum amount of heat which the pipe can transport, the Heat Transport Requirement is equated with the Heat Transport Capability Factor:

$$\int_o^L \dot{Q}\, dx = (\dot{Q}L)_{max} \tag{2-69}$$

Referring to Fig. 2-7, the axial heat flow rate $\dot{Q}(x)$ can be expressed in terms of the total heat input $\dot{Q}_t$ for each of the following regions:

Evaporator	$0 < x < L_e$	$\dot{Q}(x) = \dot{Q}_t\, x/L_\ell$
Transport Section	$L_e < x < L_e + L_a$	$\dot{Q}(x) = \dot{Q}_t$
Condenser	$L - L_c < x < L$	$\dot{Q}(x) = \dot{Q}_t (L - x)/L_c$

(2-70)

If the integration in Eq. 2-69 is carried out, an explicit expression is obtained for the total heat transport or heat flow rate $\dot{Q}_t$:

$$(\dot{Q}L)_{max} = \dot{Q}_t \left(\frac{1}{2} L_e + L_a + \frac{1}{2} L_c \right) \tag{2-71}$$

It is often convenient to define an "effective length" of the heat pipe as follows:

$$L_{eff} = \frac{1}{2} L_e + L_a + \frac{1}{2} L_c \qquad (2\text{-}72)$$

Eq. 2-69 then becomes:

$$\dot{Q}_t \, L_{eff} = (\dot{Q}L)_{max} \qquad (2\text{-}73)$$

Using Eqs. 2-63 and 2-73, the following expressions for the maximum heat flow rate $\dot{Q}_t$ is obtained:

$$\dot{Q}_t = \frac{2 K A_w (1 + n) \cos \theta_c F_\ell}{r_p L_{eff}} N_\ell \qquad (2\text{-}74)$$

It is important to note that the definition for the effective heat pipe length (Eq. 2-72) applies only for the special case of uniform heat input and heat output at two separate locations. For non-uniform heat distributions the integral of $(\dot{Q}\, dx)$ in Eq. 2-69 must be solved in order to obtain an applicable effective length to be used in Eqs. 2-73 and 2-74.

Since in the limit the maximum transport capability must equal the maximum transport requirement, Eq. 2-74 states that a given heat pipe geometry will satisfy any combination of total heat load $\dot{Q}_t$ and effective length L_{eff} which results in the same product (i.e. $(\dot{Q}L)_R$).

2.7 OTHER HEAT TRANSPORT LIMITATIONS

In addition to the capillary pumping limit discussed above, the circulation of the working fluid is restricted by several other limitations.

2.7.1 Sonic Limit

The evaporator section of a heat pipe represents a constant area vapor flow duct with mass addition through the evaporation process. The vapor velocity increases steadily along the length of the evaporator section due to the progressively increasing mass flow and reaches a maximum at the evaporator exit. It can be shown (12) that the limitations of such a flow regime are comparable to that of a converging nozzle with constant mass flow. The evaporator exit corresponds to the throat of the nozzle. The maximum vapor velocity which can exist at the evaporator exit corresponds to Mach 1. This choked flow condition is a fundamental limit on the axial vapor flow in a heat pipe. This limit does

not exclude the possibility of supersonic flow in other sections of the heat pipe. In fact, Kemme (4) (13) has reported supersonic flow conditions in the condenser section of liquid metal heat pipes.

The axial heat flux for the sonic limit is obtained by calculating the mass flow rate at Mach 1:

$$\frac{\dot{Q}}{A_v} = \rho_v \lambda V_s \tag{2-75}$$

where the sonic velocity V_s is given by the familiar equation:

$$V_s = \sqrt{\frac{\gamma R_o T}{M}} \tag{2-76}$$

At the sonic limit, therefore, the mass flow rate per unit area and the corresponding axial heat flux depend only on the properties of the working fluid and in turn the operating temperature. The limiting axial heat flux has, therefore, been included as a derived fluid property in Volume II.

The axial heat flux at sonic conditions must be evaluated using the local temperature at a choking point. This temperature is considerably lower than the stagnation temperature which is measured at the entrance of the evaporator. Stagnation and local static temperature at Mach 1 are related through the expression:

$$T_{stagn} = T\left(1 + \frac{\gamma - 1}{2}\right) \tag{2-77}$$

For liquid metals with a ratio of specific heats of 5/3 the static temperature is only 75% of the stagnation temperature at M = 1. Levy (12) presents an equation which gives the limiting axial heat flux at sonic conditions in terms of the stagnation temperature (the temperature at the beginning of the evaporator) which is often more convenient to use:

$$\frac{\dot{Q}}{A_v} = \frac{\rho_v \lambda V_s}{\sqrt{2(\gamma + 1)}} \tag{2-78}$$

In Eq. 2-78, the fluid properties, e.g., ρ_v, λ and V_s (Eq. 2-76), are evaluated at the stagnation temperature.

When the sonic limit is exceeded, it does not represent a failure as catastrophic as exceeding the capillary limit. When the sonic limit is reached, further increase in the mass flow rate and therefore the heat transfer rate can be realized only by increasing the stagnation pressure upstream of the choking point. To some extent this will occur automatically since the evaporation temperature will rise (and with it the saturation temperature and therefore the stagnation pressure) as soon as the total heat input and total heat output begin to diverge. Operation at or near the sonic limit results in large axial temperature differences along the heat pipe.

2.7.2 Entrainment Limit

Like the sonic limit the entrainment limit is also a characteristic of high axial vapor velocities. Since liquid and vapor are in direct contact along the heat pipe, separated only by the meniscus at the wick, a mutual shear force exists between them. At low relative velocities, this shear force will only add to the viscous drag in both phases. Because the vapor velocity is usually much higher than that of the liquid, the effects will be most noticeable in the liquid phase. If the relative velocity becomes too great, the interface becomes unstable and liquid droplets are torn from the wick and "entrained" in the vapor. The first observation of this phenomenon was made at Los Alamos Scientific Laboratory through the sound made by droplets striking the condenser end of the heat pipe (14).

Entrainment may be described by the Weber number which is a ratio of the inertial forces in the vapor to the tension forces in the liquid surface. The Weber number is defined as:

$$We = \frac{\rho_v \bar{V}^2}{\sigma/z} \tag{2-79}$$

where $\bar{V}$ is the average vapor velocity and z is a characteristic dimension for the surface. A Weber number of unity is generally believed to indicate the onset of entrainment. The corresponding axial heat flux is given by:

$$\frac{\dot{Q}}{A_v} = \left(\frac{\rho_v \sigma \lambda^2}{z}\right)^{\frac{1}{2}} \tag{2-80}$$

There is some uncertainty as to the proper choice of the characteristic dimension z. It is related to the wavelength of the perturbation on the liquid surface. Experimental data seems to indicate that a Weber number of unity corresponds to the onset of entrainment if z is approximately equal to the mesh size of screen material. Insufficient quantitative data is available to resolve the question of whether the characteristic dimension is related to the wire diameter (15) or the wire spacing (16). In the case of an axial groove, the groove's width has been used.

The phenomenon of entrainment reduces the amount of liquid pumped back to the evaporator by prematurely returning it to the condenser. It thus increases the circulation losses (it might be considered an internal "leak") and therein limits the amount of heat flow through the heat pipe.

2.7.3 Heat Flux Limit

In addition to the capillary, the sonic, and the entrainment limits the heat pipe performance is also limited by the evaporator heat flux. Heat is transferred into and out of the heat pipe through the pipe wall and through at least part of the wick. If the radial heat flux becomes excessive, the circulation of the working fluid can be severely affected and the heat transport capability may be controlled by the radial heat flux rather than by the axial heat transport.

The limitation of the axial heat flux is not nearly as well understood as the condenser flooding hydrodynamic limits. There appears to be no limit to the heat flux at the condenser. High condenser heat fluxes contribute, of course, directly to the heat pipe conductance but they do not affect circulation of the working fluid. The evaporator heat flux, on the other hand, has definite upper bounds which limit the axial heat transport. Unlike the previously described limits, which specify a maximum axial heat transport $\dot{Q}_t$, the heat flux limit specifies the maximum radial evaporator heat flux $\dot{q}_e$. The two quantities are related through the evaporator area A_e:

$$\dot{Q}_t = \dot{q}_e A_e \qquad (2\text{-}81)$$

Thus, for a given evaporator geometry, the heat flux limit also specifies the maximum axial heat transport.

The heat flux limit is generally considered to coincide with the onset of nucleate boiling in the wick. Heat is conducted from the heat pipe wall through the wick, and evaporation is assumed to occur at the liquid-vapor interface. This model has been substantiated by extensive experimental evidence (17, 18, 19). When boiling occurs within the wick the presence of the vapor bubbles that are generated reduce the liquid flow area and consequently decrease the transport capability.

With the onset of nucleate boiling, the hydrodynamic equations previously developed are no longer applicable since they were based on one-dimensional, laminar, liquid flow in a fully saturated wick. Breakdown of the mathematical model does not necessarily indicate a heat transfer limit. Since the hydrodynamic theory does not account for boiling in the wick, it is good design practice to define the heat flux limit as the onset of nucleate boiling.

The boiling heat flux limit corresponds to the conduction heat flux which yields a "critical" super heat ΔT_{cr} in the liquid. The boiling heat flux limit is therefore:

$$q_{max} = \frac{K_{eff}}{t_w} \Delta T_{crit} \qquad (2\text{-}82)$$

where K_{eff} is the effective thermal conductivity of the wick-liquid matrix. Models for the effective conductivity will be discussed in Section 2.8.

Marcus (20) has derived an expression for the critical super heat which is based on criteria similar to those which apply to nucleate boiling from planar surfaces.

$$\Delta T_{crit} = \frac{T_{sat}}{\lambda \rho_v} \left(\frac{2\sigma}{r_n} - (\Delta p_i)_{max} \right) \qquad (2\text{-}83)$$

where T_{sat} is the saturation temperature of the fluid and r_n is the effective radius of the critical nucleation cavity. This equation is based on the assumption that a bubble of a certain size will grow if its internal vapor pressure associated with the local superheat exceeds the restraining forces of saturation and capillary pressure. The radius of nucleation cavities, r_n, is a function of the boiling surface. Typical values for smooth surfaces are between 10^{-4} and 10^{-3} cm. For wicked surfaces, little is known about the critical radii of nucleation cavities but an upper bound is certainly the pore size of the wick.

The model predicts very conservative superheat tolerances. Even if the lower bound for the critical radius is used, the calculated critical superheat is sometimes one order of magnitude lower than that actually measured. Marcus (17) attributes this to the absence of a gaseous phase at the nucleation sites because heat pipes contain a highly degassed working fluid. However, incipient boiling is difficult to detect through temperature measurements alone and many wicks which provide for adequate venting of internally generated vapor can tolerate some nucleate boiling without affecting the hydrodynamic limit.

A definite upper heat flux limit exists for every wick, and it is reached when the vapor generated within the wick is at such a high rate that it cannot escape fast enough from the heated surface. This is equivalent to the inability of the capillary forces to replenish liquid at a sufficient rate. Boiling in the wick and the associated heat flux has been the subject of many investigations. Because of the present lack of a consistent theory that has been tested experimentally, it is premature to include this information in a Handbook.

2.8 HEAT TRANSFER

The preceding sections have dealt with the maximum heat transfer capability of the heat pipe. In this section the thermal conductance of a heat pipe which is operating at heat loads which are below the hydrodynamic or heat flux limits is discussed. When operated below any of its limits, the heat pipe is a thermal conductor of extremely high conductance. As mentioned previously, heat pipes are frequently referred to as isothermal devices. In reality their conductance is finite but very high. In defining the conductance of a heat pipe, one has to distinguish between its internal conductance and that of the interfaces between the heat pipe and the environment. Furthermore, the internal conductance is a composite of the radial heat transfer (at the evaporator and the condenser) and of the axial vapor mass transport. In most cases the conductance associated with the heat input and output mechanisms (external and internal) is much lower than the one associated with axial vapor and liquid transport. The overall conductance is therefore limited by input/output conductances--a fact which is very important in heat pipe design.

The thermal model of a fixed conductance heat pipe is shown in Fig. 2-8. The total thermal resistance, R, is composed of a series of individual resistances:

$$R = R_{ext,e} + R_{en,e} + R_{w,e} + R_{ev} + R_v + R_c + R_{w,c} + R_{en,c} + R_{ext,c} \qquad (2\text{-}84)$$

Frequently, it is more convenient to describe the heat transfer characteristics by a conductance, C, rather than a resistance, R. The two are related through:

$$C = \frac{1}{R} \qquad (2\text{-}85)$$

In terms of conductance, Eq. 2-84 becomes:

$$\frac{1}{C_t} = \frac{1}{C_{ext,e}} + \frac{1}{C_{en,e}} + \frac{1}{C_{w,e}} + \frac{1}{C_e} + \frac{1}{C_v} + \frac{1}{C_c} + \frac{1}{C_{w,c}} + \frac{1}{C_{en,e}} + \frac{1}{C_{ext,c}} \qquad (2\text{-}86)$$

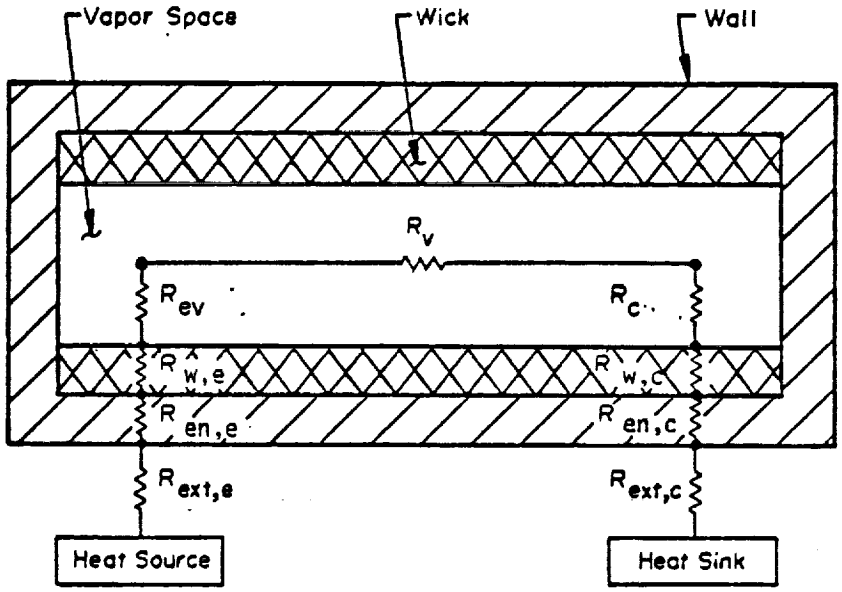

Fig. 2-8. Thermal model of a fixed conductance heat pipe

Each of the individual conductances, which are introduced by Eq. 2-86, are discussed in the following paragraphs.

(1) $C_{ext,e}$ is the conductance between the heat source and the exterior of the evaporator. Its magnitude will, in general, depend on the application of the heat pipe. When it is closely coupled to the heat source, which is most frequently the case, this conductance is directly proportional to the external evaporator area

$$C_{ext,\,e} = h_{ext,e}\ A_{ext,e} \tag{2-87}$$

The external heat transfer coefficient, $h_{ext,e}$ is a function of the type of thermal interface. Representative values can be found in Ref.(21).

(2) $C_{en,e}$ is the conductance of the heat pipe envelope (wall) at the evaporator. For cylindrical geometries

$$C_{en,e} = \left(\frac{2k\ A}{D_o\ \ln \frac{D_o}{D_i}} \right)_{en,e} \tag{2-88}$$

If the wall thickness is small compared to the diameter of the heat pipe this conductance reduces to:

$$C_{en,e} = \left(\frac{k\ A}{t} \right)_{en,e} \tag{2-89}$$

(3) $C_{w,e}$ is the conductance of the wick at the evaporator. This term is usually the most difficult one to evaluate and is frequently a very significant contributor to the overall conductance. In the absence of nucleate boiling, heat is transmitted by conduction from the heat pipe wall, through the wick, and to the liquid-vapor interface which is the site of evaporation. This conduction can be expressed in terms of an internal heat transfer coefficient, $h_{int,e}$:

$$C_{w,e} = (hA)_{int,e} \tag{2-90}$$

For some wick geometries, analytical expressions or at least approximations can be found for the internal conductance. In the case of a porous wick located at the wall of the heat pipe, the internal evaporator conductance becomes:

$$C_{w,e} = \left(\frac{2k_w A_{int}}{D_i \ln \frac{D_i}{D_v}} \right)_{en,e} \tag{2-91}$$

For thin wick structures, Eq. 2-91 reduces to a form similar to Eq. 2-89.

The effective wick conductivity k_w has been the subject of many studies (18, 19, 22). For a porous wick saturated with liquid, the effective conductivity is bracketed by the two extremes of parallel or series conduction paths:

$$\underbrace{\frac{k_s k_\ell}{\varepsilon k_s + (1 - \varepsilon) k_\ell}}_{\text{(series)}} \leq k_w \leq \underbrace{(1 - \varepsilon) k_s + \varepsilon k_\ell}_{\text{(parallel)}} \tag{2-92}$$

For metallic wicks and insulating liquids, the range of k_w covered by Eq. 2-92 is extremely broad. Conservative design would use the series conduction model. If the liquid conductivity k_ℓ is much lower than that of the solid, the series model essentially represents the conductivity of a liquid layer whose thickness is weighted by the porosity of the matrix. For the case of an annular wick, Eq. 2-92 gives the correct result if $\varepsilon = 1$ is used.

In many high performance heat pipes, the bulk of the wick is removed from the wall in order to minimize the conductive temperature gradient. A secondary wick is then employed for circumferential distribution which consists of either a very thin layer of porous material, circumferential grooves, or a combination of screen covered screw thread grooves as in the case of the inverted meniscus design (23). Screw thread

circumferential grooves have been used in most of the recently developed high performance heat pipes. References (24) and (25) provide thermal analyses of circumferential grooves.

However, these models are relatively complicated and tend to over-predict the film coefficients, particularly in the evaporator. The best design approach is to use measured values wherever possible. Film coefficients that have been obtained with various fluid/wick combinations are presented in Chapter 4. Generally, these values are for equivalent film coefficients which account for the wick conductance and the evaporation or condensation process as discussed in subsequent paragraphs.

(4) C_{ev} is the conductance associated with the vaporization process at the liquid-vapor interface. This conductance is usually very large and contributes little to the overall conductance. Cotter (1) derived an expression, based on gas kinetics, for the pressure difference between the sites of vaporization and the bulk of the vapor. This expression, in terms of a heat transfer coefficient is:

$$h = \frac{\alpha \lambda^2 \rho_v}{T} \sqrt{\frac{MW}{R_o T 2\pi}} \qquad (2\text{-}93)$$

The numerical factor (α) is of the order of 1. It accounts for the probability of condensation of an impinging vapor molecule. The vaporization conductance C_{ev} is obtained from Eq. 2-93 using a relation similar to Eq. 2-90 but based on the area of the liquid-vapor interface. In the case of axially grooved heat pipes, Kamotani (26, 27) has recently developed an expression for an equivalent evaporator film coefficient as

$$h_{eq,e} = \frac{N k_\ell}{2\pi R_v} \quad \frac{1}{k_f + \frac{k_\ell}{k_w} \frac{\delta}{S}} \qquad (2\text{-}94)$$

where:

k_p = 0.0701 for the evaporator, and 0.0221 for the condenser

(5) C_v is the thermal conductance associated with the axial vapor flow. This is the only term which, because it is generally proportional to the vapor's viscous pressure drop, is also proportional to the length of the heat pipe. The temperature drop associated with this conductance is proportional to the axial heat flow whereas all other drops are proportional to the radial heat flux.

For a given vapor pressure drop, the corresponding temperature difference can be found. Based on the definition of C_v and using the Clausius-Clapeyron Equation, the following expression is obtained:

$$C_v = \frac{\lambda \rho_v}{T} \frac{\dot{Q}}{\Delta p_v} \qquad (2\text{-}95)$$

If the vapor flow is predominantly viscous, Δp_v is proportional to $\dot{Q}$ and to the length of the heat pipe. C_v then becomes a true, axial conductance which may be compared directly to that of a solid conductor. Since this term represents the minimum temperature drop that can be experienced, heat pipes have frequently been compared on this basis to other conductors. It must be noted, however, that C_v is only a small contributor to the overall heat pipe conductance and that the comparisons are therefore not very meaningful.

(6) C_c, $C_{w,c}$, $C_{en,c}$, $C_{ext,c}$ are the conductances at the condenser end of the heat pipe and their expressions are identical to those at the evaporator. If the condenser geometry differs from that of the evaporator, the numerical values will be affected but the preceding Eqs. 2-87 through 2-94 will apply.

A combination of the individual contributions yields the overall conductance as expressed in Eq. 2-86. This expression can be simplified; since the external interfaces are not part of the heat pipe and they should be treated separately. Hence, by excluding the interface conductances and combining the contributions of wall and wick and vaporization or condensation at the evaporator or at the condenser as applicable, a simplified expression for the overall heat pipe conductance can be obtained as

$$\frac{1}{C} = \left(\frac{1}{A\,h_{eq}}\right)_e + \left(\frac{1}{A\,h_{eq}}\right)_c + \frac{1}{C_v} \qquad (2\text{-}96)$$

where A_e and A_c are the external areas of the evaporator(s) and condenser(s) and $h_{eq,e}$ and $h_{eq,c}$ are the respective combined heat transfer coefficients. Since $1/C_v$ is relatively small compared to the other two terms, Eq. 2-96 illustrates that heat pipes are best utilized where heat is to be transported over relatively large distances. The evaporator and condenser conductances are independent of the heat transport length and only the relatively small term $1/C_v$ is proportional to the heat pipe. In the limit for very short heat pipes, this insensitivity to length sometimes renders the heat pipe inferior to solid conductors because the temperature drops at the evaporator and condenser can be significant depending on the radial heat flux.

REFERENCES

1. Cotter, T. P., "Theory of Heat Pipes," Los Alamos Scientific Laboratory Report LA-3246-MS, February 1965.

2. Adamson, A. W., "Physical Chemistry of Surfaces," Interscience Publishers, New York, 1960.

3. Zisman, W. A., "Contact Angle, Wettability and Adhesion," in Advances in Chemistry Series No. 43, Ed. by Fowkes, F. M., American Chemical Society, Washington, D. C., 1965, pp. 1-51.

4. Deverall, J. E., and Kemme, J. E., "High Thermal Conductance Devices Utilizing the Boiling of Lithium and Silver," Los Alamos Scientific Laboratory, LA-3211, 1965.

5. Scheidigger, A. E., "The Physics of Flow Through Porous Media," The MacMillan Co., New York, 1960.

6. Kays, W. M., "Convective Heat and Mass Transfer," McGraw-Hill Book Co., Inc., New York, 1966.

7. Hufschmidt, E. et al., "The Shearing Effect of Vapor Flow on Laminar Liquid Flow in Capillaries of Heat Pipes," NASA TT-F-16601, October 1965.

8. Jen, H. and Kroliczek, E., "Axially Grooved Heat Pipe Study," B & K Engineering, Inc. Report No. BK012-1009 for NASA Goddard Space Flight Center, Contract No. NAS5-22562, July 1977.

9. Knight, B. W. and McInteer, B. B., "Laminar Imcompressible Flow in Channels with Porous Walls," LADC-5309.

10. Parker, G. H. and Hanson, J. P., "Heat Pipe Analysis," Advances in Energy Conversion Engineering ASME 1967 Intersociety Energy Conversion Conference, Miami, Florida, August 1967, p. 857.

11. Levy, E. K., "Theoretical Investigation of Heat Pipes Operating at Low Vapor Pressures," Trans. ASME, J. for Industry, November 1968, p. 547.

12. Levy, E. K., "Effects of Friction on the Sonic Velocity Limit in Sodium Heat Pipes," ASME Paper HPT-71-022.

13. Deverall, J. E., Kemme, J. E., and Florschuetz, L. W., "Sonic Limitations and Startup Problems of Heat Pipes," Los Alamos Scientific Laboratories, Report No. LA-4518, November 1970.

14. Deverall, J. E., "Capability of Heat Pipes," Heat Pipe Technology & Manned Space Station Appl. Technical Interchange, Huntsville, Alabama, May 27, 1969.

15. Kemme, J. E., "High Performance Heat Pipes," IEE 1967 Thermionic Specialist Conference, Palo Alto, California, October 1967, pp. 355-358.

16. Wright, P. E., Final Report for ICICLE Feasibility Study, Contract NAS5-21039, RCA, Camden, New Jersey.

17. Marcus, B. D., "Theory and Design of Variable Conductance Heat Pipes," NASA CR-2018, April 1972.

18. Soliman, M. M., Grauman, D. W., and Berenson, P. J., "Effective Thermal Conductivity of Saturated Wicks," ASME Paper No. 70-HT/SpT-40, 1970.

19. Ferrel, J. K., and Alleavitch, J., "Vaporization Heat Transfer in Capillary Wick Structures," Chemical Eng. Prog. Symposium Series V66, Heat Transfer, Minneapolis, Minn., 1970.

20. Marcus, B. D., "On the Operation of Heat Pipes," TRW Report 9895-6001-TU-000, May 1965.

21. Wright, J. P., "Thermal Investigation and Analytical Modeling of Heat Pipe Thermal Interface Techniques," Rockwell International, June 1973.

22. Goring, R. L. and Churchill, S. W., "Thermoconductivity of Heterogeneous Materials," Chemical Engineering Prog. 57, No. 7, 53-59 (1961).

23. Saaski, E. W., and Hamasaki, R. H., "Study of a High Performance Evaporative Heat Transfer Surface," NASA CR 152008, May 1977.

24. Berger, M. E., and Feldman, K. T., Jr., "Analysis of Circumferentially Grooved Heat Pipe Evaporators," ASME Paper 73-Wa/Ht-13, 1973.

25. Schneider, G. E., and Yovanovich, M. M., "Thermal Analysis of Trapezoidal Grooved Heat Pipe Walls," Report to Department of Communications, Ottawa, Ontario, 1975.

26. Kamotani, Y., "Evaporator Film Coefficients of Grooved Heat Pipes," 3rd International Heat Pipe Conference, 1978.

27. Kamotani, Y., "Thermal Analysis Program for Axially Grooved Heat Pipes; Its Description and Capabilities," to be published.

VARIABLE CONDUCTANCE HEAT PIPE THEORY

The conventional fixed conductance heat pipe discussed in Chapter 2 is a completely passive device. It is not restricted to a fixed operating temperature but adjusts its temperature according to the heat load and the sink condition. Although its thermal conductance is very high, it is nevertheless a nearly constant parameter.

However, there are many potential heat pipe applications in which a specific operating temperature range is desired along certain portions of the pipe even though source and sink conditions are changing. In those cases, it becomes necessary to actively or passively control the heat pipe so that it maintains the desired operating temperature range. Temperature control is obtained by varying one or several of the conductances that make up the heat pipe's overall thermal conductance. Similarly there exist many applications where heat pipe operation as a (1) thermal diode or (2) a thermal switch is required. In either case, the objective is for the heat pipe to operate at the limits of variable conductance as an effective heat conductor or as a thermal insulator. Again, it is necessary to introduce an active or passive control feature to effect this behavior. Traditionally, variable conductance has been used to describe control provided by "gas-loaded" heat pipes. As discussed in the next section there are four types of variable conductance pipes: (1) gas-loaded heat pipes; (2) excess-liquid heat pipes; (3) liquid flow-modulated heat pipes; and (4) vapor flow-modulated heat pipes.

This chapter discusses the different methods for obtaining variable conductance operation and the associated theory. Fixed conductance heat pipe theory is still applicable to determine the transport capability of the heat pipe. Variable conductance theory, as presented in Sections 3.2 through 3.4, consists of the analysis and mathematical models that define the particular control technique and the associated variable conductance operation of the heat pipe.

3.1 TECHNIQUES FOR VARYING HEAT PIPE CONDUCTANCE

The basic conductance model of a heat pipe is presented in Section 2.8. For ease of reference, a slightly simplified model is shown in Fig. 3-1 in which the evaporator and condenser conductances are lumped together. In this model, C_e represents the conductance between the heat source and the vapor in the heat pipe, C_v is the internal resistance

along the length of the pipe, and C_c is the conductance between the heat pipe vapor and the ultimate heat sink. The overall conductance C between the source and the sink is given by Eq. 3-1.

$$C = \frac{1}{\frac{1}{C_e} + \frac{1}{C_c} + \frac{1}{C_v}} \qquad (3\text{-}1)$$

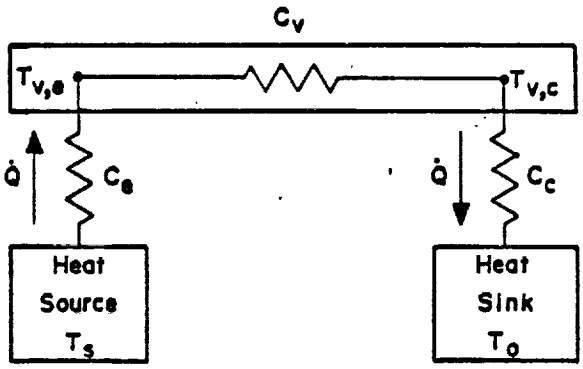

Fig. 3-1. Conductance model of heat pipe

In principle, a variable heat pipe conductance can be achieved by modulating any one or several of the individual conductances that make up the overall conductance. A number of techniques exist to achieve variable conductance, and they can be grouped into the following four categories:

1. Gas-Loaded Heat Pipe

This technique consists of introducing a fixed amount of non-condensible gas into the heat pipe which during operation will form a "plug" which blocks the vapor flow. A schematic of a gas-loaded VCHP is presented in Fig. 3-2. Typically, a reservoir is added to accommodate the gas when "full-on" heat pipe operation is required. As vapor flows from the evaporator to the condenser, it sweeps the non-condensing gas which accumulates in the cold end of the heat pipe. The gas therein forms a barrier to the vapor flow and effectively "shuts off" that portion of the condenser which it fills. The length of the plug and therefore the condenser conductance depends on such factors as the system's operating temperature, heat source and sink conditions, reservoir size

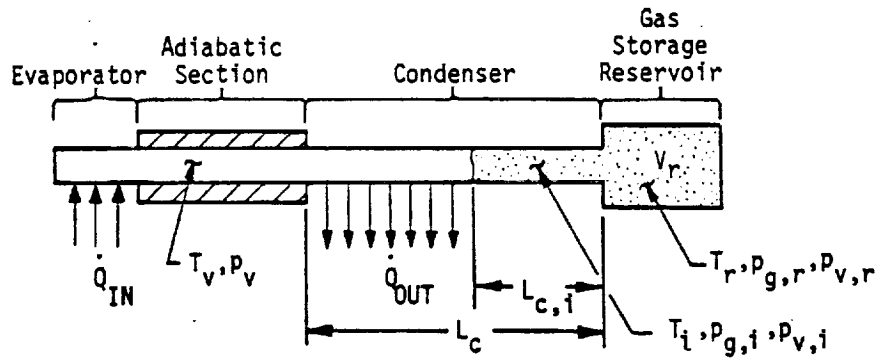

Fig. 3-2. Gas-loaded variable conductance heat pipe

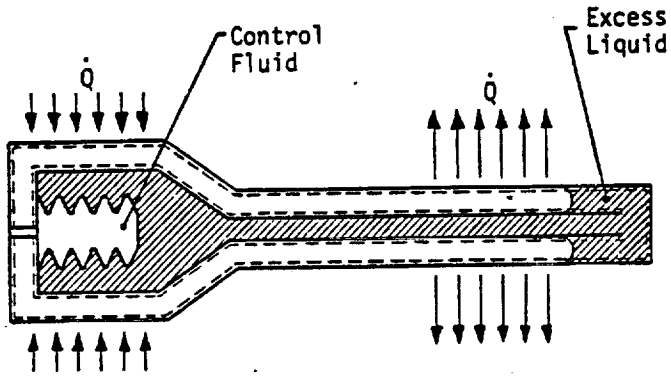

a. Variable Conductance

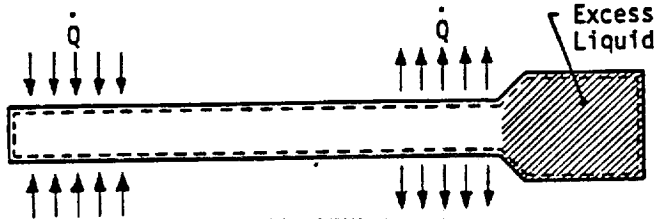

b. Thermal Diode

Fig. 3-3. Schematics of excess-liquid heat pipes

and reservoir temperature, etc. The influence of these parameters as well as the various methods for obtaining gas-loaded VCHP control are discussed in the next section. It should also be noted that gas blockage can also be used to effect diode and switching operations; however, the transients associated with the "shutdown" or "switching" operations can be prohibitive with a gas-loaded system (1).

2. Excess-Liquid Heat Pipe

This approach is analogous to the "gas-loaded" heat pipe except that excess liquid accumulates as a slug in the condenser end rather than a non-condensible gas. Control with this technique tends to be less sensitive to variations in sink conditions; however, the actual designs can be more difficult to implement. Fig. 3-3a shows one method for obtaining variable conductance with excess liquid. Again a reservoir is utilized and it is located inside the heat pipe envelope. The effective volume of the reservoir is varied by means of a bellows which contains an auxiliary fluid in equilibrium with its vapor. Adjustment of the bellows to changes in system temperature changes the reservoir volume therein allowing the excess liquid to move into or out of the condenser.

Fig. 3-3b illustrates a thermal diode heat pipe which utilizes liquid blockage to "shut off" the heat piping action in the reverse direction. In the normal forward mode operation the excess liquid is swept into the reservoir at the condenser end. When conditions arise (e.g. an increase in sink temperature due to orbital conditions, etc.) which cause the condenser temperature to rise above the evaporator, the direction of vapor flow is reversed. The excess liquid is then driven from the reservoir into the normal evaporator section thus blocking the vapor flow and inactivating that section for heat rejection. Thus, the heat source is insulated from the hot condenser end with the result that the heat piping action is only effective in the forward mode.

3. Liquid Flow Control

Liquid flow control involves either interrupting or impeding the condensate return in the wick in order to "dry-out" part or all of the evaporator. This technique achieves control of the evaporator conductance by affecting the

circulation of the working fluid and therein creating a hydrodynamic failure in the evaporator section.

Liquid flow control is limited generally to providing "on - off" control for diodes and thermal switches when the heat source is a dissipative one since the hydrodynamic failure will result in a non-uniform temperature distribution at the heat source. However, for fixed temperature sources, continuous modulation of the heat pipe conductance by varying the wick flow resistance is acceptable since partial evaporator dryout simply results in reduced heat transfer into the pipe.

Fig. 3-4a shows a liquid trap diode heat pipe for aerospace application. In this case, a wicked reservoir is located at the evaporator end. This reservoir does not communicate with the main wick; therefore, when the temperature gradient is reversed,liquid evaporates at the hot side of the pipe and then condenses and is trapped within the reservoir. As a result, the wick becomes partially saturated and ultimately the condensate cannot return to the heat input section and the heat piping action is effectively shut "off."

A gravity operated diode heat pipe is shown in Fig. 3-4b. Here a reversal of the temperature gradient causes the liquid to collect at the bottom of the pipe where it cannot be pumped back up against the gravitational force.

4. Vapor Flow Control

Vapor flow control involves throttling or interrupting the vapor as it proceeds from the evaporator to the condenser. This creates a pressure drop between the two sections and hence a corresponding temperature drop. A schematic of a vapor modulated variable conductance heat pipe is given in Fig. 3-5a. A bellows and auxiliary fluid are used to effect the throttling action. An increase in heat load or source temperature causes a rise in the vapor temperature which in turn causes the control fluid to expand and partially close the throttling valve therein creating a pressure differential. This method of control is substantially limited by the fact that the evaporator to condenser pressure differential must not exceed the capillary

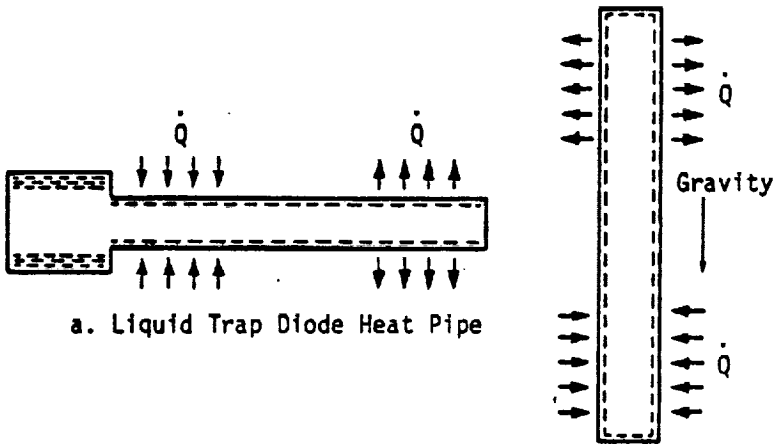

a. Liquid Trap Diode Heat Pipe

b. Gravity Operated Diode Heat Pipe

Fig. 3-4. Schematics of liquid-flow modulated heat pipes

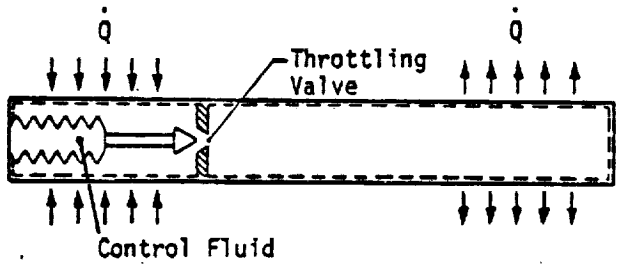

a. Vapor Modulated Thermal Conductance

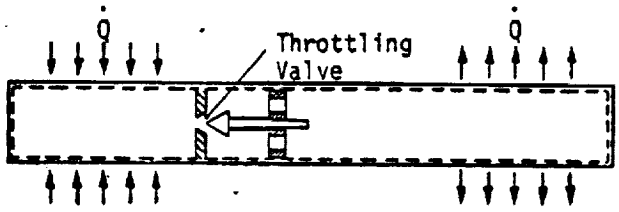

b. Vapor Modulated Thermal Diode

Fig. 3-5. Schematics of vapor-flow modulated heat pipes

pressure developed by the fluid/wick combination. If the valve arrangement is reversed to that shown in Fig. 3-5b, a diode action is achieved when conditions arise which reverse the normal temperature gradient.

3.2 VARIABLE CONDUCTANCE WITH GAS-LOADED HEAT PIPES

The principle of this technique is the formation of a gas plug at the condenser end of the pipe which prevents vapor from condensing in the part blocked by the gas. This plug is the result of introducing a fixed amount of a non-condensible gas into the heat pipe. In the absence of circulation of the working fluid (i.e., without heat transport) the gas is uniformly distributed within the vapor space except for a small amount which is dissolved in the liquid phase of the working fluid. During operation a steady flow of vapor exists from the evaporator to the condenser. The gas is swept by the vapor to the condenser. Unlike the vapor, it does not condense but forms a "plug" at the condenser end of the heat pipe.

Variable conductance variation through the addition of a non-condensible gas is particularly attractive because it accomplishes passive control of the vapor temperature. In a conventional (fixed conductance) heat pipe, the vapor temperature adjusts itself in order to meet the heat rejection requirements for a given sink condition. Thus, if the heat load and/or sink temperature increases, the vapor temperature will also rise. In a gas-loaded heat pipe, the fixed amount of gas occupies part of the condenser; the length of the gas plug being dependent on the vapor (and sink) temperature. If the heat load is increased, the vapor temperature tends to rise as in the fixed conductance heat pipe. However, the corresponding increase in vapor pressure of the working fluid compresses the gas plug, thereby increasing the size of the active condenser. This results in a higher conductance which effectively opposes the tendency of the vapor temperature to increase. Similarly, if the heat source and/or sink temperature decreases, the vapor temperature and pressure tend to drop which permits the gas plug to expand, the conductance of the heat pipe to decrease, and the vapor temperature decreases to be minimized. A gas-loaded heat pipe therefore reduces fluctuations of the operating temperature and behaves as a self-controlled VCHP.

3.2.1 Flat-Front Theory

A simplified model of a gas-loaded heat pipe whose condenser is partially blocked is shown in Fig. 3-6. The corresponding gas and vapor distributions that apply during operation are also presented. As indicated in this figure, the interface between the gas and vapor is not a sharp one because it is controlled by mass diffusion and axial conduction effects which are discussed in a later section. However, a good understanding of the operational characteristics, and certainly preliminary designs,can be obtained by utilizing a mathematical model which assumes that a "flat-front" exists between the vapor and gas. The following assumptions are employed with this model:

(1) Steady state conditions exist.

(2) The interface between the active and shut-off portions of the pipe is very sharp.

(3) The total pressure is uniform throughout the pipe (i.e. the vapor temperature drop is negligible).

(4) Axial conduction can be neglected.

(5) The gas-vapor mixture obeys the Ideal Gas Law.

In addition, if the heat transfer to the environment can be expressed in terms of a heat transfer coefficient h_c, the condenser conductance is proportional to the active condenser length $L_{c,a}$ and is defined as

$$C_c = (h\,P)_c\, L_{c,a} \tag{3-2}$$

These assumptions and the following Eqs. completely describe the operation of a gas-loaded heat pipe.

(A) Conservation of Mass

$$m_g = m_{g,i} + m_{g,r} \tag{3-3}$$

(B) Law of Additive Partial Pressures

$$\left.\begin{aligned} p_v &= p_{v,i} + p_{g,i} \quad \text{(inactive condenser)} \\ p_v &= p_{v,r} + p_{g,r} \quad \text{(reservoir)} \end{aligned}\right\} \tag{3-4}$$

(c) Ideal Gas Equation of State

$$(pV)_g = (mRT)_g \tag{3-5}$$

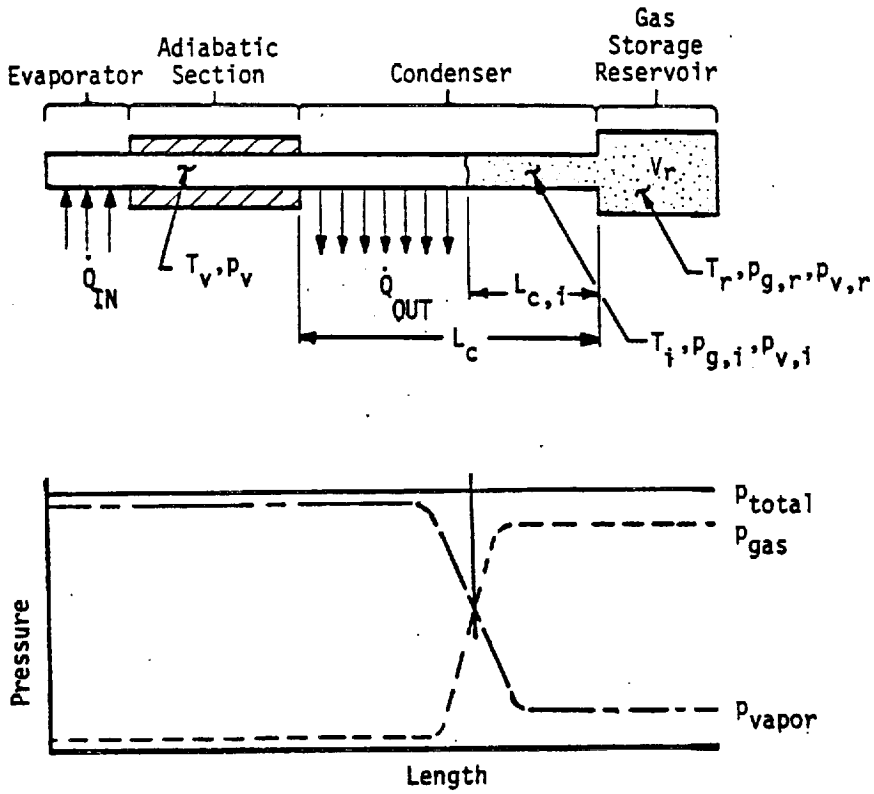

Fig. 3-6. Distribution of gas and vapor in a gas controlled VCHP

The reservoir size and gas load are determined by the following two extremes of operation:

(a) Maximum Condition -- Maximum heat load at the highest sink temperature.

Optimum operation of the heat pipe under this condition will have the heat pipe's condenser fully "open." Thus the maximum condition determines the reservoir size required to contain the non-condensible gas. Eqs. 3-4 and 3-5 can be solved to give

$$V_r = (m\,R)_g \left[\frac{P_v - P_{v,r}}{T_r}\right]^{-1}_{max} \tag{3-6}$$

(b) Minimum Condition -- Minimum heat load at the lowest sink temperature.

Operation at the minimum condition requires that part or all of the heat pipe's condenser and adiabatic sections be "shut-off" consistent with the temperature control requirements. Hence, the gas load must be sufficient to block that portion of the pipe required to satisfy the minimum condition. The solution of Eqs. 3-3 thru 3-5 gives

$$m_g = \left[\frac{p_v - p_{v,o}}{R_g T_o}\right]_{min} V_{v,im} + \left[\frac{p_v - p_{v,r}}{R_g T_r}\right]_{min} V_r \qquad (3\text{-}7)$$

where $V_{v,im}$ is defined as the volume of the vapor space in the inactive part of the heat pipe at the minimum condition.

The following two terms are defined for the purpose of simplifying these Eqs:

$$\Psi_o \equiv \frac{p_v - p_{v,o}}{T_o} \; ; \quad \Psi_r \equiv \frac{p_v - p_{v,r}}{T_r} \qquad (3\text{-}8)$$

The storage volume and gas charge required for any gas-controlled heat pipe can now be determined by the simultaneous solution of Eqs. 3-6 and 3-7 as

$$\frac{V_r}{V_{v,im}} = \frac{\Psi_{o,min}}{\Psi_{r,max} - \Psi_{r,min}} \qquad (3\text{-}9)$$

$$(m\,R)_g = V_r\,\Psi_{r,max} \qquad (3\text{-}10)$$

These equations apply, in general, to gas-controlled heat pipes. Before proceeding to their application to the various types of gas-controlled heat pipes, it is important to understand how they relate to temperature control.

The most important parameter in a thermal control system is the temperature control required (i.e., control sensitivity). This parameter is essentially the allowable variation in heat source temperature (ΔT_s). Once the required heat source temperature control has been defined, the corresponding maximum and minimum heat pipe vapor temperatures are determined from:

$$T_v = T_s - R_s \dot{Q} \qquad (3\text{-}11)$$

For a constant resistance R_s between the heat source and heat pipe, Eq. 3-11 defines the allowable variations of T_v for variations in T_s and $\dot{Q}$.

The vapor pressure ($p_{v,max}$ and $p_{v,min}$) corresponding to the required vapor temperature limits are then determined from saturation conditions for the working fluid. Thus, while the temperature control required does not appear explicitly in the equations defining the storage requirements, it does enter implicitly through the heat pipe vapor pressures.

One final comment which applies to the design of gas-controlled heat pipes is that the tighter the control required, the larger the reservoir size. For a specific type of VCHP and fixed reservoir end conditions, as $p_{v,min}$ approaches $p_{v,max}$ ($\Psi_{r,min}$ approaches $\Psi_{r,max}$), the denominator of Eq. 3-9 decreases and the required storage volume increases. When the denominator becomes zero or negative, no further improvement in temperature control can be obtained with the type of VCHP being investigated.

Once the design has been established, the heat pipe's conductance or steady state operation for a given set of conditions can be determined from Eqs. 3-9 and 3-10 and the heat transfer requirement (Energy Eq.) which can be expressed as

$$\dot{Q} = (hP)_c \, L_{c,a} \, (T_v - T_o) \tag{3-12}$$

Since

$$L_{c,a} = L_c - L_{c,i} = L_c - \dot{V}_{v,i}/A_v \tag{3-13}$$

It follows that

$$\frac{L_{c,a}}{L_c} = \frac{\dot{Q}}{\dot{Q}_{max}} = 1 - \frac{V_r}{A_v L_c} \left[\frac{\Psi_{r,max} - \Psi_r}{\Psi_o} \right] \tag{3-14}$$

A thermal analysis of a system which utilizes a gas-loaded heat pipe requires the simultaneous solution of the Energy Equation and the heat pipe's Mass Balance. Hence, in order to locate the gas interface for a given heat load and sink condition, one must assume a vapor temperature and then verify that Eq. 3-14 is satisfied for the specified heat load or iterate accordingly and then calculate the active length.

3.2.2 Types of Gas-Loaded Heat Pipes

A variety of different types of gas-loaded heat pipes have been developed which can be divided into wicked and non-wicked reservoir systems.

3.2.2.1 Wicked Reservoir Systems

A reservoir wick is used to provide a return path for any liquid that collects in the reservoir either through diffusion and condensation of the vapor or through accidental spillage of the working fluid. The presence of a wick saturated with liquid establishes a saturation partial vapor pressure of the working fluid which is in equilibrium with the reservoir temperature.

The reservoir wick may be an extension of the heat pipe wick or it may be an entirely different type of wick. Since the reservoir wick generally only has to satisfy a minimal heat transport requirement, a very simple design such as multiple layers of screen attached to the reservoir wall is sufficient. At the maximum condition, the vapor in the reservoir reduces the volume available for gas storage. However, at the minimum condition, the saturated vapor reduces the amount of gas required to fill the reservoir and therefore reduces the storage requirements. Several conditions can be factored into the design which affect the reservoir temperature and therefore the control characteristics of the VCHP, and they are as follows.

(a) Cold Reservoir

The simplest variable conductance heat pipe is commonly referred to as a "cold reservoir" type. As shown in Fig. 3-7, its reservoir is in thermal equilibrium with the sink condition (i.e., $T_r = T_o$). The storage volume requirement for a cold reservoir system is:

$$\frac{V_r}{V_{v,im}} = \frac{\Psi_{o,min}}{\Psi_{o,max} - \Psi_{o,min}} \tag{3-15}$$

and its gas charge requirement is:

$$(mR)_g = V_r \ \Psi_{o,max} \tag{3-16}$$

The location of the gas front is given by:

$$\frac{L_{c,a}}{L_c} = 1 - \frac{V_r}{A_v L_c} \left[\frac{\Psi_{r,max} - \Psi_o}{\Psi_o}\right] \tag{3-17}$$

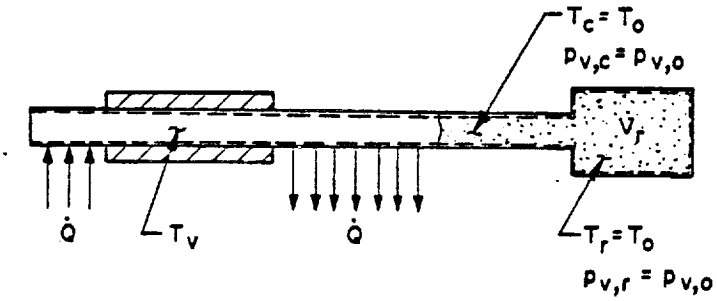

Fig. 3-7. Self-controlled VCHP with a wicked, uncontrolled reservoir

The "cold reservoir" VCHP is generally the easiest one to fabricate and integrate with another system and therefore the least expensive. However, because the reservoir has a wick and is in equilibrium with the sink temperature, its control capability is limited. In particular, unless relatively coarse temperature control is satisfactory, the cold reservoir type is suited for those applications where the maximum sink temperature is substantially less than the operating temperature and only moderate variations in heat source and sink temperature occur.

(b) Reservoir at Constant Temperature

A relatively simple extension of the cold reservoir system is one in which the reservoir is interfaced with some other component, structural member, etc., whose temperature is relatively insensitive to variations in the sink condition (i.e., T_r = constant). This system is capable of far greater control than an equivalent cold reservoir type. Its storage volume requirement can be determined from:

$$\frac{V_r}{V_{v,im}} = \frac{\Psi_{o,min}}{\Psi_{r,max} - \Psi_{r,min}} \tag{3-18}$$

and its gas charge requirement is:

$$(mR)_g = V_r \ \Psi_{r,max} \tag{3-19}$$

The location of the interface is given by Eq. 3-14, i.e.

$$\frac{L_{c,a}}{L_c} = \frac{\dot{Q}}{\dot{Q}_{max}} = 1 - \frac{V_r}{A_v L_c}\left[\frac{\Psi_{r,max} - \Psi_r}{\Psi_o}\right]$$

A VCHP with a temperature controlled, wicked reservoir is far less sensitive to variations in the sink temperature than one whose reservoir is coupled to the sink temperature. Conversely, for a specified control sensitivity and sink temperature range, the VCHP with a temperature controlled reservoir will require a much smaller reservoir size. The only restriction with a controlled reservoir system is that the reservoir temperature must be less than the minimum vapor temperature.

When passive methods cannot be used to maintain the reservoir at a constant temperature, a reservoir heater can be employed. This is a type of active control wherein a feedback controller is used to regulate a reservoir heater such that the reservoir temperature is kept constant under varying sink conditions. Minimum heater power requirements result if the reservoir is maintained at a temperature just slightly above the maximum sink temperature. The equations defining the storage requirements are identical to those for the passive system; however, when active control is utilized it is generally better to control the source temperature rather than the reservoir.

(c) Feedback VCHP

Each of the preceeding systems requires an infinite storage volume in order to provide absolute control of the heat pipe temperature (i.e., $\Delta T_v = 0$). Even if nearly absolute control of the vapor temperature could be obtained practically, this would not guarantee that the heat source temperature (which is really the parameter of interest) would be maintained constant. As indicated by Eq. 3-11, there is always a finite thermal impedance between the heat source and the heat pipe vapor temperature. Consequently, even though the vapor temperature is kept constant, unacceptable heat source temperature fluctuations could result from variations in the heat load.

Under these circumstances, or when the desired control cannot be obtained with practical reservoir sizes, an active feedback system can be employed. In the feedback system, the vapor temperature decreases with increasing heat load or vice versa, thereby permitting absolute control (i.e., $\Delta T_s = 0$, $\Delta T_v = - R_s \Delta \dot{Q}$) of the heat source. The active feedback system is essentially the same as the heated reservoir system discussed previously, except that, instead of monitoring reservoir temperature and maintaining it constant, a controller senses the heat source temperature and regulates the reservoir temperature to derive the desired control.

In order to minimize the reservoir size, the auxiliary heater should keep the reservoir near the vapor temperature at the condition of minimum heat load and lowest sink temperature. This results in larger power requirements for the feedback system than for the heated reservoir type. However, the auxiliary power required is relatively small; its magnitude being associated primarily with the transient requirements (2). At the condition of maximum heat load and highest sink temperature, in order to achieve full utilization of the reservoir for gas storage, the reservoir temperature should approach the sink temperature. Thus, in the feedback system the reservoir temperature will vary between the maximum sink temperature and the minimum conditions. The storage requirements for a feedback system are defined by the general Eqs. 3-9 and 3-10. For the optimum steady-state case where $T_{r,min} = T_{v,min}$ and $T_{r,max} = T_{o,max}$,

$$\frac{V_r}{V_{v,im}} = \frac{\Psi_{o,min}}{\Psi_{o,max}} \tag{3-20}$$

and its gas charge requirement is:

$$(mR)_g = V_r \Psi_{o,max} \tag{3-21}$$

Again the location of the interface is determined from Eq.(3-14), i.e.

$$\frac{L_{c,a}}{L_c} = \frac{\dot{Q}}{\dot{Q}_{max}} = 1 - \frac{V_r}{A_v L_c}\left[\frac{\Psi_{r,max} - \Psi_r}{\Psi_o}\right]$$

However, with a feedback system the desired temperature control is specified and therefore the required vapor temperature is known. The location of the interface and the variable conductance operation will in this case consist of determining the reservoir temperature that is needed to give the required conductance. The following analysis applies:

(1) Solve the vapor temperature required to satisfy the specified conditions from Eq. 3-11.

$$T_v = T_s - R_s \dot{Q}$$

(2) Solve for the corresponding conductance or interface location using Eq. 3-12.

$$L_{c,a} = \dot{Q}/(h\,P)_c\,(T_v - T_o) \qquad (3\text{-}22)$$

(3) Use Eq. 3-14 to determine the reservoir temperature that will give the required interface location.

3.2.2.2 Non-Wicked Reservoirs

One other type of gas-controlled heat pipe is a system which utilizes a non-wicked reservoir. As shown in Fig. 3-8, the reservoir is thermally coupled to the evaporator or heat source. This is done to prevent liquid from condensing in the reservoir and not being able to return because there is no capillary interconnection. The reservoir is non-wicked to avoid saturation conditions at temperatures equal to or greater than the heat pipe vapor temperature. Saturation conditions would, of course, prevent gas storage in the reservoir. Because there is no interconnection between the heat pipe wick and the reservoir, any fluid from the heat pipe that is accumulated in the reservoir, due to spillage or diffusion, must diffuse back out during start-up. This can result in relatively long start-up times (e.g., several hours) for this type of system.

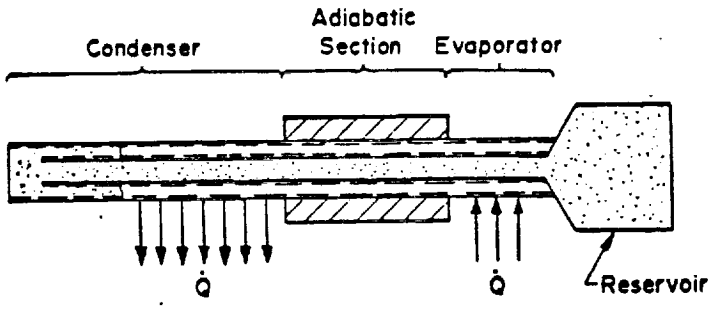

Fig. 3-8. VCHP with reservoir thermally coupled to the evaporator

Under normal operating conditions, vaporized working fluid which has diffused from the condenser will exist within the reservoir. As Marcus (3) points out, the partial pressure of this vapor will not correspond to the reservoir temperature but to the temperature at the mouth of the reservoir where the wick ends. Generally, a feeder tube which is in equilibrium with the sink condition is employed between the reservoir and the condenser section. Consequently, under the assumptions of the flat front model, the partial pressure of vapor in the reservoir corresponds to the sink temperature, i.e.

$$p_{v,r} = p_{v,o} \tag{3-23}$$

The storage volume requirement for a "hot reservoir" system is therefore:

$$\frac{V_r}{V_{v,im}} = \frac{\Psi_{o,min}}{\left[\frac{T_o}{T_r}\,\Psi_o\right]_{max} - \left[\frac{T_o}{T_r}\,\Psi_o\right]_{min}} \tag{3-24}$$

and the gas charge requirement is:

$$(mR)_g = V_r\left(\frac{T_o}{T_r}\,\Psi_o\right)_{max} \tag{3-25}$$

where the reservoir temperature is equal to the heat source or heat pipe evaporator temperature. Hence, the basic improvement that is realized when compared to a wicked "cold" reservoir system is that derived from compression of the gas within the reservoir.

The location of the interface is obtained from:

$$\frac{L_{c,a}}{L_c} = 1 - \frac{V_r}{A_v L_c} \frac{\left(\frac{T_o}{T_r}\psi_o\right)_{max} - \frac{T_o}{T_r}\psi_o}{\psi_o} \qquad (3\text{-}26)$$

3.2.3 Diffusion Effects

The theory of gas loaded VCHP's presented in the preceeding sections is based on a sharp interface (flat front model) between active and inactive portions of the condenser. An ideal distribution does not exist in reality. The actual "front" is controlled by diffusion within the gas-vapor interface and by axial conduction in the wall. A typical diffuse front is shown in Fig. 3-9. It is seen that the "average" temperature in the inactive part of the condenser is somewhat higher than the sink temperature and that the average partial vapor pressure is higher than that corresponding to the sink temperature. This causes the temperature set point of the VCHP to be higher than predicted by "flat front" theory for the particular gas inventory.

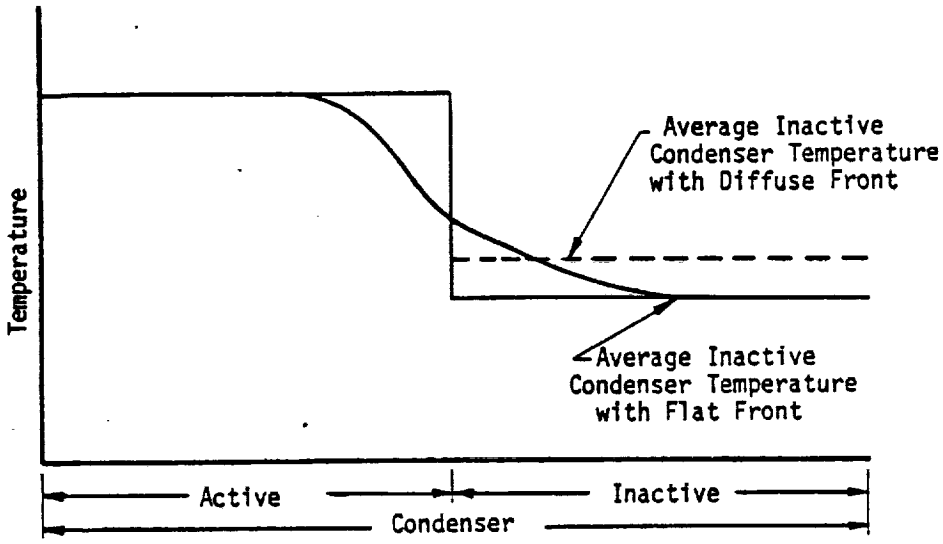

Fig. 3-9. Temperature distribution in the condenser for flat front and diffuse front models

In non-wicked reservoir heat pipes, this effect can be quite pronounced. The partial vapor pressure in a non-wicked reservoir is theoretically equal to the partial pressure in the inactive condenser section. If the interface moves close to the end of the condenser ($C_c \sim (C_c)_{max}$), the tail of the diffuse front may extend into the reservoir and raise the vapor pressure in the reservoir. The deviation from prediction using the flat front model is more pronounced in a non-wicked reservoir heat pipe since the effects of increased partial vapor pressure involve the entire reservoir. Marcus (3) conducted experiments to test the flat front theory. He instrumented a VCHP with an internal non-wicked reservoir to measure the actual temperature profiles. Using a theoretical approach, similar to the one presented in Section 3.2.1, he computed the vapor temperature as a function of active condenser length. In order to account for the diffuse temperature distribution he integrated the molar gas density along the inactive condenser section using the actually measured temperatures. The agreement between theory and experiment is very good, indicating that the flat front model does predict the control capability of the pipe accurately provided that appropriate average temperature for the inactive portion of the condenser and the reservoir are used.

A complete model of the diffuse interface in a gas-loaded heat pipe must include: (1) heat transfer between the condenser and environment; (2) axial conduction in the walls, wicks, and fins; (3) binary mass diffusion between the vapor and gas; and (4) radial wick resistance. The theory of a diffuse gas front is rather complicated and is not included. A detailed model as well as the method of solution and numerical results are given by Marcus (3).

3.2.3.1 Numerical Analysis of Diffuse Vapor Gas Front

Marcus (3) reports the results of a parametric study which evaluates the effect of wall conductivity, working fluid, and operating temperature on the vapor-gas interface. The results can be summarized as follows:

(1) Axial conduction in the pipe wall plays a substantial role in defining the vapor-gas interface. Typical temperature profiles along the condenser are shown in Fig. 3-10. One clearly sees that wall conductance tends to spread the front over the condenser.

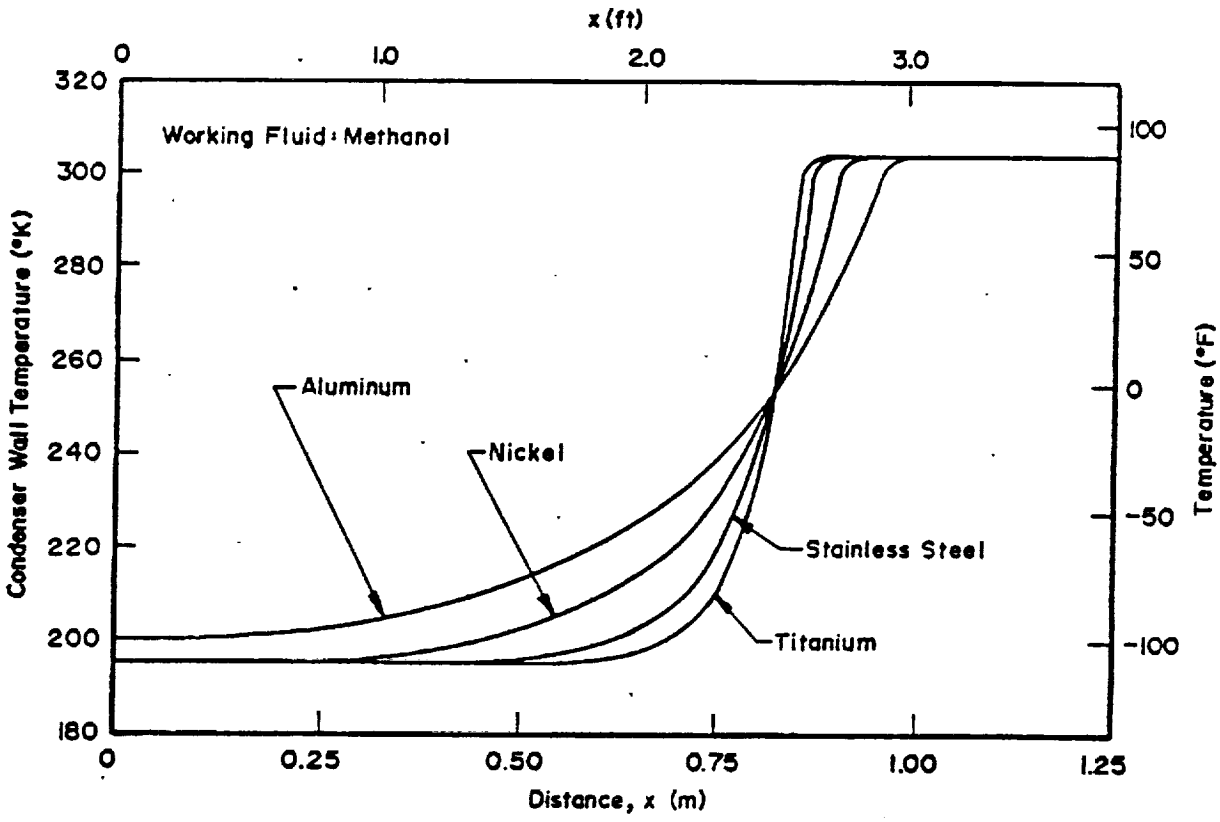

Fig. 3-10. Effect of axial wall conduction on the condenser temperature profile

(2) The effect of working fluid on the temperature profiles is insignificant (Fig. 3-11). This suggests that heat transport by mass diffusion is minimal and that axial conduction dominates.

(3) The operating temperature does not significantly alter the profile of the vapor-gas interface. Typical effects are shown in Fig. 3-12.

The above results are typical for heat pipes for spacecraft temperature control. There is no reason to believe that other gas controlled heat pipes would not exhibit the same qualitative behavior.

One important conclusion can be drawn from this study. Since heat transport by mass diffusion appears to be insignificant when compared to axial conduction, the temperature profile in the vicinity of the interface is determined to a first approximation by

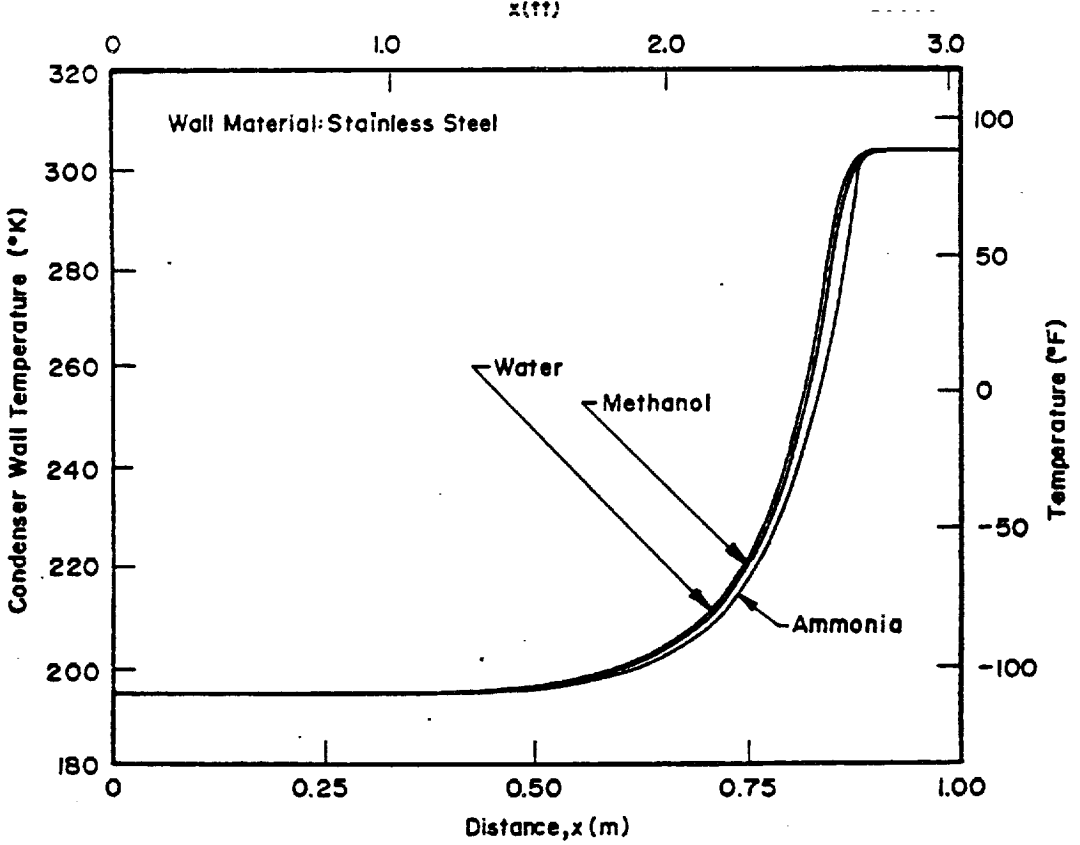

Fig. 3-11. Effect of working fluid on the condenser temperature profile

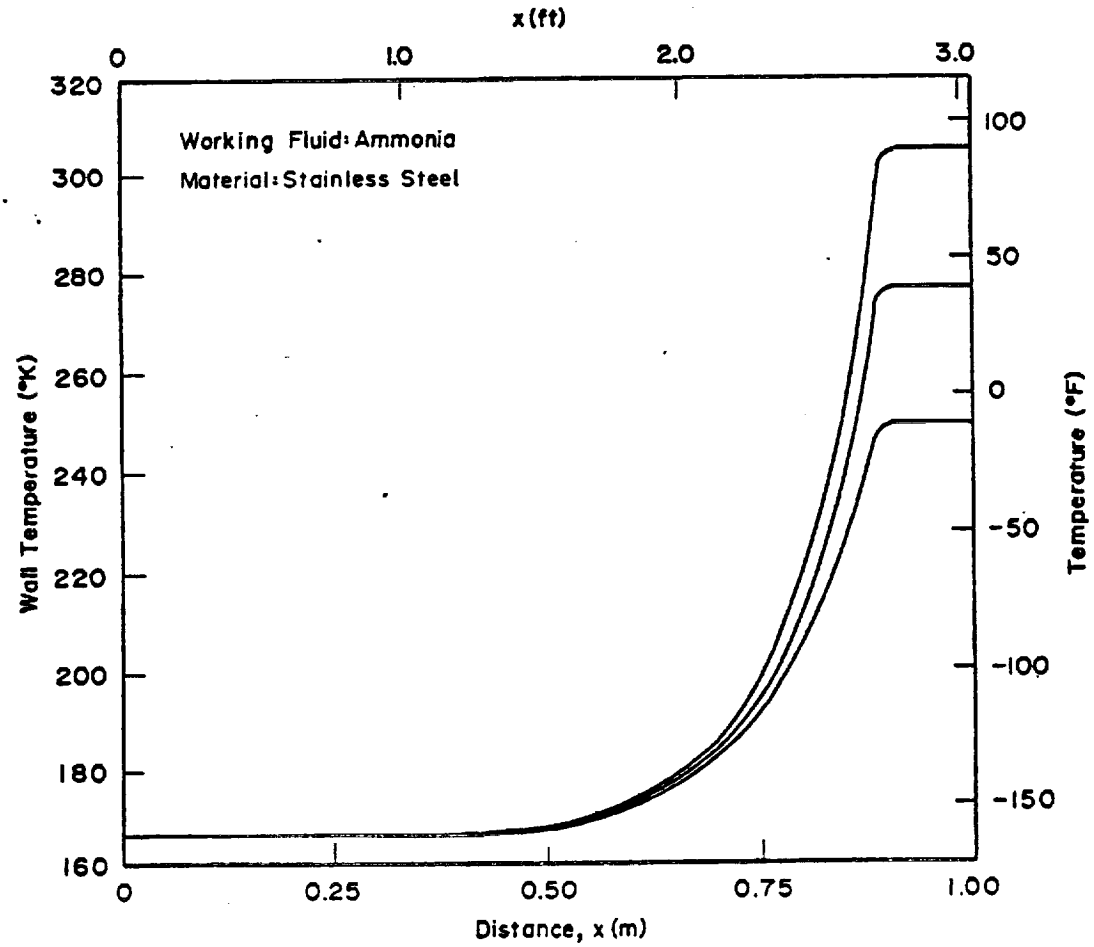

Fig. 3-12. Effect of operating temperature on the condenser temperature profile

conduction and by heat transfer to the environment. Thus, a conventional "fin" equation (4) will, in most cases, adequately describe the temperature profile along the heat pipe.

The flat front model predicts the conductance of the heat pipe satisfactorily if a realistic temperature profile is used to calculate the effective condenser temperature. Treating the inactive portions of the condenser as a fin provides an excellent approximation of the temperature profile and represents a first order refinement to the flat front model.

The detailed numerical analysis that is available with the "Gas Pipe" Program (5) provides information which cannot be obtained using the simple closed-form solution. An important example of this is the determination of the freeze-out rate of the working fluid which will occur when conditions exist which will cause the condenser and/or reservoir temperature to drop below the fluid's melting point. When this occurs a finite amount of vapor will continuously diffuse into that region and freeze there.

3.2.4 Gas Absorption Reservoir

One of the more recent innovations for improving the design of a gas-controlled heat pipe consists of replacing the gas storage volume with a much smaller gas absorption reservoir (6). For a number of gas/fluid combinations, it can be shown that it is volumetrically more efficient to store gas as a dissolved solute than dispersed as a gas in a vapor reservoir. The absorption reservoir consists of a wick matrix which supports the liquid in a 1-g environment. Under conditions of vapor-liquid equilibrium, the concentrations of non-condensible gas in the two phases are related by:

$$C_{g\ell} = \alpha\, C_{gv} \qquad (3\text{-}27)$$

where:

$C_{g\ell}$ = Molar gas density in the liquid phase

C_{gv} = Molar gas density in the vapor phase

The factor α is the Ostwald coefficient and is a constant for dilute solutions. Hence, the larger the Ostwald coefficient, the greater the amount of gas absorption into the liquid phase versus the vapor phase. In addition to requiring values of α which are greater than one, efficient storage volumes are realized when the volume of the liquid in the condenser is small. This is generally the case with aerospace heat pipes. If "flat-front" theory is

used, it follows that the volume required for a gas absorption reservoir in a general gas controlled application (e.g., Eq. 3-9) is given by:

$$\frac{V_{r,ga}}{V_{v,im}} = \frac{\Psi_{o,min}}{\Psi_{r,max} - \Psi_{r,min}} \quad \frac{\theta_c}{\theta_r} \tag{3-28}$$

where:

$$\theta_c = 1 + \beta_c (\alpha\eta_c - 1) \quad \text{and} \quad \theta_r = 1 + \beta_r (\alpha\eta_r - 1) \tag{3-29}$$

with

β_c = Fraction of condenser filled with wick/fluid composite

β_r = Fraction of reservoir filled with wick/fluid composite

η_c = Fraction of wick/fluid composite filled with liquid in the condenser

η_r = Fraction of wick/fluid composite filled with liquid in the reservoir

The void fractions η_c and η_r are generally equal to the porosity (ε) of the condenser and reservoir wick structures.

A comparison of Eq. 3-28 with Eq. 3-9 shows that the savings to be realized with a gas absorption reservoir are:

$$\frac{V_{r,ga}}{V_r} = \frac{\theta_c}{\theta_r} \tag{3-30}$$

In general the most efficient gas storage will be obtained with liquid-gas combinations which have large values for their Ostwald coefficient. Reservoir size reductions on the order of 1/5 to 1/10 can be realized with values of 10 to 20 for α. Unfortunately, such combinations are possible but common control gases do not satisfy this criterion. Table 3-1 lists several room temperature liquid-gas combinations which have high solubility.

3.2.5 Transients with Gas-Controlled Heat Pipes

The performance of heat pipes during transients is still only partially understood. This is particularly true for variable conductance heat pipes which represent control elements within a thermal system. A detailed discussion of transient behavior is beyond the scope of this Manual but a summary of the salient points is presented.

TABLE 3-1. ROOM TEMPERATURE LIQUID-GAS COMBINATIONS HAVING HIGH SOLUBILITY

Solvent	Solute	Temperature (°C)	Ostwald Coefficient
Hexane	n-Propane	25	23.6
Benzene	n-Propane	25	16.0
Benzene	n-Pentane	16	312.0
Methanol	Propane	25	3.4
Methanol	Carbon Dioxide	12	4.1
Methanol	Butane	12	28.0
Methanol	Sulfur Dioxide	25	83.0
Methanol	Carbon Dioxide	59	39.0
Water	Ammonia	25	40.7
Water	Sulfur Dioxide	25	34.0
Water	Methanol	100	254.0

The transient performance of fixed conductance heat pipes has been discussed by several investigators in Refs. 7 through 12. Most of this work has been concerned with the start-up dynamics of liquid-metal heat pipes whose working fluid is frozen (i.e., solid) at room temperature conditions. The presence of a non-condensing gas which reduces the transport length tends to alleviate start-up conditions associated with the low transport capability of working fluids when they are at low vapor pressures. Reference 12 treats the start-up of cryogenic heat pipes whose working fluids are supercritical at room temperature. In this case,since any non-condensible gas that might be present in the pipe is greatly compressed, its effect on start-up will be negligible.

Transient discussions of the various types of gas-loaded heat pipes can be divided into three groups--wicked reservoir, non-wicked reservoir, and feedback controlled pipes.

3.2.5.1 Wicked Reservoir Heat Pipes

The partial pressure of the vapor everywhere in a wicked reservoir heat pipe is in equilibrium with the local wick temperature. Diffusion effects may be neglected except for establishing the vapor-gas interface. The transient behavior of wicked reservoir gas-loaded pipes can therefore be adequately described by considering the sensible heat

capacities of the various heat pipe elements and the conductance between them. The position of the vapor-gas interface is assumed to be in equilibrium at all times with the pressure and temperature distributions. Consequently, transient behavior can be predicted using ordinary thermal modeling techniques.

3.2.5.2 Non-Wicked Reservoir Heat Pipes

In a non-wicked reservoir, the partial vapor pressure in the reservoir is established by diffusion. The length of the diffusion path between the nearest point of saturation, i.e., the end of the condenser and the reservoir, may be long and diffusion rates often dominate the transient response. Although the transient behavior of non-wicked reservoir heat pipes is by no means fully developed, successful correlation of the "hot" reservoir heat pipe flown in the Ames Heat Pipe Experiment (AHPE) has been obtained (13).

Another phenomenon which is peculiar to non-wicked reservoir heat pipes is the mechanism for removal of liquid working fluid from the reservoir. Ordinarily, the non-wicked reservoir contains only non-condensing gas and some working fluid vapor. Liquid may accidentally be spilled into the reservoir, as for example either as a result of handling or as a result of vibrations during launch. If the spillage occurs during handling, the bulk of the liquid can usually be removed by proper orientation. If this happens during launch and is then immediately followed by a 0-g environment, no such removal mechanism exists. In either case, some liquid will remain in the reservoir. Under these conditions, when the heat pipe is started-up, the vapor pressure in the reservoir will correspond to the saturation pressure of the liquid at the reservoir rather than the condenser temperature. Since the reservoir temperature is always higher than the condenser temperature, some of the gas will be forced out of the reservoir and the heat pipe's set point will be changed. In the extreme case, corresponding to a reservoir temperature equal to the evaporator temperature, all of the gas will be forced out. Since the reservoir volume normally exceeds the condenser volume, the latter will be completely blocked and serious overheating of the heat source may result. These abnormal conditions will prevail until the liquid is evaporated from the reservoir and recaptured by the wick.

3.2.5.3 Feedback Controlled Gas-Loaded Heat Pipes

Feedback systems exhibit a rather complex transient behavior. These systems contain all the elements of a typical control loop and are subject to the same performance characteristics. Unlike other variable conductance heat pipes, feedback systems can possess unstable

regimes in which oscillations may occur. Thermal feedback systems are more stable than electrical feedback systems; however, their stability should be established for each application.

Closely related to stability is the existence of "overshoot" and "undershoot" of the control temperature. A typical response for a feedback controlled gas-loaded heat pipe, in which the source temperature is regulated, is shown in Fig. 3-13. Changes in the heat load and/or in the sink temperature cause the source temperature to temporarily deviate from the set point. As illustrated, the feedback system regains control and the set point is restored.

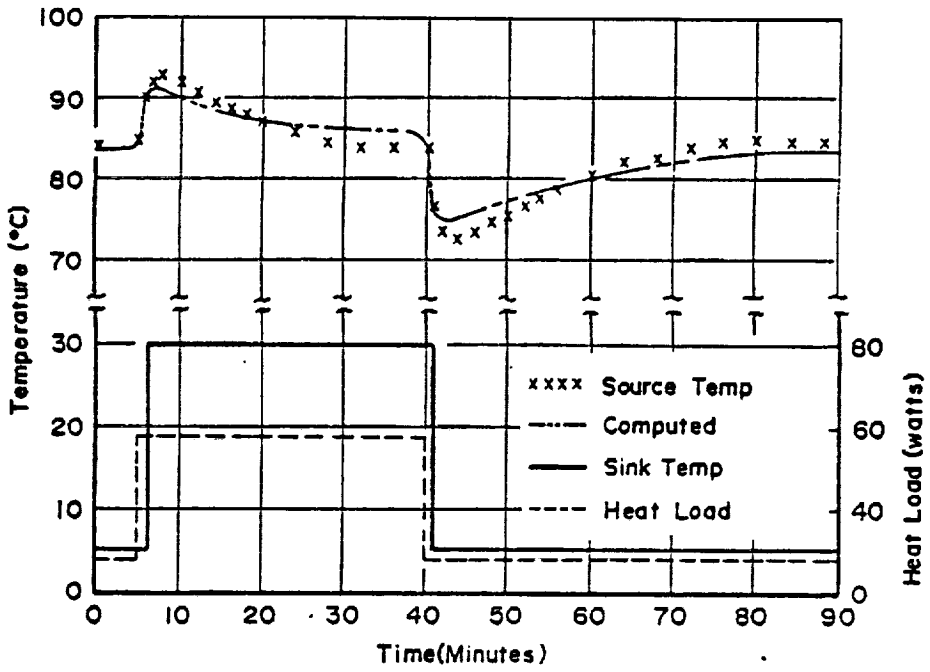

Fig. 3-13. Transient response of heat source with electrical feedback controlled heat pipe

A lumped parameter model of a heat pipe feedback loop is presented in Reference 2 which shows that the response of the heat source is controlled by the following two time constants:

$$\tau_r \equiv (m\ C_p\ R)_r$$

$$\tau_s \equiv (m\ C_p\ R)_s$$

where m_r and $C_{p,r}$ are the mass and the lumped specific heat of the reservoir, and m_s and $C_{p,s}$ are the mass and the lumped specific heat of the heat source. R_r is the thermal resistance between the reservoir and the sink, and R_s is the thermal resistance between the heat source and the heat pipe evaporator. The response time is minimized if the ratio τ_r/τ_s is small. Since the time constant of the heat source is frequently determined by the application, the only available alternative is to make τ_r as small as possible. The most desirable method of minimizing τ_r is to minimize the heat capacity m_r of the reservoir. By closely coupling (thermally) the reservoir to the sink (small R_r), a reduction in the reservoir time constant can be achieved but this is generally undesirable since it increases the auxiliary power required to maintain the reservoir at the selected temperature during steady state operation.

3.3 OTHER VARIABLE CONDUCTANCE HEAT PIPES

Most of the aerospace applications to date have utilized gas-loaded heat pipes for their thermal control requirements. However, demand for diode and switching operations is increasing, particularly for temperature control of low temperature and cryogenic detector systems (14). Although gas-loaded heat pipes can be adapted to accommodate these other thermal control functions, more efficient operation can be obtained passively by utilizing some of the other variable conductance techniques.

3.3.1 Excess Liquid Heat Pipe

This technique is closely related to non-condensing gas control. Variable conductance is achieved by inactivating part of the condenser by using an incompressible liquid. The most convenient

Fig. 3-14.

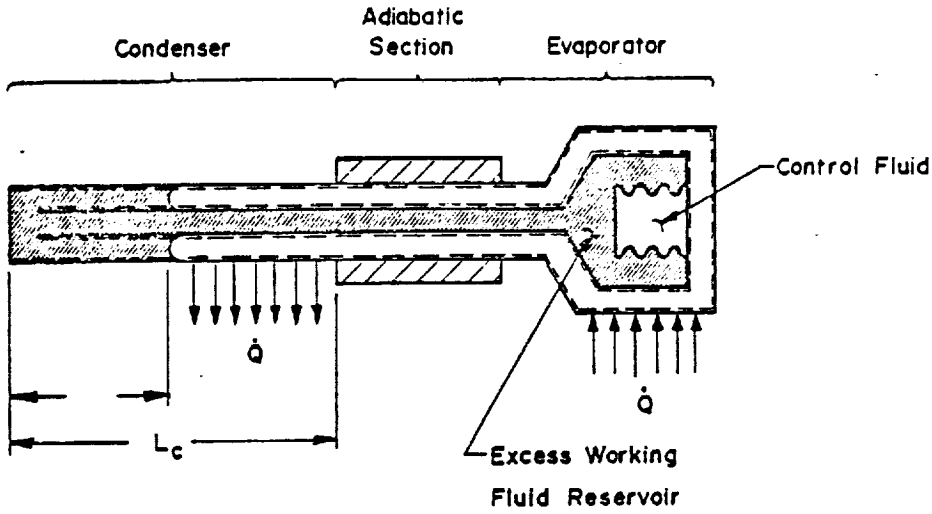

Fig. 3-14. Variable conductance through condenser flooding with liquid

Excess working fluid is contained in a reservoir which is located inside the heat pipe envelope. The effective volume of the reservoir is varied by means of a bellows which contains an auxiliary fluid in equilibrium with its vapor. Expansion of the bellows forces liquid working fluid out of the reservoir and into the condenser. This technique provides self-control of the source temperature; that is, increasing the heat source and/or the sink temperature causes the conductance to increase and this has the effect of minimizing the tendency for the source temperature to change.

The control characteristics can be developed using a model similar to the one in Section 3.2.1. Assuming that the fraction of the working fluid occupied by the wick and the vapor space is approximately constant (or negligible as in the case of the vapor), conservation of mass of the excess working fluid requires:

$$V_{ex} = V_r - V_b + A_v L_i \tag{3-31}$$

where V_r is the sum of the volumes of the reservoir and the capillary tube, V_b is the volume of the bellows containing the auxiliary control fluid, and V_{ex} is the volume of the excess fluid. Because the excess fluid is in the liquid state, conservation of mass corresponds to conservation of volumes. The volume occupied by the bellows (V_b) is related to the pressure difference between the working fluid and the auxiliary fluid through:

$$V_b = V_{bo} + \frac{A_b^2}{k}(p_a - p_v) \tag{3-32}$$

where V_{bo} is the equilibrium volume of the bellows, A_b is the bellows area, and k is the bellows spring rate.

Combining Eqs. 3-31 and 3-32 together with Eq. 3-12 yields the following expression for the active condenser length:

$$\frac{L_{c,a}}{L_c} = 1 - \frac{V_{ex} - V_r + V_{bo}}{A_v L_c} + \frac{A_b^2}{k A_v L_c} (p_v - p_a) \qquad (3\text{-}33)$$

Because of the incompressibility of the liquid, this system is less sensitive to changes in the sink temperature than gas-loaded heat pipes. Good control is achieved if:

(a) The cross-sectional area of the bellows is large

(b) The spring rate of the bellows is small

(c) The slope of the vapor pressure curve of the working fluid is larger than that of the auxiliary fluid

In addition to providing an insensitivity to changes in the sink temperature, temperature control using excess working fluid generally requires smaller storage reservoirs. Also, the interface between vapor and liquid is not subject to the diffusion effects. These system advantages must be weighed against some disadvantages. Gravity tends to cause the excess fluid to puddle in the condenser rather than form a well-defined interface as shown in Fig. 3-14. In addition, the sink temperature must always be above the freezing point of the working fluid because the inactive part of the condenser will be approximately at sink temperature and freezing would form a solid plug preventing any further control. Finally, sloshing of the excess fluid can be a problem, and containment of the excess fluid as well as the auxiliary fluid must be taken into account.

3.3.2 Liquid Flow Control

Liquid flow control represents probably the most viable technique for accomplishing diode and/or switching operations. Two basic methods exist: (1) the liquid trap which starves the heat pipe of its working fluid; and (2) liquid blockage which impedes the vapor flow and therefore the "heat-piping" action. A detailed summary of diode heat pipe technology is presented in Ref. 15. Significant aspects of the two techniques of liquid flow control are presented in the next sections.

3.3.2.1 Liquid Trap

The liquid trap technique is based on the tendency of liquid to accumulate at the coldest portion of the heat pipe, except as displaced by surface tension and gravity forces. The liquid trap is a reservoir provided at the evaporator end and is in good thermal contact with the evaporator to hold the liquid during and after reversal of the heat pipe operation. As shown in Fig. 3-15, the liquid trap contains a wick structure which does not communicate with the wick in the heat pipe.

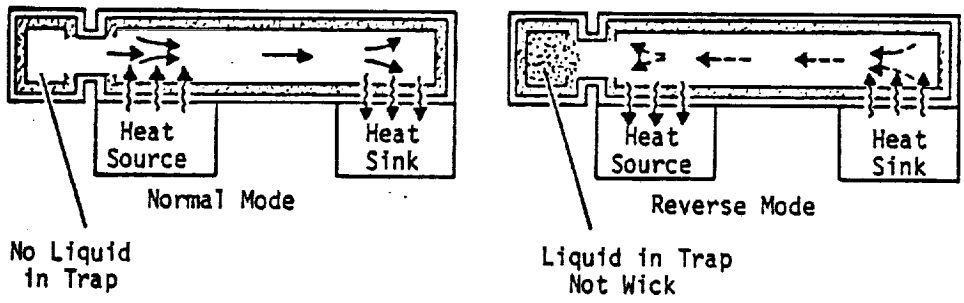

Fig. 3-15. Liquid trap diode operation

In the normal mode of operation the trap is dry. When the liquid trap end becomes the cold end of the heat pipe, condensation begins to occur within the trap, as well as in the evaporator end. As liquid accumulates in the trap, the heat pipe wick becomes underfilled causing a fairly rapid reduction in transport capability. The reduction in transport capability can be quite significant with only a few percent reduction of the liquid charge below 100% fill. This holds for both arterial wicks and axial grooves. For reduction of the transport capability to the order of less than 1% of the original value, however, it may be necessary to dry out the heat pipe wick completely, with all the liquid in the trap. Depending on the specific design the above phenomenon could also lead to a very rapid partial shutdown of the diode and a slower approach of the complete shutdown situation with minimum reverse heat flow. The trap volume should be sufficient to accommodate the entire fluid inventory of the heat pipe. Therefore, wicks having a small liquid volume are particularly attractive. The liquid trap technique combined with axially grooved wicks is an excellent combination and provides a simple and reliable design.

3.3.2.2 Liquid Blockage

The liquid blockage technique is dependent upon excess liquid shifting naturally from one end to the other as hot and cold ends are interchanged. Under reverse-mode operation, the excess liquid must have a volume sufficient to block the vapor space of the cold end and a large part of the transport section to minimize conduction heat transfer. As shown in Fig. 3-16, a reservoir is provided at the normal condenser end to obtain excess liquid under normal-mode conditions. The reservoir size must be slightly larger than the evaporator and transport section vapor space volumes, to allow for changes in liquid density with temperature. To keep the reservoir size small, the vapor space in the evaporator and adiabatic sections has to be kept small. This is automatically achieved with various arterial wicks. However, when axial grooves are intended to be used, an insert in the evaporator and at least part of the adiabatic section should be provided to reduce the vapor space. This, however, could cause a serious reduction in the forward-mode transport capability. Without an insert it would in general be impossible to hold a liquid plug in the vapor space against gravity during 1-g testing. Therefore, axial groove wicks cannot be used for the liquid blockage technique. The liquid blockage technique is most attractive for cryogenic applications where, under normal-mode operation, the evaporator is relatively short compared with the condenser and transport sections. This arrangement minimizes the excess liquid required for blockage.

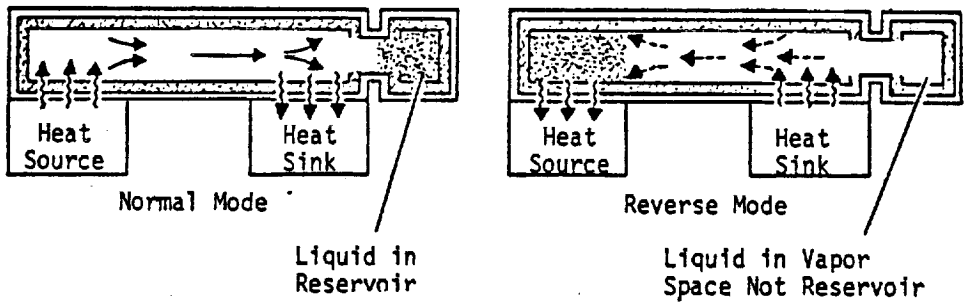

Fig. 3-16. Liquid blockage diode operation

The limitation of the liquid blockage technique is the ground testing requirement. In a gravity environment the vapor space in the blocked sections of the shutoff diode must hold the liquid. This means that the vapor space has to be small enough to insure that the respective capillary head, Δp, will support the gravity head of the liquid slug (Fig. 3-17). The condition for blockage of the vapor space in ground level testing can be derived to be:

$$\Delta p = \rho_\ell \, g \, D = \frac{2\sigma}{t_v} \tag{3-34}$$

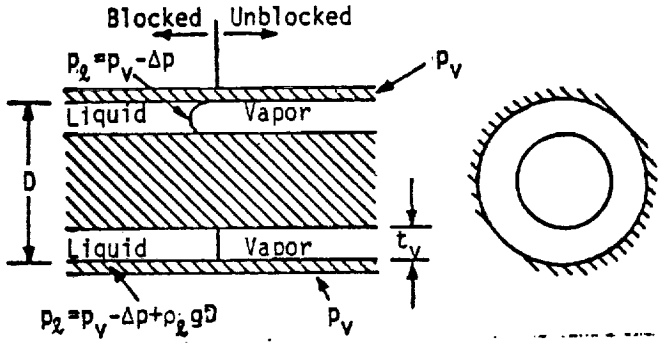

Fig. 3-17. Liquid blockage of vapor space (Ref. 16)

This requirement results in very narrow vapor spaces and consequently large vapor pressure drops during normal heat pipe operation. The heat pipe capacity is therefore limited and this type of diode is restricted to smaller heat transport applications, and the use of working fluids such as ammonia, which combine good capillary rise characteristics with small vapor losses.

One method for avoiding this problem that has been developed is referred to as a "blocking-orifice" design (16). This consists of inserting an orifice plate around the heat pipe wick at the point where blockage ends (e.g., Fig. 3-18). The opening in the orifice place is located at the bottom of the pipe as shown in Fig. 3-18. The orifice height may be greater or less than the annular vapor passage height, t_v. The use of large vapor passage areas more than compensates for the additional vapor pressure loss introduced by the orifice.

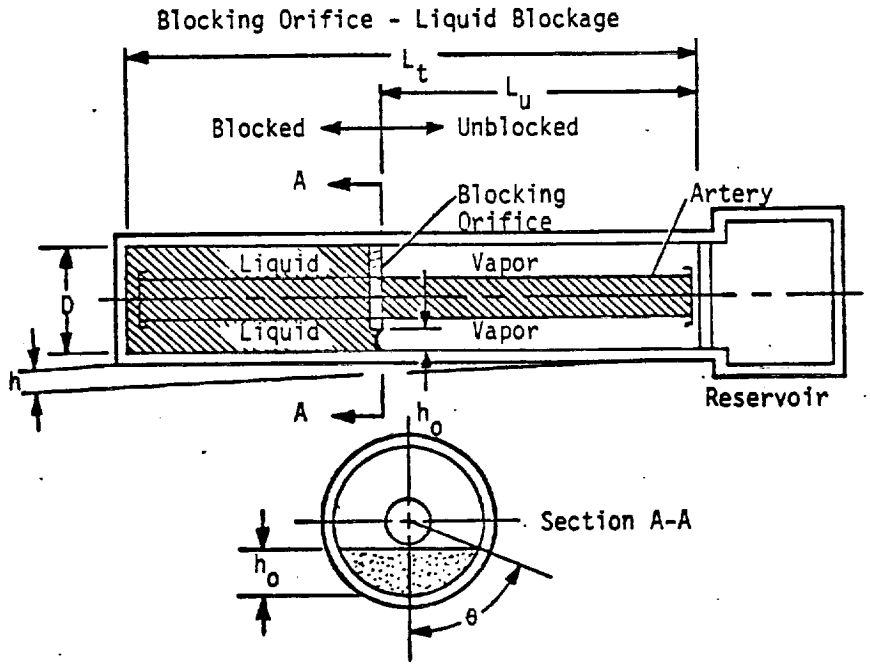

Fig. 3-18. Liquid blockage with a blocking orifice (Ref. 16)

If the pipe is tilted with the blocked end high, the equation for hydrostatic equilibrium for the design defined in Fig. 3-18 can be written as:

$$\rho_\ell \, g \, (h_o + \frac{hL_u}{L_t}) = \frac{2\sigma}{h_o} \qquad (3\text{-}35)$$

from which the maximum orifice height can be determined as:

$$h_o = 0.5 \left\{ \left[\left(\frac{hL_u}{L_t} \right)^2 + \frac{8\sigma}{\rho_\ell g} \right]^{.5} - \frac{hL_u}{L_t} \right\} \qquad (3\text{-}36)$$

3.3.3 Vapor Flow Control

The interruption of the vapor flow between the evaporator and condenser will result in a pressure difference in the vapor and, because of saturation conditions, a corresponding temperature difference. For a given axial heat flow rate, varying the temperature difference is equivalent to varying the heat pipe's conductance. The principle of this technique is shown schematically in Figs. 3-19 and 3-20. The vapor flow can be modulated by an external signal, e.g., the current of the electromagnet in Fig. 3-19, or the system can be self-controlled as shown in Fig. 3-20. (13).

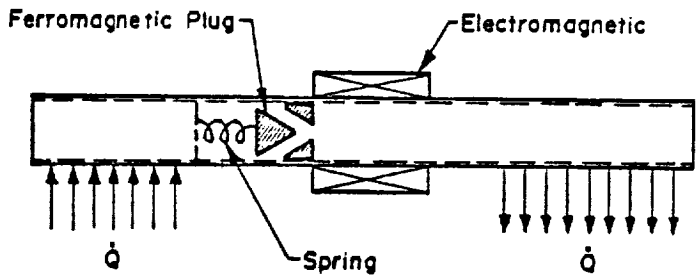

Fig. 3-19. Vapor flow control using external signal

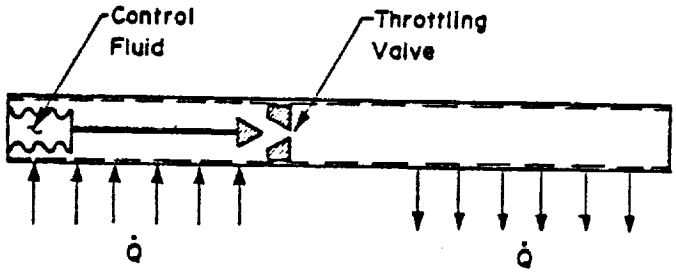

Fig. 3-20. Self-controlled vapor-modulated heat pipe

Vapor control represents a direct method of varying the axial conductance of the heat pipe. It does not, as with other techniques, render part of the condenser or evaporator ineffective. The entire evaporator and condenser are isothermal during all modes of operation since the pressure and temperature differential occurs across the throttle mechanism.

The obvious advantage is partially offset by the limited control range. The pressure difference created by the throttle must never exceed the capillary pressure of the wick. If the capillary pressure is exceeded, the vapor will "bubble" through the wick and around the throttle and the control capability will be lost. In a vapor flow-controlled heat pipe, the wick must be capable of providing sufficient capillary pressure to overcome the hydrodynamic losses and the pressure difference created for control purposes. From a hydrodynamic point of view, the wick must therefore be overdesigned.

The temperature difference which corresponds to a given pressure difference is obtained from the Clausius-Clapeyron equation (17).

$$\frac{\Delta T_v}{\Delta p_r} = \frac{T}{\lambda \rho_v} \tag{3-37}$$

In order to achieve large temperature differences (large variations of the conductance) with small pressure differences, the vapor density of the working fluid should be low. Vapor control is most effective if a fluid is selected which has a low vapor pressure at the operating temperature.

References

1. Brennan, P. J., and Groll, M., "Application of Axial Grooves to Cryogenic Variable Conductance Heat Pipe Technology," presented at 2nd International Heat Pipe Conference, April 1976.

2. Bienert, W. B., and Brennan, P. J., "Transient Performance of Electrical Feedback Controlled Variable Conductance Heat Pipes."

3. Marcus, B. D., "Theory and Design of Variable Conductance Heat Pipes," NASA CR-2018, April 1972.

4. Krieth, F., "Principles of Heat Transfer," International Textbook Company, Scranton, Pa., 1958.

5. Marcus, B. D., Fleishman, G. L., and Edwards, D. K., "User's Manual for the TRW GASPIPE 2 Program," NAS2-5503, October 1973.

6. Saaski, E. W., "Heat Pipe Temperature Control Utilizing a Soluble Gas Absorption Reservoir," NASA CR-137792, February 1976.

7. Cotter, T. P., "Heat Pipe Startup Dynamics," IEEE 1967 Thermionic Conversion Specialist Conference, October 1967.

8. Deverall, J. E., "Capability of Heat Pipes," Heat Pipe Technology & Manned Space Station Appl. Technical Interchange, Huntsville, Alabama, May 27, 1969.

9. Kemme, J. E., "High Performance Heat Pipes," IEEE 1967 Thermionic Specialist Conference, October 1967, pp. 355-358.

10. Kemme, J. E., "Heat Pipe Capability Experiments," Proceedings of Joint AEC/Sandia Labs., Heat Pipe Conference 1, SC-M-66-223, October 1966, pp. 11-26.

11. Shlossinger, A. P., "Heat Pipe Devices for Space Suit Temperature Control," TRW Systems Report No. 06462-6005-R0-00, November 1968.

12. Colwell, G.T. "Prediction of Cryogenic Heat Pipe Performance," Annual Report for 1975 under Grant No. NSG-2054, Feb. 1, 1976.

13. Eninger, J. E., Luedke, E. E., and Wanous, D. J., "Flight Data Analysis and Further Development of Variable-Conductance Heat Pipes," NASA CR-137782, February 1976.

14. Sherman, A., and Brennan, P. J., "Cryogenic and Low Temperature Heat Pipe/Cooler Studies for Spacecraft Application," AIAA Paper No. 74-753, July 1974.

15. Groll, M., and Munzel, W. D., "Design and Development of a Heat Pipe Diode," Phase I: Design, Prepared for ESTEC, Contract No. 2993/76/NL/PP (SC), July 1977.

16. Kosson, R. L., Quandrini, J. A., and Kirkpatrick, J. P., "Development of a Blocking-Orifice Thermal Diode Heat Pipe," AIAA Paper No. 74-754, July 1974.

17. Reid, R. C., and Sherwood, T. K., "The Properties of Gases and Liquids - Their Estimation and Correlation," McGraw-Hill Book Co., Inc., New York, 1958.

HEAT PIPE DESIGN

The development of a practical heat pipe design requires the application of the theory presented in Chapters 2 and 3 in combination with a variety of considerations including physical, thermal and mechanical constraints; application requirements; materials properties; fabrication, processing and testing limitations; as well as reliability and safety. At the outset the designer is faced with a number of optional solutions including non-heat pipe design alternatives. The objective of this chapter is to illustrate practical design procedures that are required for the successful development and application of heat pipe hardware.

4.1 DESIGN PROCEDURE

Fig. 4-1 is a flow chart of the major steps to be followed in the design of a heat pipe. The first step in the design process is to identify the performance requirements. Once the specifications for a heat pipe application have been defined, the design selection and evaluation process can be initiated. Three basic considerations are applicable to the development of any heat pipe design:

(1) Selection of the working fluid

(2) Selection of the wick design

(3) Selection of the container design

For a given application, several possible combinations of working fluid, wick structure and container design can be selected to satisfy the specifications. Other considerations such as thermal control techniques (e.g., active or passive gas controlled variable conductance) will also affect the heat pipe's design. As in any design optimization, the final design represents an iteration among the various design factors, and very often an adjustment of the performance requirements or design constraints. A detailed discussion of those factors which determine a heat pipe's design is given in Section 4.2.

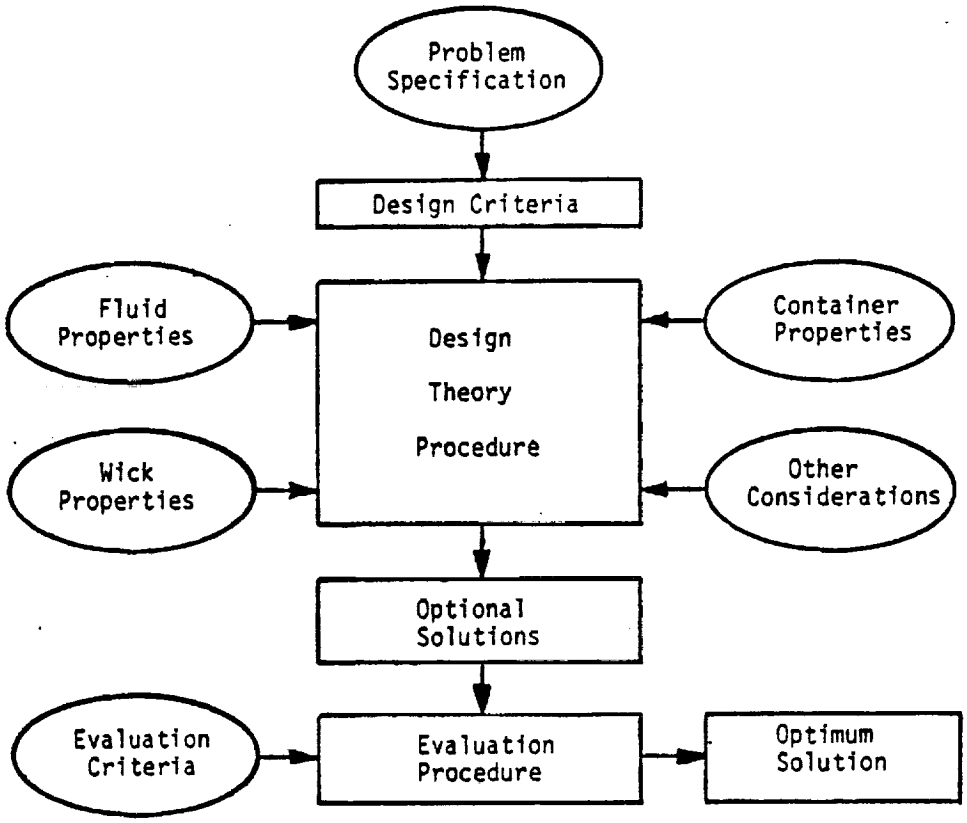

Fig. 4-1. Flow chart of heat pipe design procedure

4.2 PROBLEM DEFINITION AND DESIGN CRITERIA

The basic performance requirements of the specific application must be established before any design effort can be initiated. These parameters include operating temperature range, heat load requirements, allowable temperature drops, thermal control requirements, and size, weight and geometry limitations. In addition, design and operational constraints associated with testing, operational limits under gravitational or acceleration loads, mechanical, thermal interface requirements, storage and operational lifetimes, pressure containment specifications, toxicity requirements, and provisions for structural support must also be established. Also the type of application, aerospace or commercial, and ultimately cost must be considered. A specification should be prepared to organize and delineate the various requirements. This specification should be thorough and complete since it will be the document used for the design, development, and test efforts. A listing of the requirements which may be included in the heat pipe specification and their impact on the heat pipe design is given in Table 4-1.

TABLE 4-1 PROBLEM DEFINITION AND DESIGN CRITERIA

Requirement	Impact on Heat Pipe Design
Operating Temperature Range	Choice of working fluid; pressure retention
Thermal Load	Heat Pipe diameter, number of heat pipes, wick design, and choice of working fluid
Transport Length	Wick design
Temperature Uniformity and Overall ΔT	Evaporator and condenser wick design, conductive path length trade-off, heat pipe geometry
Physical Requirements	Size, weight structural strength and geometry
Acceptance & Quality Testing	"One-G" environment operation and correlation with "Zero-G" operation
Ground Testing	Degrees of freedom in orientation, limits on operating during testing
Dynamic Environment	Operation under acceleration loads, structural integrity
Thermal Environment	Pressure retention during non-operating temperature cycles
Man Rating	Pressure Vessel Code; Fluid Toxicity
Mechanical Interfacing	Mounting provisions, provisions for thermal interfacing
Transient Behavior	Choice of working fluid, wick design, variable conductance type
Reliability	Leak tightness requirements, material compatibility, processing care and control, redundancy

4.2.1 Operating And Non-Operating Thermal Environment

This requirement represents the primary constraint on the selection of the working fluid. Freezing point and critical temperature define the operating limits of a fluid. However, in practice, the useful temperature range must be well within these limits. Clearly defined upper and lower operating temperature bounds are therefore required for proper selection of the working fluid. In addition, it is often necessary to define maximum and minimum non-operating temperature conditions. Upper temperature limits can affect the pressure containment design and may impact working fluid degradation and materials compatibility. The minimum non-operating temperature on the other hand can affect the heat pipe's start-up behavior especially if operation is to be initiated from a frozen or low vapor temperature state at which point the pipe has negligible heat transport capacity.

Sink temperature variations and temperature control requirements are the most significant design constraints associated with thermal control heat pipes. They can affect the selection of variable conductance heat pipe design working fluids and reservoir size. For diode designs, the variation in sink temperature determines the degree of shutdown required and the maximum permissible reverse conductance.

4.2.2 Thermal Load

The specification of the thermal load consists of defining the distribution of heat addition and heat removal. Multiple heat input and heat output sections as well as adiabatic sections can exist, but a good definition of their axial and circumferential distributions must be available. This is necessary to properly evaluate their effect on the transport requirements and the heat pipe temperature drops. The power density and distribution of any heat addition will also determine whether a boiling limit could occur in the evaporator section(s). Finally, the transient nature of the heat loads should also be defined where tight temperature control and variable conductance operation are required.

4.2.3 Transport Length

The transport length is an equivalent distance over which the heat must be carried. This requirement, in combination with the thermal load distribution, determines the transport requirement $(QL)_{req}$ which directly affects the choice of working fluid and wick design.

4.2.4 Temperature Uniformity and Overall Temperature Drop

The degree of temperature uniformity and the overall heat pipe temperature drop will determine the evaporator and condenser designs as well as affecting the choice of working fluid and the wick design.

4.2.5 Physical Requirements

Size, weight, and geometry limitations as specified by the application, when considered with the performance requirements, must be such that a practical heat pipe design can be obtained.

4.2.6 Acceptance and Qualification Testing

A detailed discussion of typical heat pipe test requirements is given in Chapter 8. In addition to thermal performance tests, leak tests, compatability tests, and pressure tests are also often required to verify that the various performance and design requirements have been attained. Thermal performance test requirements must be related to 0-g as well as 1-g behavior. When 0-g applications are specified, the test elevation for 1-g performance verification should be such that 1-g effects such as "puddling" are minimized. However, since the 1-g test elevation affects the choice of working fluid and the wick design, this elevation should not be overly prohibitive. Leak and pressure tests are generally defined as part of the fabrication process; their specified levels affect the container and closure designs.

4.2.7 Dynamic Environment

Capillary forces are relatively small, and therefore operation of a heat pipe against adverse acceleration loads is limited. The frequency and nature of acceleration loads must be defined and imposed as operational constraints on the heat pipe if operation under these conditions is required. In addition, the heat pipe may be subjected to a dynamic environment, and the heat pipe must be designed to withstand these dynamic loads without damage or degradation in performance.

4.2.8 Man Rating

Exposure to personnel during processing, testing, handling, shipping, installation and operation requires heat pipes that are safe and free of hazards. Safety standards associated with the toxicity of the working fluid, the fluid's vapor pressure, and pressure retention are additional constraints which must be placed on the heat pipe design.

Industry standards such as the ASME Boiler Code (35) for pressure vessels and safety regulations for the handling of hazardous materials are used in defining hazard-free design requirements.

4.2.9 Thermal/Mechanical Interface

Thermal/mechanical interfaces affect container design and the thermal performance of the heat pipe. To achieve good thermal interfaces, it is first necessary to define the mechanical interface requirements. The surface flatness and finish of an interface have a strong influence on the system's temperature gradients. Interface filler materials improve the performance of mechanical interfaces. However, restrictions are often imposed on their use for space applications because of the outgassing associated with many of these materials.

4.2.10 Transient Behavior

Start-up is best accomplished by using a working fluid which is initially saturated. When this is not possible, as in the case of many cryogenic or liquid metal heat pipes, the wick should be designed to give good transport during the priming operation. When a variable conductance heat pipe is required, the transient behavior will depend to a large extent on the type of VCHP employed and the choice of the working fluid.

4.2.11 Reliability

Four failure mechanisms impose limitations on the life of any heat pipe--these are fluid leakage, non-condensible gas generation, wick degradation, and fluid property degradation. The life of the heat pipe is defined as the total time span from the time of final pinch-off to the end of use as defined by application requirements. This total time span determines the minimum leak-tightness requirement. This parameter is critical since heat pipes operate with a very small fluid inventory, and small continuous leaks can cause the heat pipe to become inoperable.

The working fluid must be compatible with the container and wick materials in order to avoid generation of non-condensible gases. Again, for extended life requirements, even extremely small rates of non-condensible gas generation can be detrimental. This is especially true for heat pipes which have very small condenser regions. Non-condensible gases are swept from the evaporator to the condenser region; and, if excessive gas is generated, unacceptable condenser blockage can result.

Wicks can degrade due to erosion or an accumulation of particulate matter which impedes the liquid flow through the wick. Similarly, fluid properties can degrade due to chemical reactions. It is important that realistic lifetimes be defined so that they can be demonstrated with meaningful accelerated life tests (see Section 8.1.1.2).

4.2.12 Temperature Control Sensitivity

Temperature control requirements often determine the type of variable conductance technique that must be employed. Cold-wicked reservoir VCHP's can provide adequate temperature control for moderate heat load and sink temperature variations. A feedback controlled VCHP is capable of providing absolute temperature control for very severe variations of heat load and sink temperatures. For any variable conductance pipe, the required degree of temperature control will affect the choice of the working fluid and the reservoir size.

4.3 WORKING FLUID SELECTION

A variety of physical, chemical, and thermodynamic properties of a particular working fluid must be evaluated to determine whether or not that fluid is suitable for the specific heat pipe application. The general considerations which apply to candidate fluids are:

(1) Operating temperature range

(2) Liquid transport factor

(3) Vapor phase properties

(4) Wicking capability in body-force field

(5) Thermal conductivity

(6) Fluid operating pressure

(7) Fluid compatibility and stability

A number of heat pipe fluids and their operating temperature range are summarized in Table 4-2. These are categorized into three operating temperature ranges: cryogenic (Group 1), intermediate (Group 2), and high temperature (Group 3). Properties which directly affect heat pipe design and performance are given in Figs. 4-2 through 4-13. A detailed listing of the fluid properties together with a computer program for tabulating fluid properties (HPF) is presented in Volume II of this manual. The effects of these various parameters on the selection of a working fluid are discussed below.

TABLE 4-2. SELECTED PROPERTIES OF HEAT PIPE WORKING FLUIDS

FLUID	FORMULA	GROUP	MOLECULAR WEIGHT	MELTING POINT		NORMAL BOILING POINT		CRITICAL TEMPERATURE		CRITICAL PRESSURE		TEMPERATURE RANGE OF TABULATED DATA	REFERENCES*
				°K	°F	°K	°F	°K	°F	$10^5 Nm^{-2}$	Psia	(°K)	
1. Helium	He	1	4.0	1.3	-457.3	4.2	-452.1	5.2	-450.3	2.3	33.4	2.4 - 4.0	1
2. Hydrogen	H_2	1	2.0	14.0	-434.4	20.4	-423.0	33.0	-400.3	12.9	187.2	14 - 33	1, 2, 7
3. Neon	Ne	1	20.2	24.5	-415.6	27.1	-410.9	44.4	-379.8	26.5	384.5	27 - 44	1, 3, 7
4. Oxygen	O_2	1	32.0	54.3	-361.8	90.2	-297.3	154.8	-181.1	50.9	738.6	55 - 154	1, 2, 3, 7
5. Nitrogen	N_2	1	28.0	63.1	-346.0	77.3	-320.4	126.2	-232.4	34.0	493.3	65 - 125	1, 2, 3, 5
6. Argon	A	1	39.9	83.8	-308.8	87.3	-302.5	150.9	-188.1	50.0	725.5	85 - 150	1, 3, 4
7. Propane	C_3H_8	1	44.1	85.5	-305.8	231.1	43.7	370.0	206.3	42.6	618.1	190 - 367	1, 6, 9
8. Freon -14	CF_4	1	88.0	89.4	-298.7	145.5	-197.8	227.7	-49.8	37.4	542.7	130 - 222	14
9. Ethane	C_2H_6	1	30.1	89.9	-297.8	184.5	-127.6	305.5	90.2	49.1	712.4	100 - 305	1, 3, 6, 9
10. Methane	CH_4	1	16.0	90.7	-296.4	111.4	-259.2	190.5	-116.8	46.4	673.3	91 - 190	1, 3, 5, 6
11. Freon -13	$CClF_3$	1	104.5	93.2	-291.9	191.7	-114.6	302.3	84.5	39.0	565.9	163 - 293	1, 3
12. Butane	C_4H_{10}	1	58.1	134.8	-217.0	272.7	31.2	425.0	305.3	38.0	550.7	260 - 350	1, 3, 5, 6, 9
13. Freon -21	$CHCl_2F$	1	102.9	138.2	-210.9	282.1	48.1	451.4	352.8	51.8	751.8	213 - 450	1, 3, 5
14. Freon -11	CCl_3F	1, 2	137.4	162.2	-167.8	296.9	74.7	471.2	388.5	44.1	639.9	293 - 413	1, 3, 5
15. Methanol	CH_3OH	2	32.0	175.2	-144.3	337.9	148.5	513.2	464.1	79.5	1153.0	273 - 503	1
16. Toluene	C_7H_8	2	92.1	178.1	-139.1	383.7	231.0	593.9	609.3	41.6	603.6	275 - 473	1, 5, 6
17. Acetone	$(CH_3)_2CO$	2	59.1	180.0	-135.7	329.4	133.2	508.2	455.1	47.6	690.0	250 - 475	5, 6
18. N-Heptane	C_7H_{16}	2	100.2	182.6	-131.0	371.6	209.2	540.2	512.7	27.4	397.6	273 - 473	1, 5, 6
19. Ammonia	NH_3	1, 2	17.0	195.5	-107.8	239.8	-28.0	405.6	270.4	112.9	1638.0	200 - 405	1, 2, 3, 5
20. M-Xylene	C_8H_{10}	2	106.2	225.3	-54.1	412.3	282.5	619.2	654.9	36.5	529.6	275 - 473	1, 6
21. Mercury	Hg	2, 3	200.6	234.3	-37.9	630.1	674.5	1763	2714	1510	21910	280 - 1070	1, 7, 8
22. Dowtherm E		2	147.0			453.4	356.4	690.2	785.0	40.3	584.7	283 - 610	13
23. Water	H_2O	2	18.0	273.2	32.0	373.2	212.0	647.3	705.4	221.2	3210	273 - 643	1
24. Benzene	C_6H_6	2	78.1	278.7	42.0	353.3	176.2	562.6	553.0	49.2	713.9	280 - 560	1, 5
25. Dowtherm A		2	166.0	285.2	53.6	531.1	496.4	801.2	982.4	40.2	583.3	373 - 670	1
26. Cesium	Cs	3	132.9	301.6	83.2	943.0	1237.8	2050	3230	117.0	1698.9	400 - 1500	1, 7
27. Potassium	K	3	39.1	336.4	145.8	1032.2	1398.3	2250	3590	160.0	2322	400 - 1800	1, 7
28. Sodium	Na	3	23.0	371.0	208.1	1152.2	1614.3	2500	4040	370.0	5369	400 - 1500	1, 7
29. Lithium	Li	3	6.9	453.7	357.0	1615.0	2447.0	3800	6380	970.0	14074	500 - 2100	1, 7
30. Silver	Ag	3	107.9	1234	1761	2450.0	3950.3	7500	13040	336.0	4875	1600 - 2400	7, 8, 12

*References for fluid properties are listed in Chapter 1 of Volume II

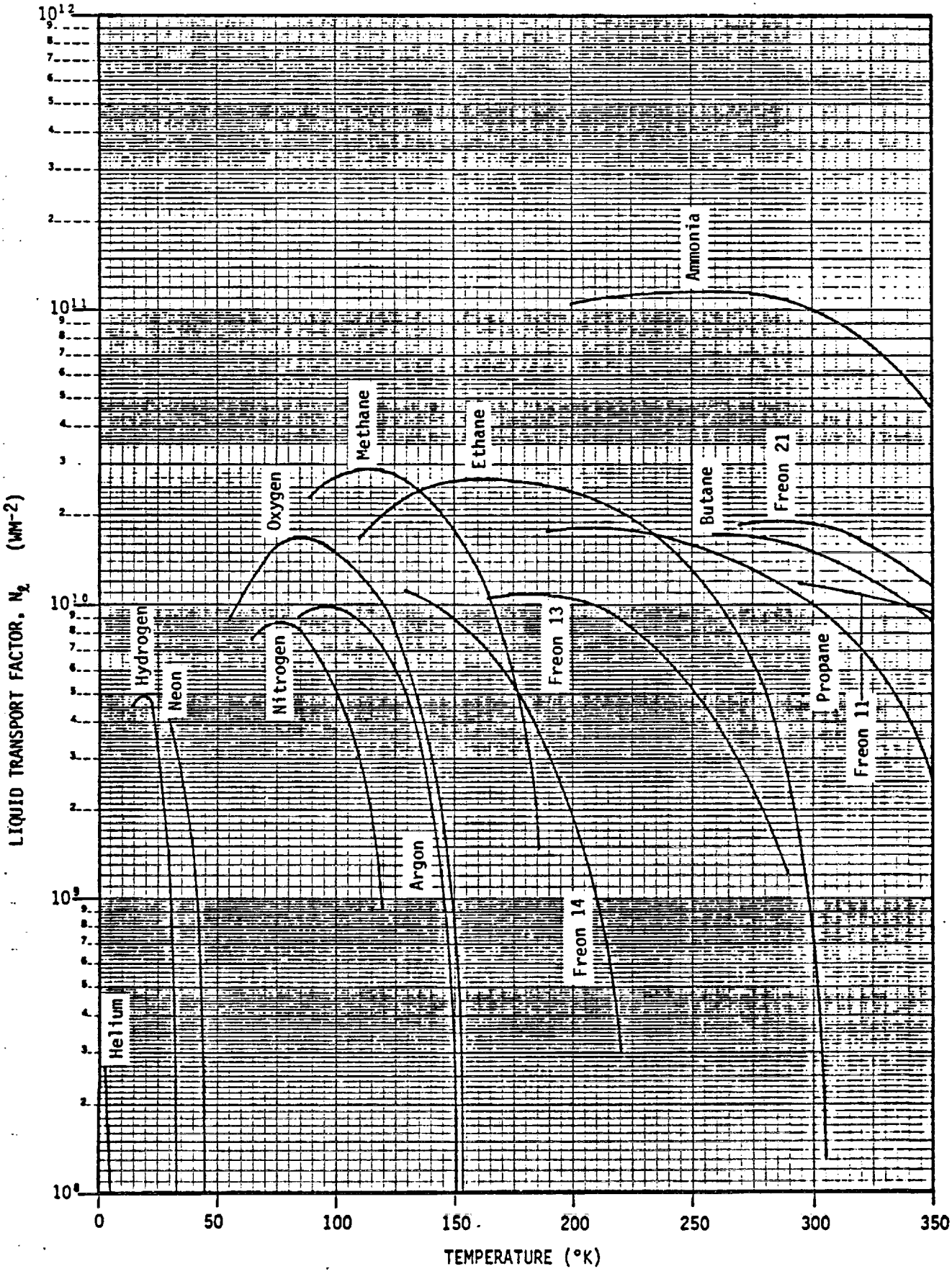

Fig. 4-2. Liquid transport factor: Group 1

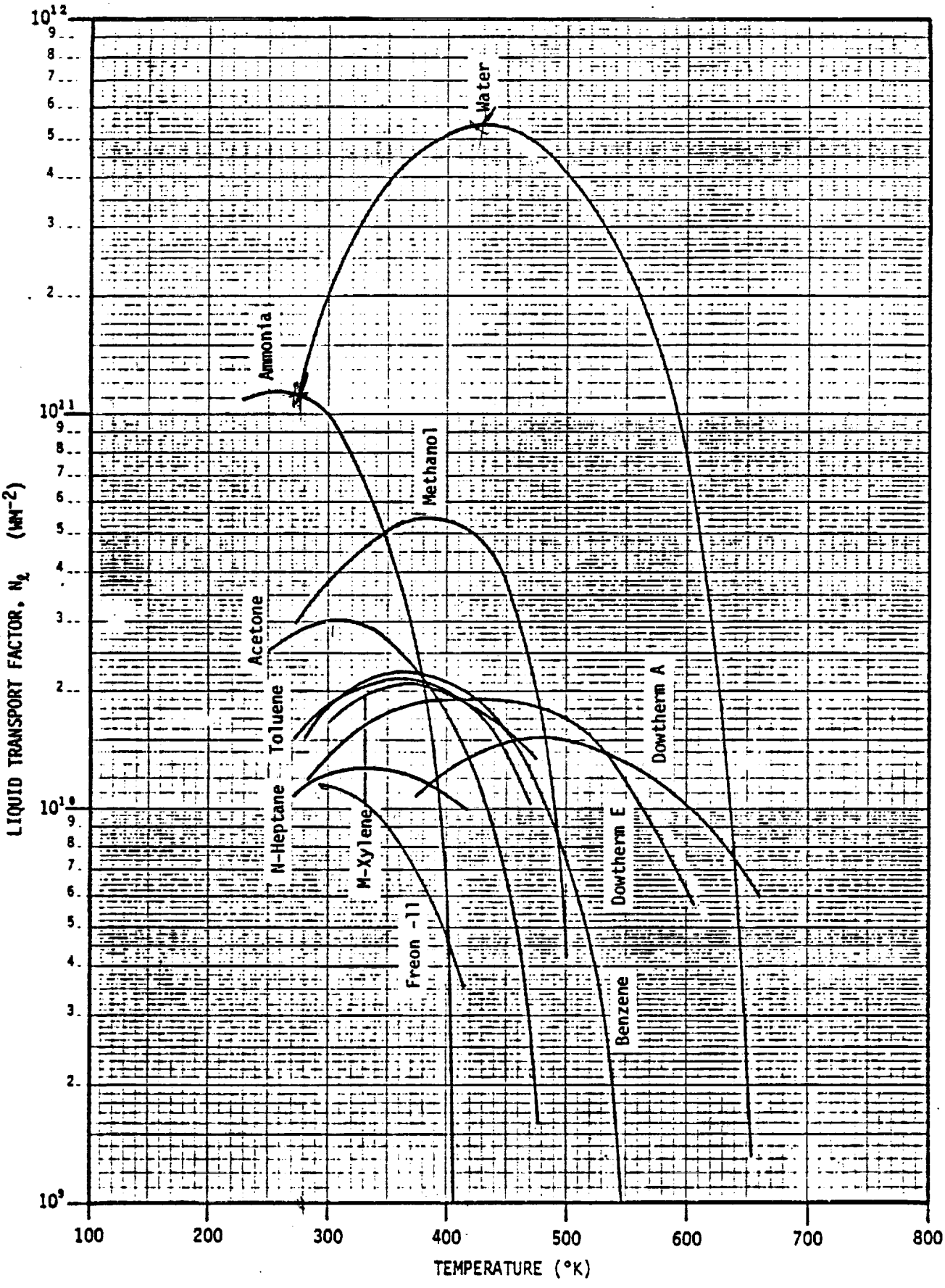

Fig. 4-3. Liquid transport factor: Group 2

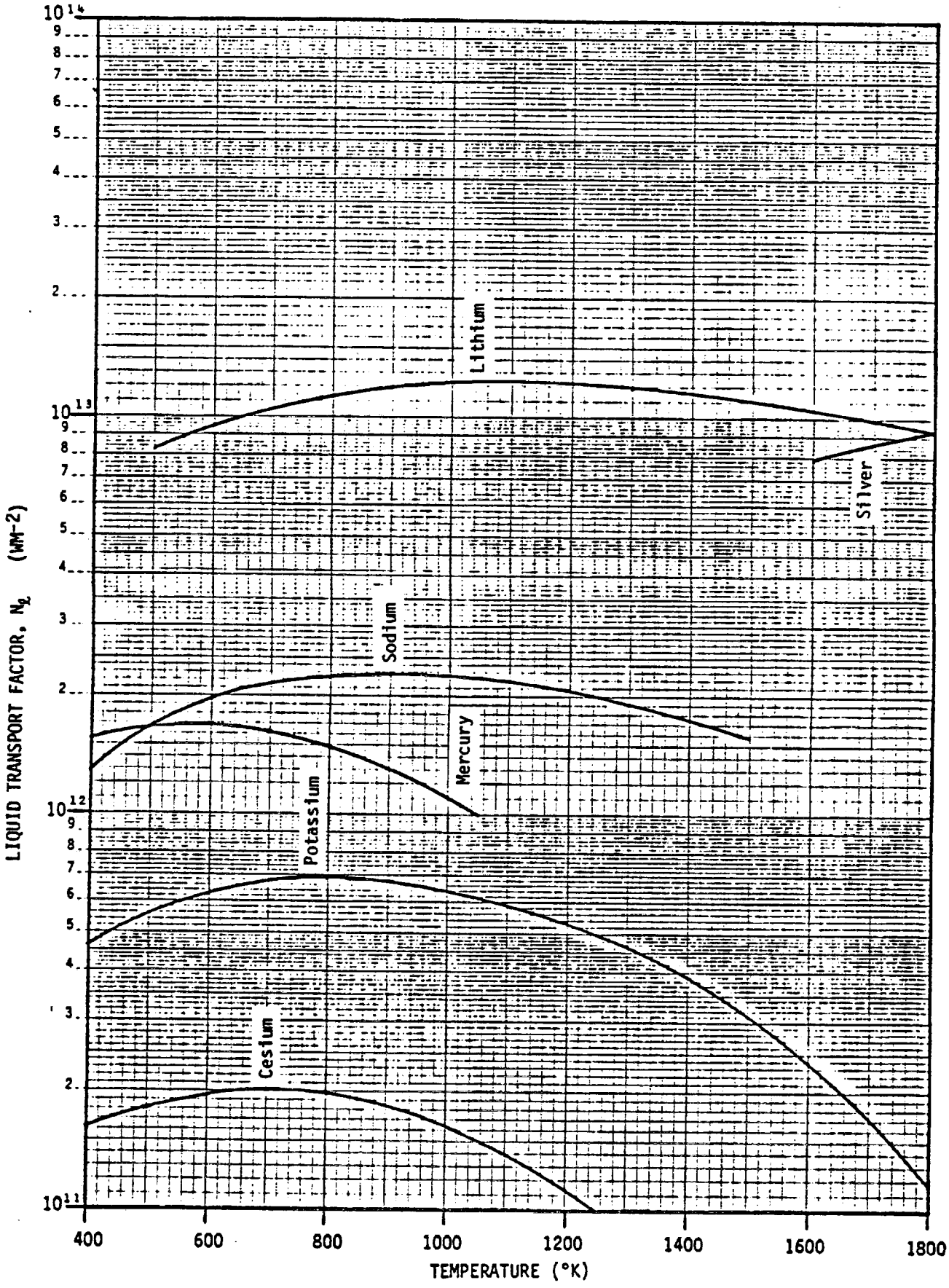

Fig. 4-4. Liquid transport factor: Group 3

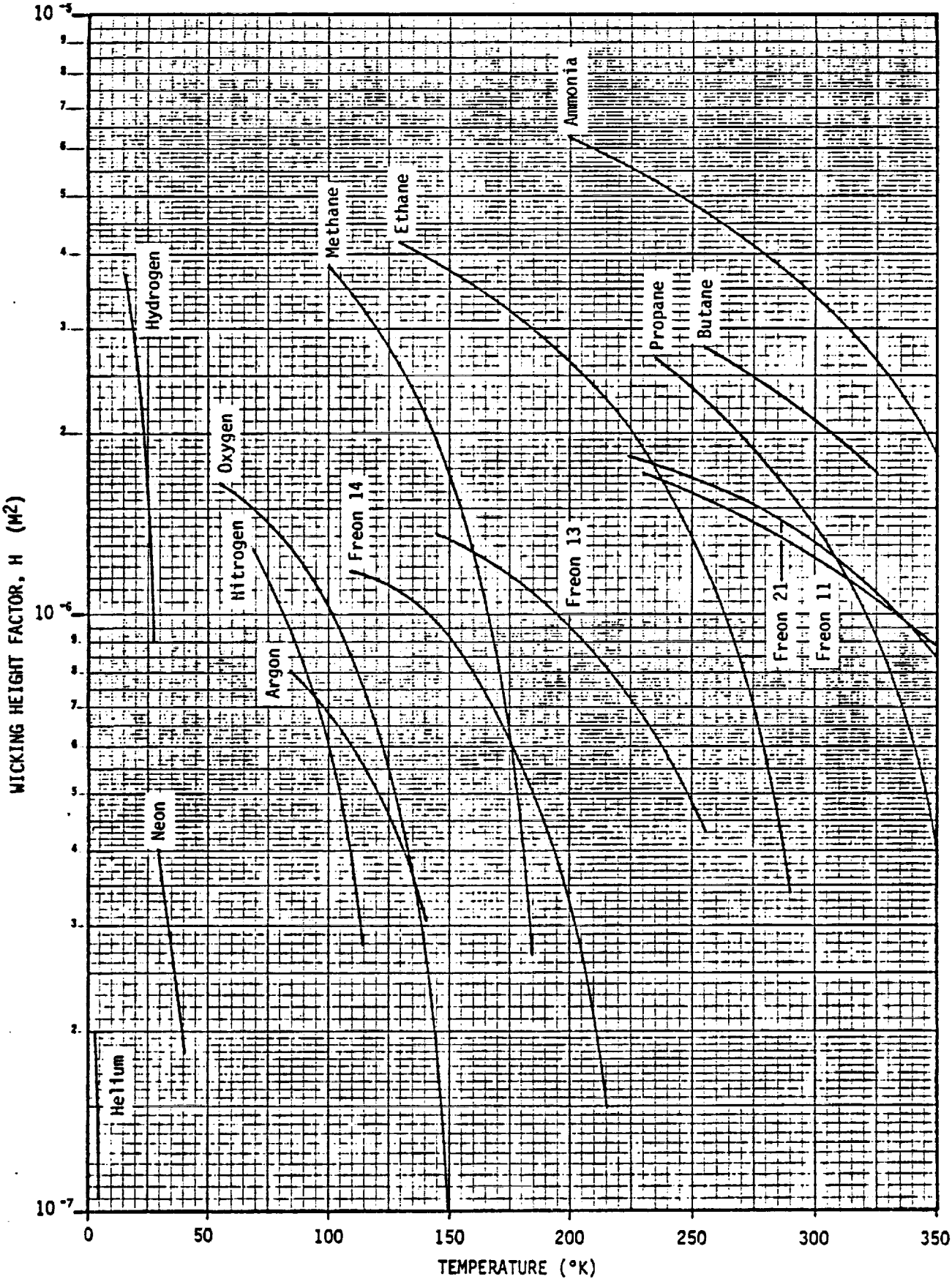

Fig. 4-5. Wicking height factor: Group 1

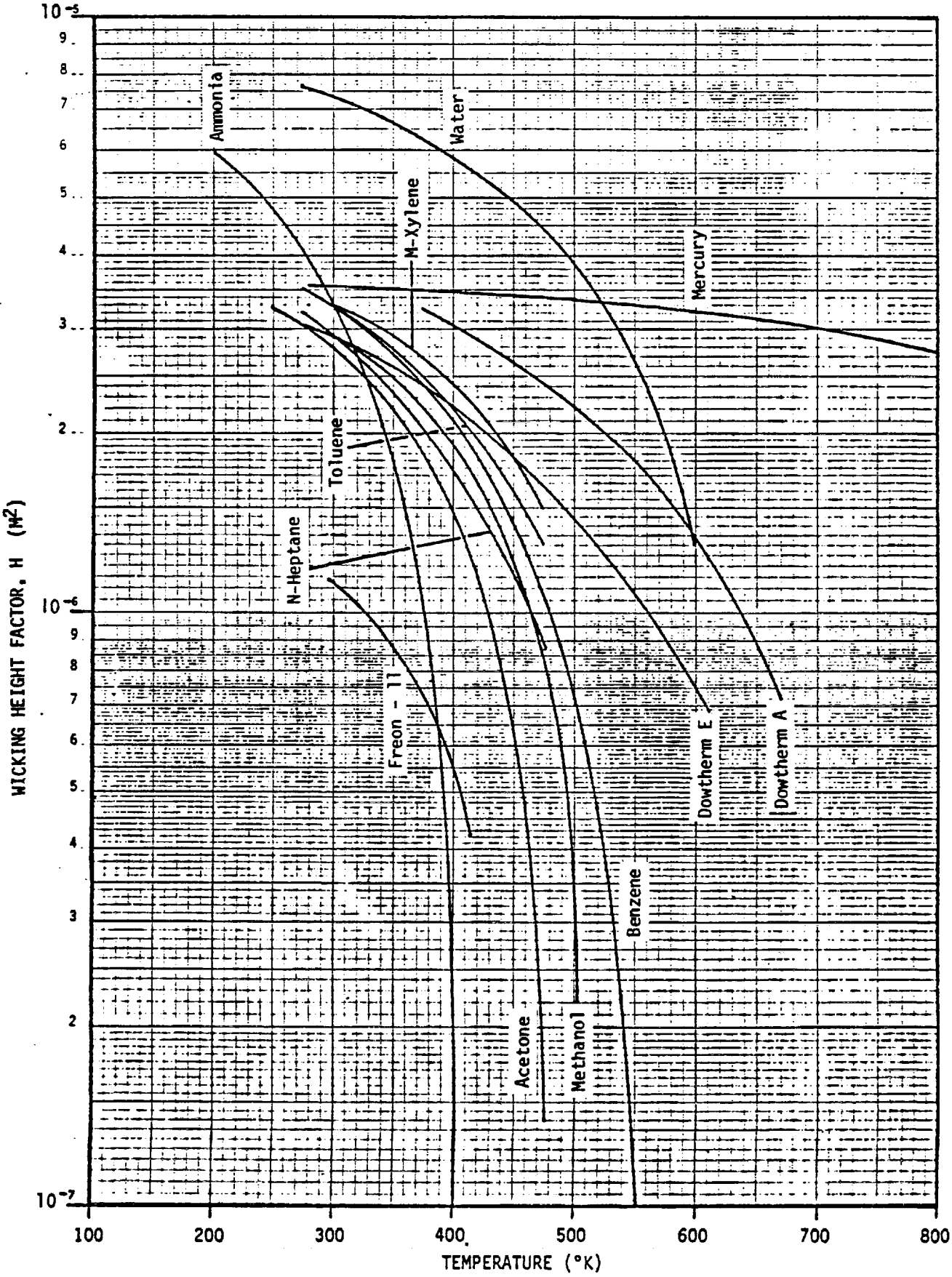

Fig. 4-6. Wicking height factor: Group 2

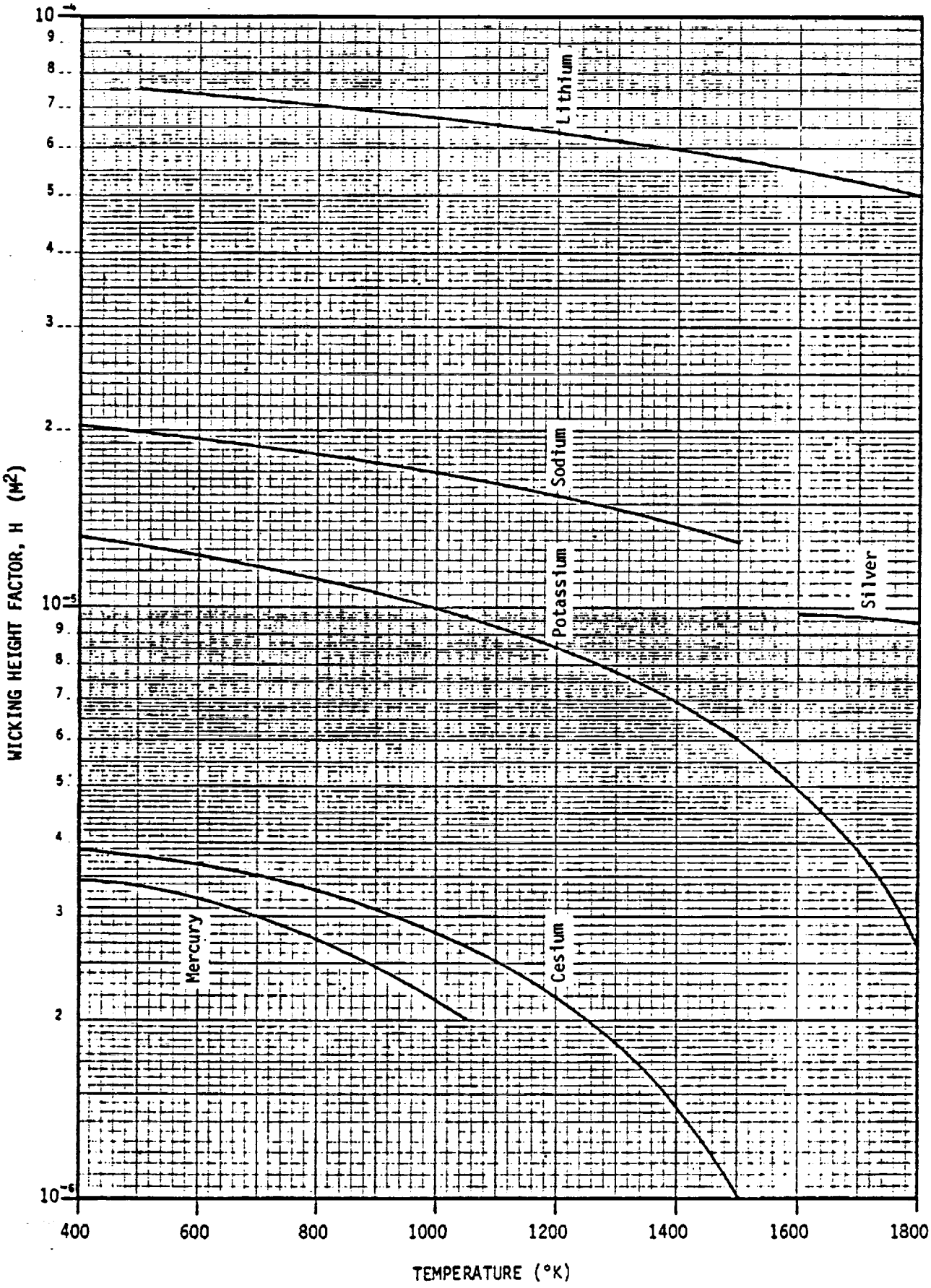

Fig. 4-7. Wicking height factor: Group 3

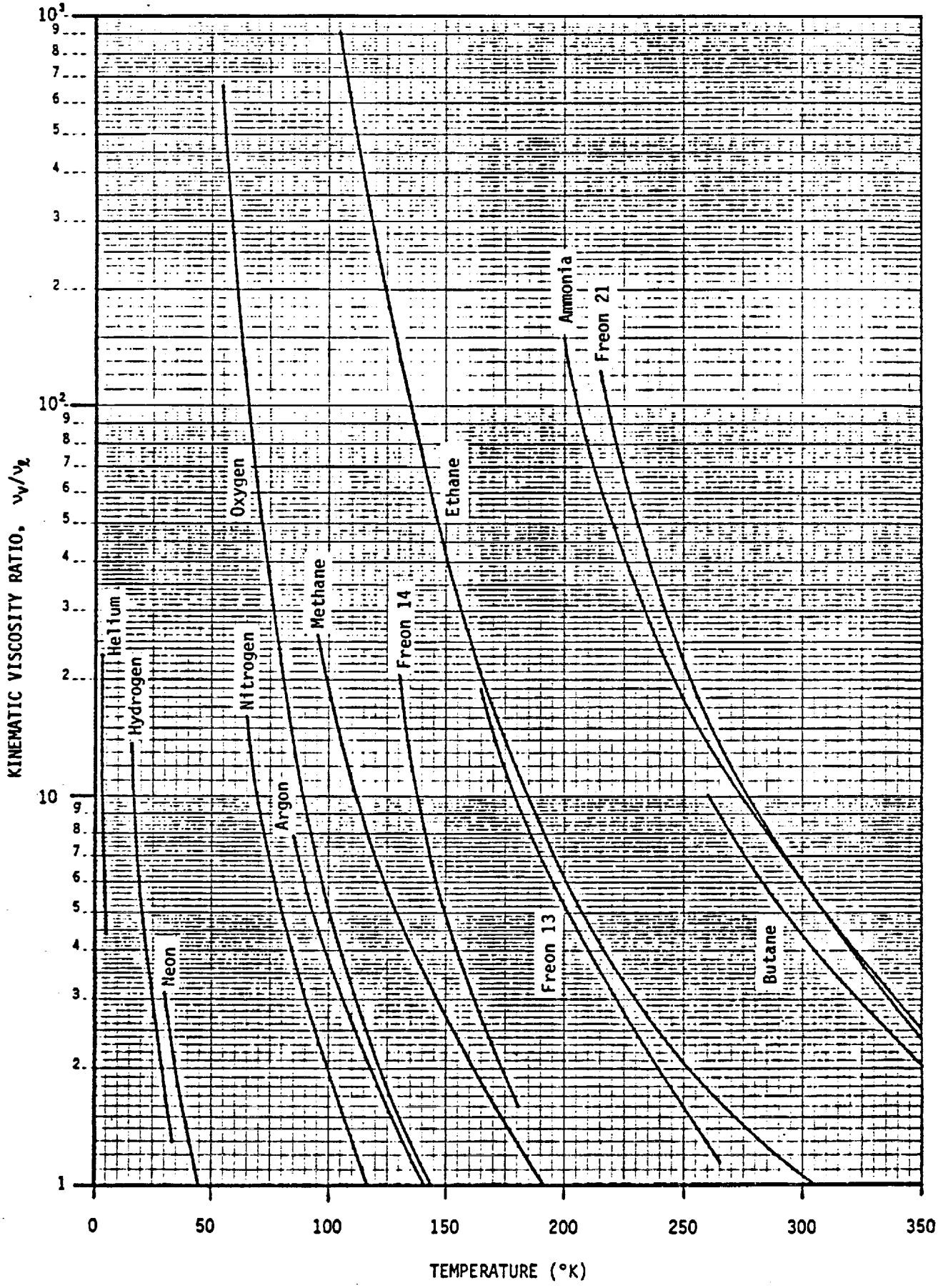

Fig. 4-8. Kinematic viscosity ratio: Group 1

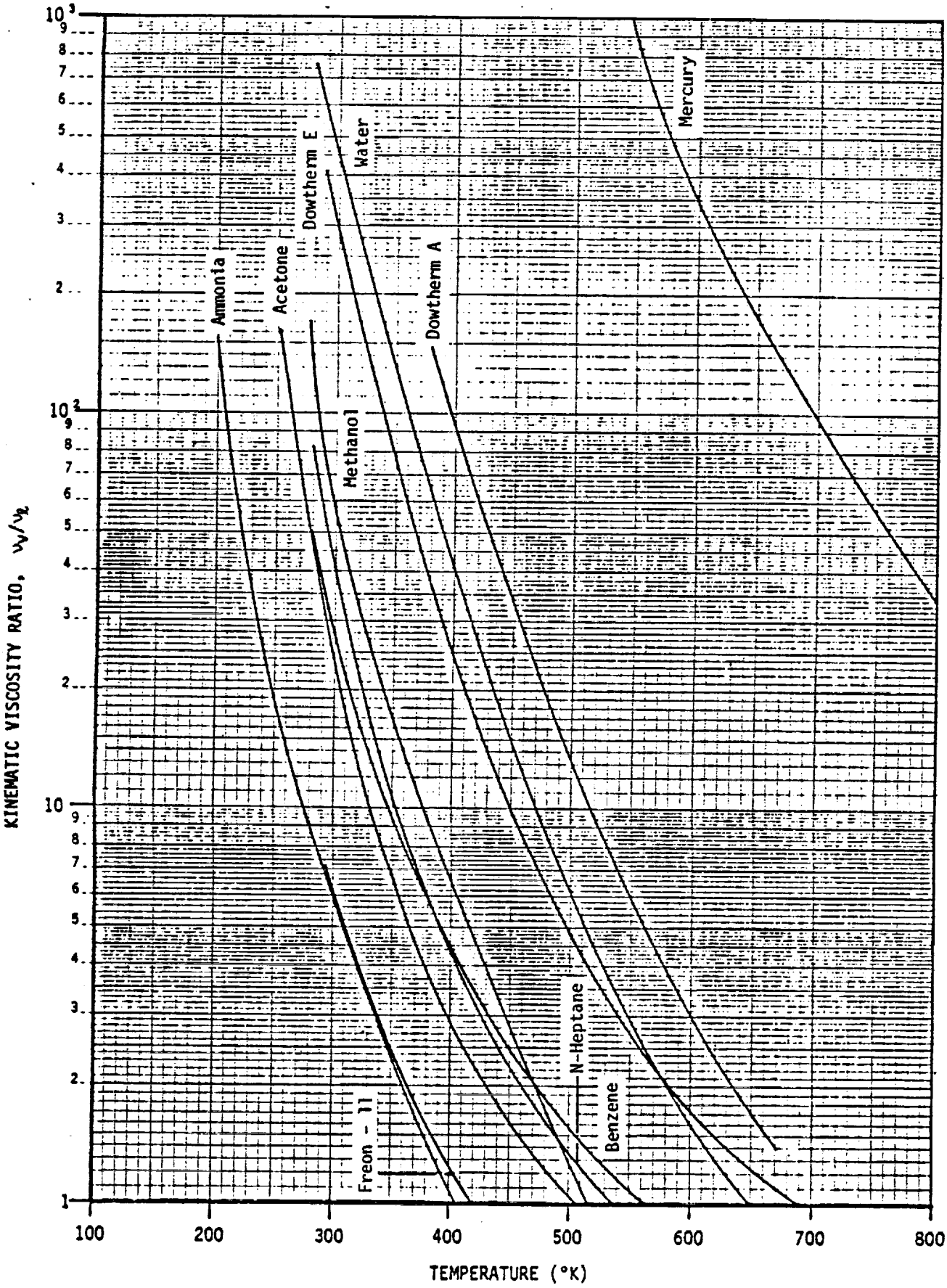

Fig. 4-9. Kinematic viscosity ratio: Group 2

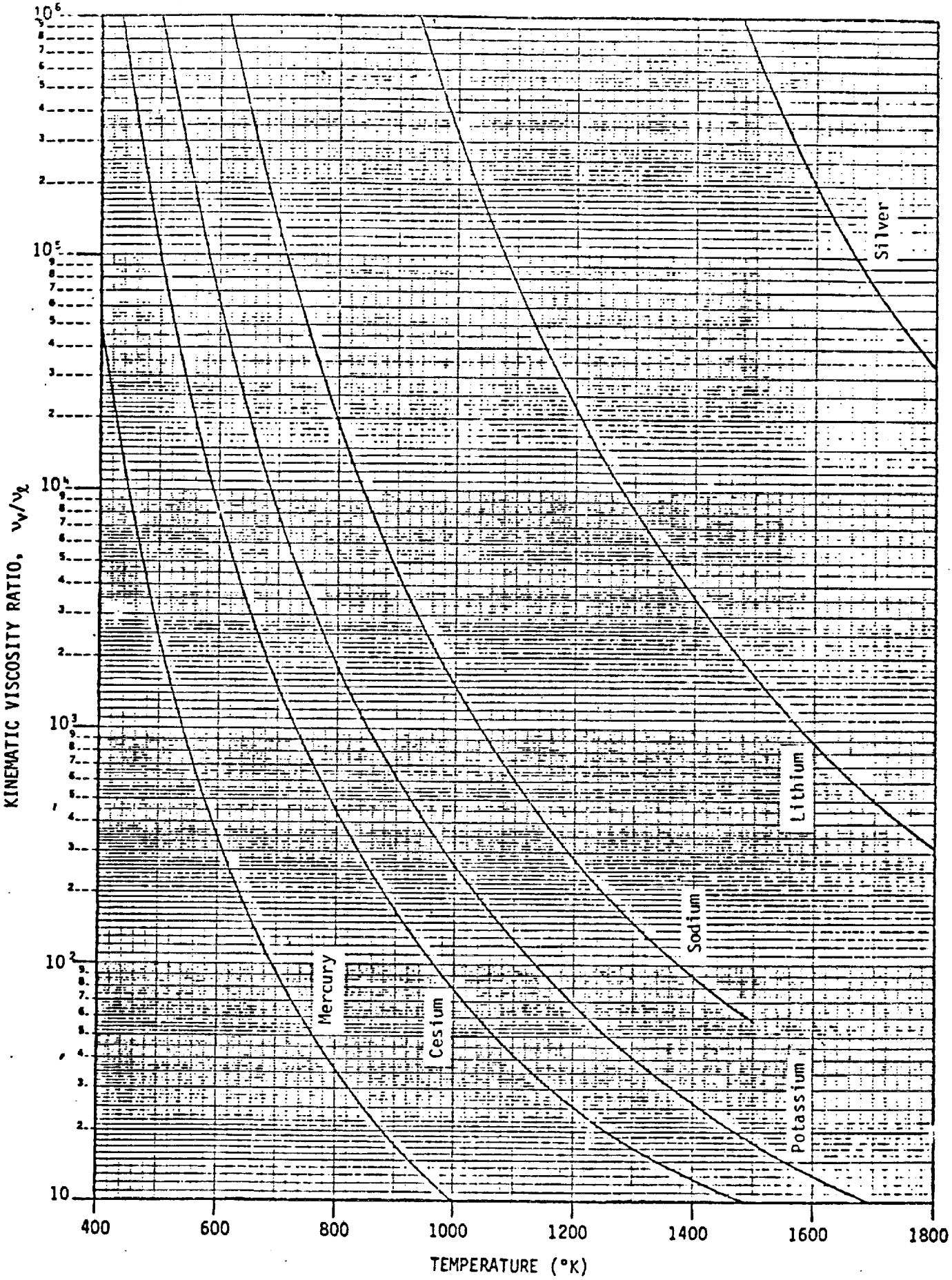

Fig. 4-10. Kinematic viscosity ratio: Group 3

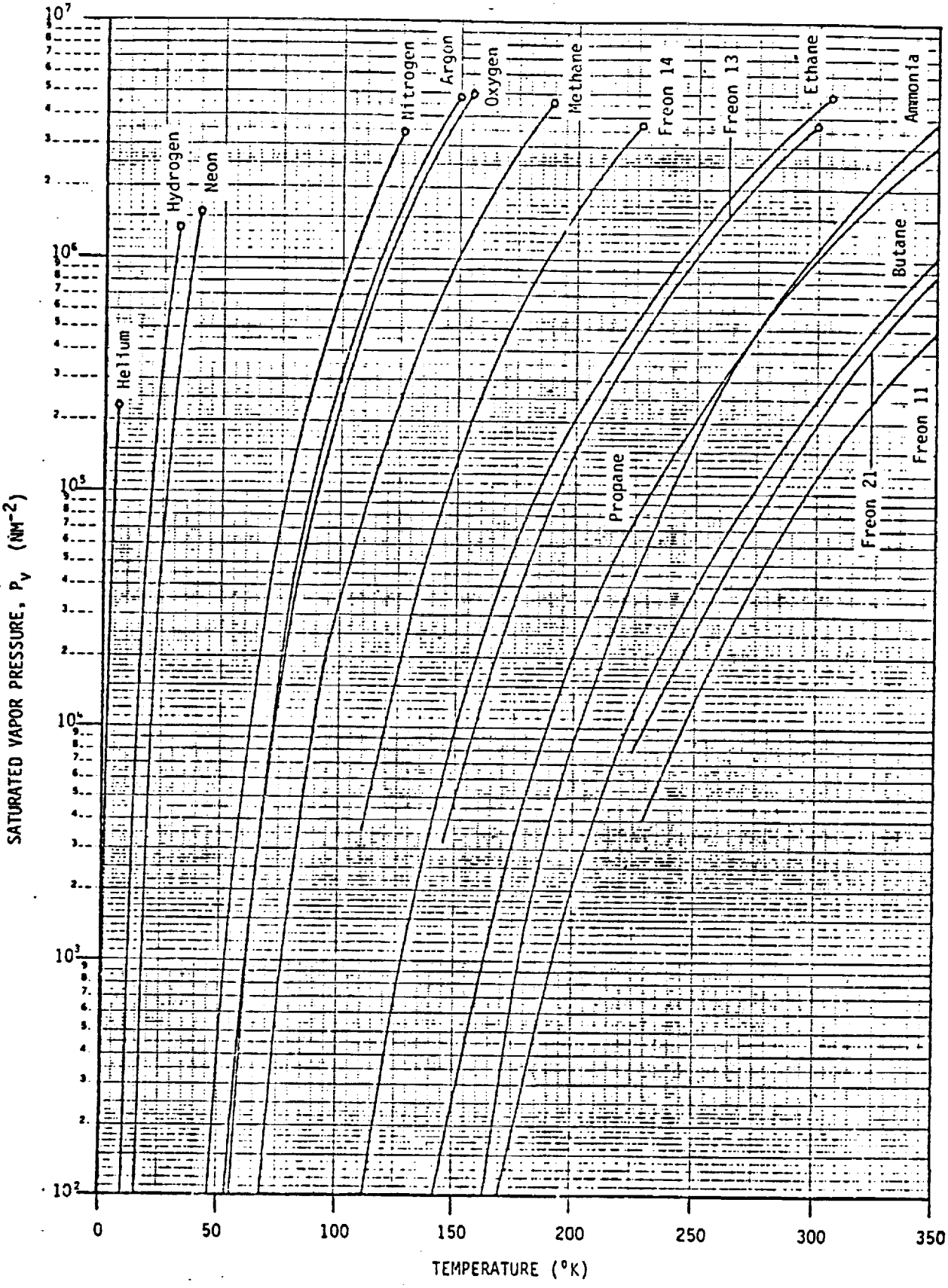

Fig. 4-11. Saturated vapor pressure: Group 1

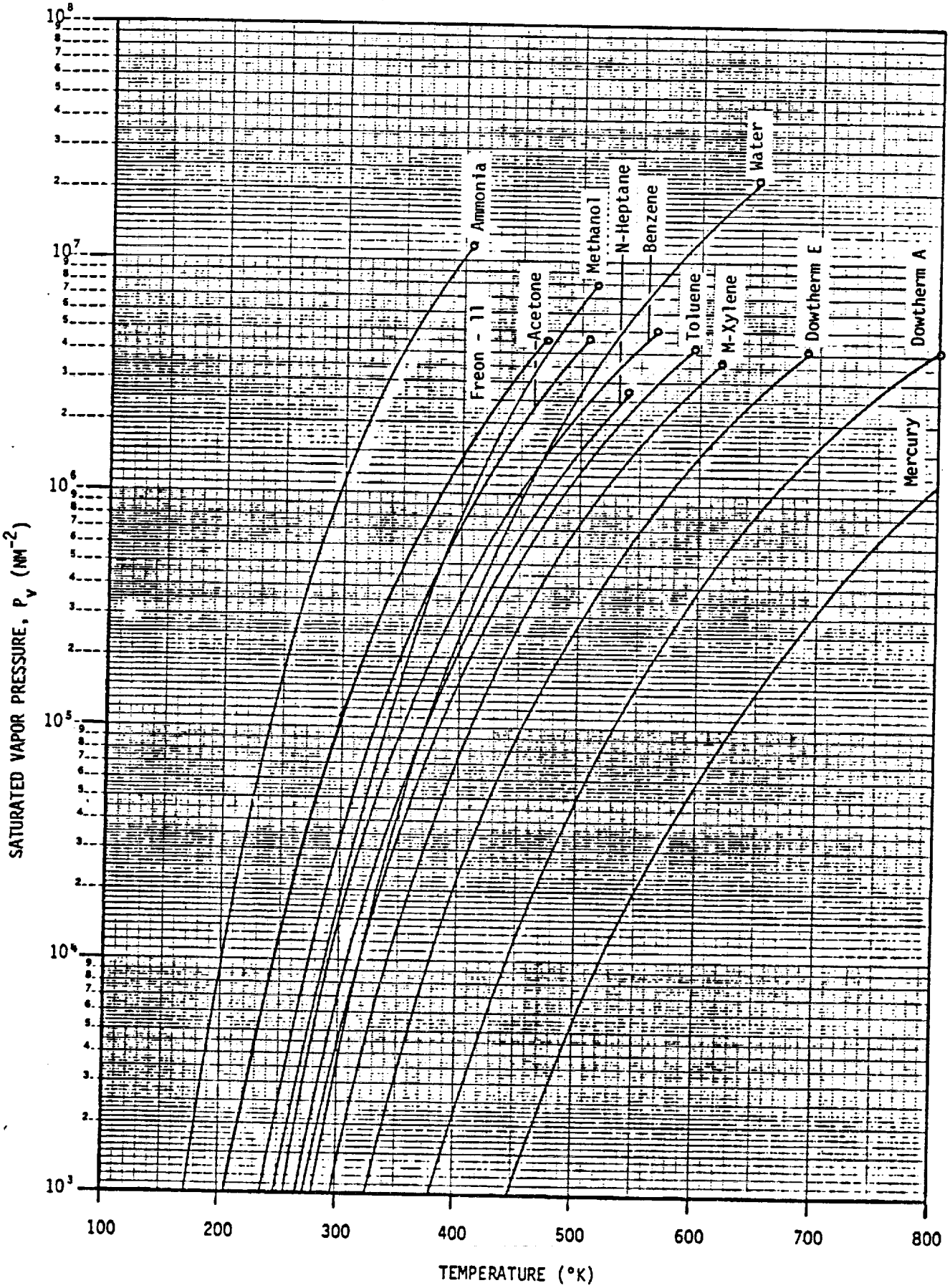

Fig. 4-12. Saturated vapor pressure: Group 2

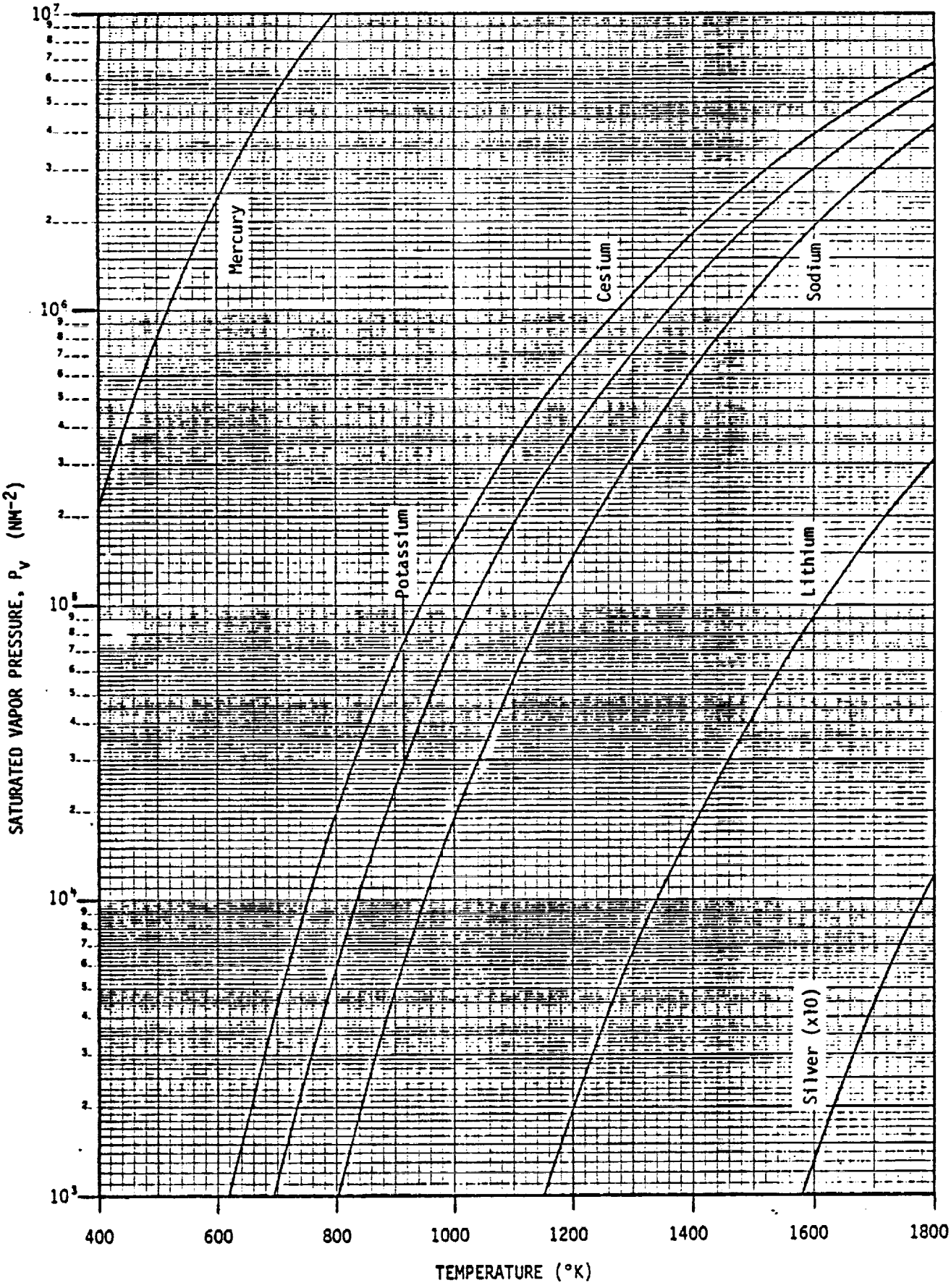

Fig. 4-13. Saturated vapor pressure: Group 3

4.3.1 Operating Temperature Range

Since a heat pipe cannot function below the freezing point or above the thermodynamic critical point of its working fluid, a fluid should be chosen whose useful temperature range spans the operating temperature limits of the heat pipe. The lower temperature limit relates to adverse vapor effects such as the sonic limit, entrainment limit, or simply excessive vapor viscous and liquid/vapor shear pressure drops. As a "rule of thumb", the lowest operating temperature should be greater than the temperature corresponding to a vapor pressure of 0.1 atmosphere. Conversely, the upper limit of the operating temperature should be kept below the critical point to avoid low values of surface tension and latent heat which result in poor capillary pumping and excessive liquid losses. Operation below the critical point will also avoid excessive containment pressure requirements.

4.3.2 Liquid Transport Factor

The capillary pumping ability of the working fluid is best described by the "Liquid Transport Factor," N_ℓ. This factor states that the highest performance of the heat pipe is obtained with a fluid which has a high surface tension, high liquid density, high latent heat of vaporization, and a low viscosity. In Figs. 4-2 to 4-4 the Liquid Transport Factor is plotted versus temperature for selected fluids in the three basic operating temperature regions. Notice that each curve contains a rather broad maximum near the fluids normal boiling point. The decrease in the Liquid Transport Factor on the low temperature side is due to the increase in liquid viscosity. On the high temperature side, the decrease occurs because the latent heat, liquid density, and liquid surface tension all decrease more rapidly than the liquid viscosity. The Liquid Transport Factor decreases to zero at the critical temperature as the latent heat and surface tension become zero.

For heat pipes operating in the absence of body forces and for conditions where the vapor pressure drop is negligible, the capillary pumping limit is directly proportional to N_ℓ. However, in the general design case, there is no simple grouping of fluid properties which serves as an exact basis for selection. Therefore, the N_ℓ factor can only serve as a figure of merit for candidate heat pipe working fluids. To finalize the choice of fluid, a parametric evaluation must be conducted which includes the liquid transport factor, vapor losses, wicking height requirements, and thermal conductance.

4.3.3 Liquid Wicking Capability in a Body-Force Field

As discussed in Chapter 2, the presence of body forces can influence the relative performance of various heat pipe working fluids because:

(1) The body-force head is subtracted from the maximum capillary head in determining the capillary pumping available to overcome flow losses.

(2) The body-force head must be overcome by surface tension effects in order to prime the wick configuration.

Since in both cases the problem is one of surface tension forces working against body forces, the ratio of these forces represents a basis of fluid comparison. In terms of fluid properties, this ratio is proportional to the "Wicking Height Factor."

$$H_\ell \equiv \frac{\sigma}{\rho_\ell g}$$

Thus, to minimize adverse body-force effects, the designer should select a working fluid which has a high value for this parameter. For the purpose of comparison, the Wicking Height Factor is given in Figs. 4-5 through 4-7 for various working fluids as a function of temperature. It decreases with increasing temperature since the surface tension decreases faster than the liquid density.

4.3.4 Kinematic Viscosity Ratio

The Liquid Transport Factor N_ℓ and the Wicking Height Factor H_ℓ defined above provide figures of merit for the liquid phase of the working fluid. The relative merit of the vapor phase can be described by the "Kinematic Viscosity Ratio."

$$\frac{\nu_v}{\nu_\ell} \equiv \frac{\mu_v}{\mu_\ell} \frac{\rho_\ell}{\rho_v}$$

This parameter in combination with wick and vapor channel properties defines the proportion of viscous vapor to liquid flow losses. To minimize adverse vapor effects (viscous and shear losses), low values of this parameter are desirable. As shown in Figs. 4-8 through 4-10, the Kinematic Viscosity Ratio decreases with increasing temperature.

4.3.5 Pressure Containment

Adequate attention must be given to evaluating the heat pipe design for all possible temperature environments to which the heat pipe could be subjected. In the case of cryogenic and low temperature heat pipes, storage at ambient temperature or shipping conditions will usually result in substantial internal pressures. Similarly, there exist various applications where the heat pipe must be bonded to another system component. In many cases it is advantageous to bond the heat pipe after it has been charged. Provision must be made in the heat pipe design to contain the resulting pressure or the fabrication process must be specified to avoid this potential excessive pressure condition.

At saturation condition, the vapor pressure is readily determined (e.g., Figs. 4-11 thru 4-13). If the critical point of the fluid is exceeded, the designer can calculate an approximate pressure by using the simple equation of state for an ideal gas.

$$p V = n R T \tag{4-1}$$

This equation holds, with a fair degree of accuracy, for highly superheated vapors. In order to calculate internal pressures, which are fairly accurate throughout the entire superheated vapor region, more complex equations of state (developed from empirical data) must be utilized. One of the best known and most useful such equations is the Beattie-Bridgeman Equation of State (1). The equation is:

$$p = \frac{R T (1 - e')}{v_n^2} (v_n + B) - \frac{A}{v_n^2} \tag{4-2}$$

where:

$$\left.\begin{aligned} v_n &= \text{Specific Volume (liters/gm-mole)} \\ v_n &= \text{(Volume x Molecular Weight)/mass} \\ A &= A_o \left(1 - \frac{a}{v_n}\right) \\ B &= B_o \left(1 - \frac{b}{v_n}\right) \\ e' &= \frac{c}{v_n T^3} \end{aligned}\right\} \tag{4-3}$$

A_o, a, B_o, b, and c are constants that must be determined experimentally for each fluid. The constants for a number of fluids are given in Table 4-3. If the constants are not available for a particular fluid, it is suggested that the ideal gas equation be used and a safety factor of 2.5 to 3 be applied to the working stress of the heat pipe container material.

TABLE 4-3. CONSTANTS FOR THE BEATTIE-BRIDGEMAN EQUATION OF STATE (1)

GAS	Ao	a	Bo	b	10^{-4} x c
Ammonia	2.3920	0.17031	0.03415	0.19112	476.87
Argon	1.2907	0.02328	0.03931	0.0	5.99
n-Butane	17.7940	0.12161	0.24620	0.09423	350.00
Ethane	5.8800	0.05861	0.09400	0.01915	90.00
Helium	0.0216	0.05984	0.01400	0.0	0.0040
n-Heptane	54.5200	0.20066	0.70816	0.19179	400.00
Hydrogen	0.1975	-0.00506	0.02096	-0.04359	0.0504
Methane	2.2769	0.01855	0.05587	-0.01587	12.83
Methanol	33.3090	0.09246	0.60362	0.09929	32.03
Neon	0.2125	0.02196	0.02060	0.0	0.101
Nitrogen	1.3445	0.02617	0.05046	-0.00691	4.2
Oxygen	1.4911	0.02562	0.04624	0.004208	4.8
Propane	11.9200	0.07321	0.18100	0.04293	120.00

Units: Pressure in atmospheres; volume in liters/gm-mole; temperature in ^{o}K; R = 0.08206 atm-liters/gm-mole - ^{o}K

4.3.6 Heat Transfer

Although the heat pipe has been frequently considered an isothermal heat transfer device, a thermal gradient must always exist between the heat input and output regions during operation. This gradient is determined by the radial heat flux and the thermal conductance of the heat pipe wall and the wick material saturated with the working fluid. The effective conductance of various wick designs is discussed more fully in Section 4.4. As far as the selection of the working fluid is concerned, it is desirable to choose the fluid with the highest thermal conductivity since film coefficients are directly proportional to this property. Liquid phase thermal conductivities for various heat pipe fluids are given in Fig. 4-14. The thermal conductivity of a given fluid tends to decrease with increasing temperature.

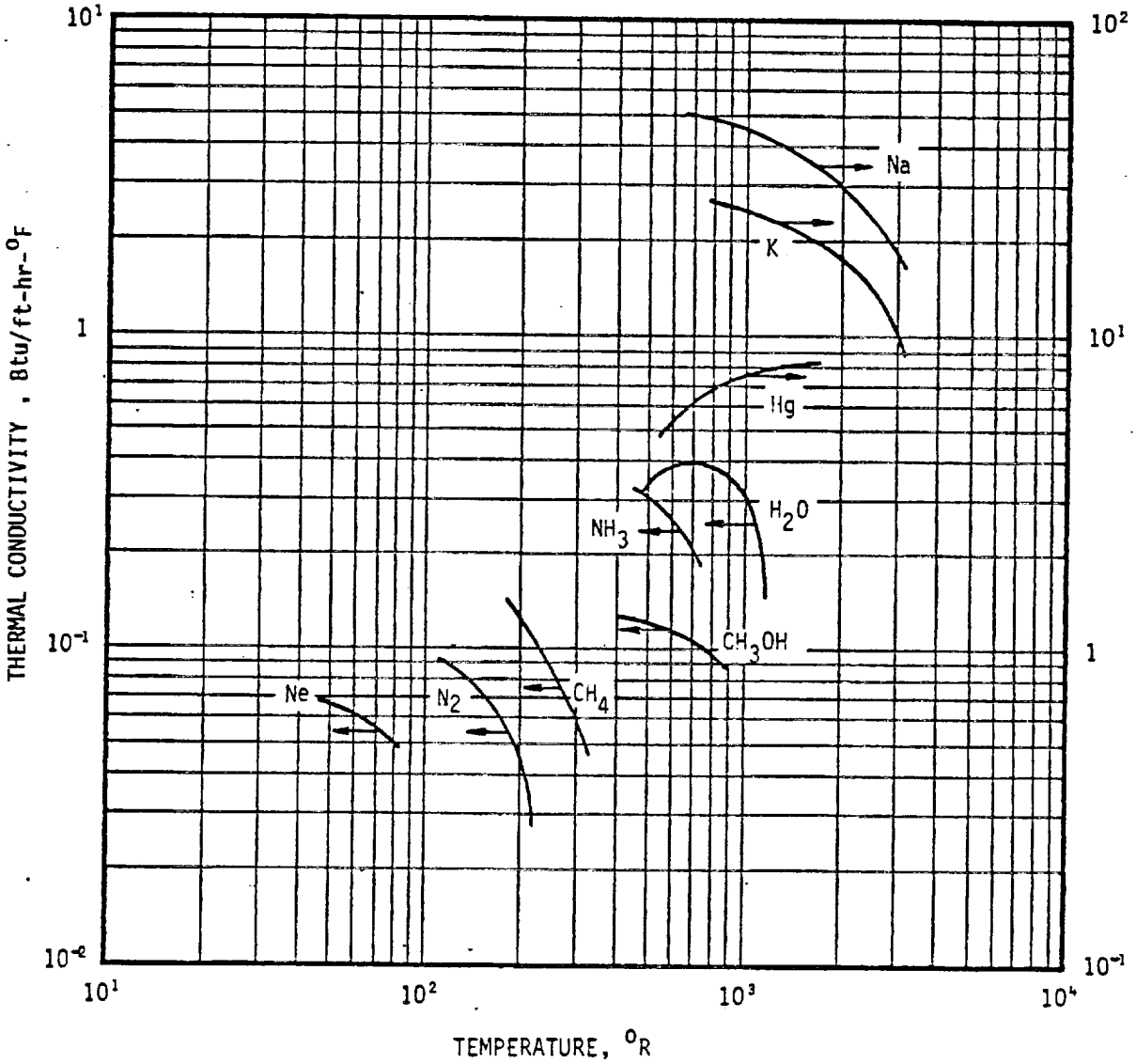

Fig. 4-14. Liquid thermal conductivity for several heat pipe working fluids at saturated state (One °R = 0.5556 °K , 1 Btu/ft-hr-°F =1.730 W/m-°K)

The designer must also consider the radial heat transfer in the evaporator, especially if boiling would seriously degrade hydrodynamic performance. The criteria for nucleation have been discussed in Chapter 2. Assuming the critical radius in Eq. 2-83 for the critical superheat is equal to the wick pore size, the pertinent fluid property grouping for superheat tolerance is $\sigma/(\lambda \rho_\ell)$. This parameter, multiplied by the liquid thermal conductivity, yields a measure of the fluid's radial heat transfer tolerance with respect to nucleation. The Nucleation Tolerance Factor is defined as:

$$N_{TF} \equiv (k \sigma/\lambda \rho)_\ell \qquad (4\text{-}4)$$

and is plotted versus vapor temperature in Fig. 4-15 for selected working fluids. The higher the value of N_{TF} the greater the heat flux that can be tolerated without nucleate boiling.

4.3.7 Fluid Compatibility

A major factor in the selection of a working fluid is its compatibility with other materials in the heat pipe system. In contrast to most corrosion problems, the structural integrity of the tube wall is not the primary consideration. One of the factors that is critical to the performance of a heat pipe is the amount of non-condensible gas that is generated. The gas could result from materials outgassing or chemical reactions. This gas collects in the condensing region and causes condenser blockage. An example of this is the hydrolysis of water which occurs in aluminum/water heat pipes.

Corrosion and erosion of the container and wick can also result in a change in the wetting angle as well as in the permeability, porosity, or capillary pore size of the wick. Solid precipitates resulting from corrosion and erosion are transported by the working fluid to the evaporator region where they are deposited when the liquid vaporizes. This leads to an increased resistance to fluid flow which results in lowering the Heat Flux Limit in the evaporator.

The compatibility and stability of working fluids and heat pipe materials at the intended operating temperatures must be established by testing. A widely used approach to compatibility testing is to employ the actual heat pipe hardware and monitor the rate of gas generated. As mentioned previously, non-condensible gas generated within a heat pipe collects at the end of the condenser, blocking vapor flow and causing a local temperature drop (see Fig. 4-16). Thus, by monitoring the temperature distribution along a heat

pipe operating at constant temperature,the rate of gas generation can be determined. Several such compatibility tests have been performed by many different experimenters and laboratories. Typical results are listed in Table 4-4.

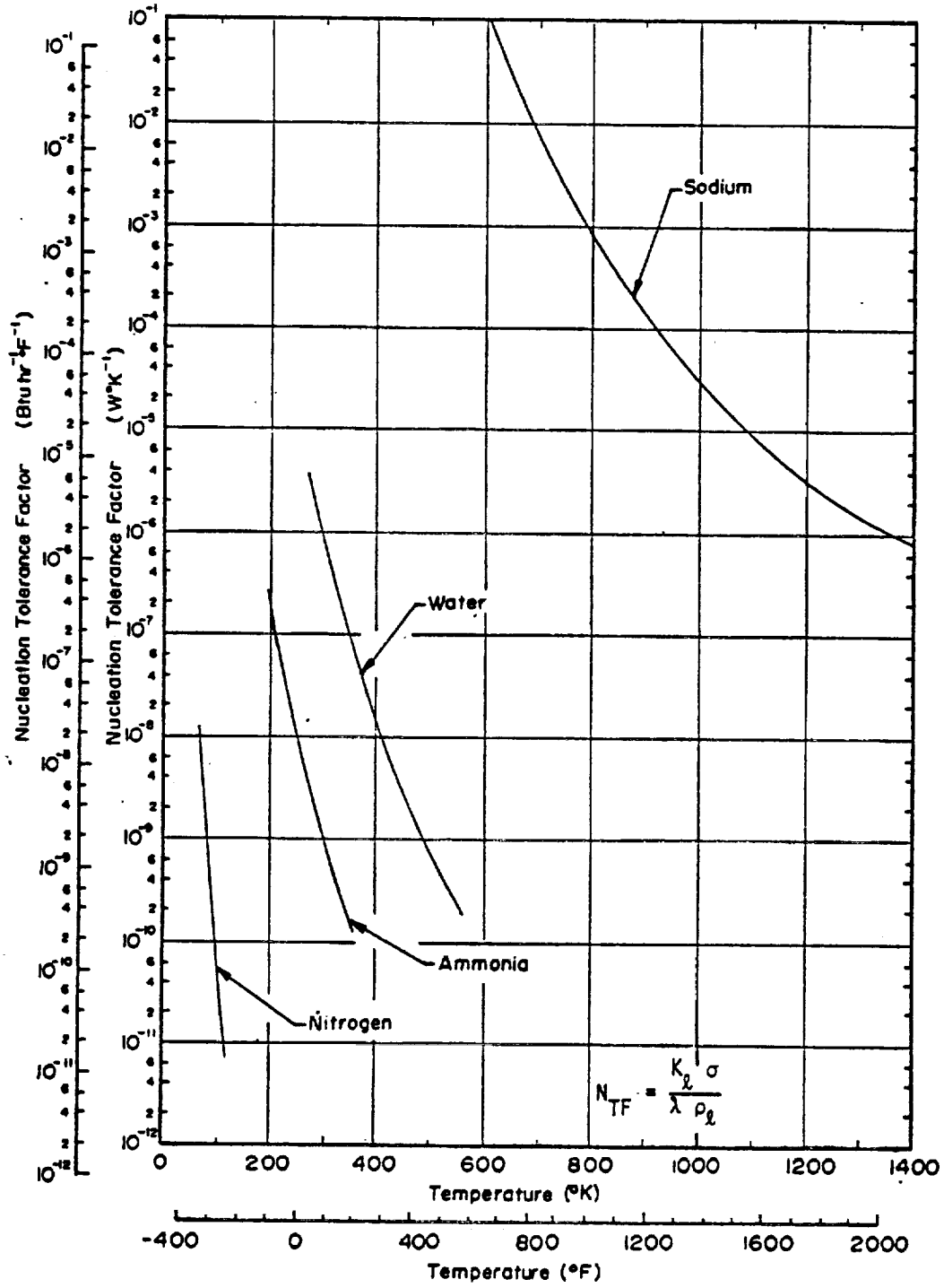

Fig. 4-15. Nucleation tolerance factors of several commonly used working fluids

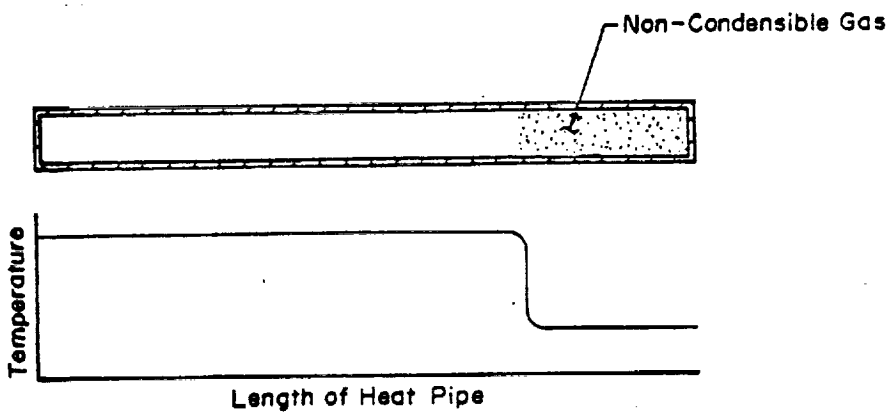

Fig. 4-16. Effect of gas build-up on temperature uniformity of heat pipe

TABLE 4-4. GENERALIZED RESULTS OF EXPERIMENTAL COMPATIBILITY TESTS *

	Aluminum	Stainless Steel	Cold rolled steel	Iron	Copper	Brass	Silica	Nickel	Inconel	Tungsten	Tantalum	Molybdenum	Rhenium	Titanium	Niobium
Water	I	C*			C		C	C	I					C	
Ammonia	C	C	C	C				C							
Methanol	I	C		C	C	C	C	C							
Acetone	C	C			C	C	C								
Freon - 11	C														
Freon - 21	C			C											
Freon - 113	C														
C_6F_6					C		C								
n-butane	C														
n-pentane	C	C													
n-heptane	C														
Benzene	C														
Toluene	I														
Dowtherm A		C			C		C								
Dowtherm E	I	C*	I		C	I									
DC 200	C	C			C			C							
DC 209					C										
Perchloroethylene					C		C								
Dimethyl Sulfide					C		C								
Monsanto CP-9					C		C								
Monsanto CP-32(pyridene)	I				C										
Monsanto CP-34	I														
Lithium		I						I	I	C	C	C		I	C
Sodium		C						C	C					I	C
Potassium								C						I	
Cesium														C	C
Mercury		C#						I	I		I	I		I	I
Lead		I						I	I	C	C			I	I
Indium		I						I	I	I	I	I			I
Silver										C	C		I		

C = Compatible
I = Incompatible
* Sensitive to Cleaning
# I with Austenitic SS

* See Chapter 7 for detailed Compatibility Test Results

4.4 WICK DESIGN

The wick provides the necessary flow area for liquid return from the condenser to the evaporator and also provides the pores required to develop capillary pumping. The properties of the wick are characterized by the permeability K and an effective pumping radius r_p. These properties and the wick cross-sectional area A_w determine the ability of the heat pipe to overcome hydrodynamic losses.

The choice of a wick design for a specific heat pipe application is determined by trade-offs between a number of interrelated parameters. First, the wick should be capable of providing a high capillary pressure which is equivalent to processing a small effective pore radius. Second, it should be capable of supporting high flow rates which means that the wick should have a high permeability and therefore a large effective pore radius. Finally, in many designs, the wick is directly in the heat flow path and therefore its thermal conductivity is an important consideration.

4.4.1 Basic Properties

As was discussed in Chapter 2, often the only way to obtain accurate values for the various properties of wicks is by experimental measurements. However, reasonable estimates for preliminary evaluations can be made for several configurations. Various types of capillary structures which have been employed in the past are illustrated in Fig. 4-17. These include capillary cylinders (tubes) made of porous material such as wire mesh screen, rectangular and annular flow channels also made of porous material, grooves of various geometries formed in the wall of the heat pipe container, matrices of multiple layers of wire mesh screen, packed spheres, and sintered fibers. Typical wick designs employing the above are discussed in Section 4.4.2. Properties for each are summarized in Table 4-5.

Working estimates for values of the effective pore radius (r_p) and permeability can be easily determined for well defined wick geometries such as the cylindrical, rectangular and annular flow channels. These capillaries are characterized by a constant cross-sectional flow area. The effective pore radius and the permeability can be obtained from the following expressions, (2,3):

$$r_p = \frac{2A}{W_p} \qquad (4\text{-}5)$$

$$K = \frac{D_h^2}{2\,(f \cdot Re)} \qquad (4\text{-}6)$$

where:

$D_h = \frac{4A}{W_p}$ Hydraulic Diameter

A = Cross Sectional Flow Area of the Capillary

W_p = Wetted Perimeter

$f \cdot Re$ = The Product of the Fanning Friction Factor and the Reynolds Number

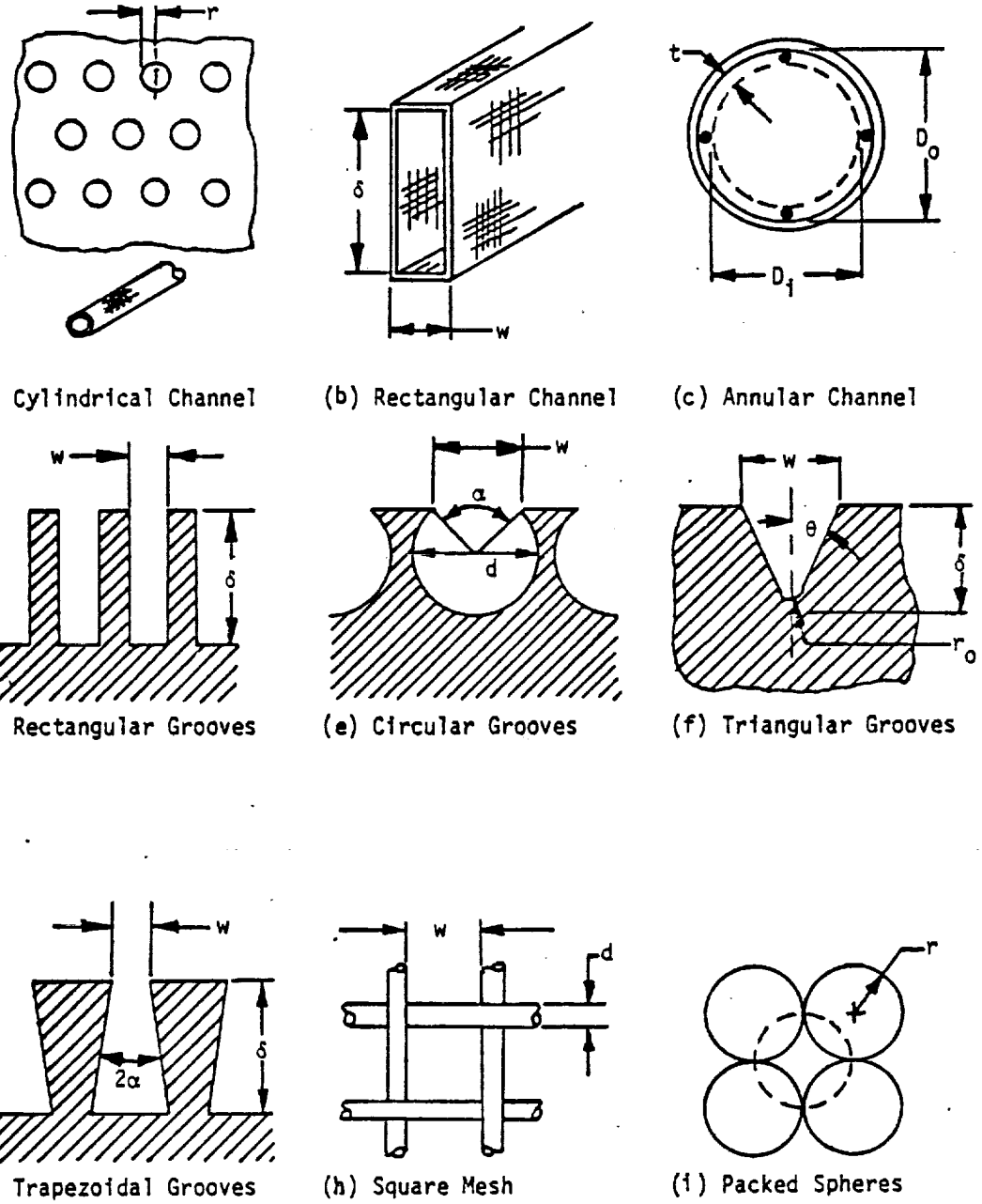

(a) Cylindrical Channel (b) Rectangular Channel (c) Annular Channel

(d) Rectangular Grooves (e) Circular Grooves (f) Triangular Grooves

(g) Trapezoidal Grooves (h) Square Mesh (i) Packed Spheres

Fig. 4-17. Typical capillary wick designs

TABLE 4-5. CAPILLARY PROPERTIES

TYPE	EFFECTIVE PORE RADIUS r_p	PERMEABILITY K	COMMENTS	REFERENCE
1. Cylindrical	r	$r^2/8$	$(f \cdot Re) = 16$	2,3
2. Rectangular	$\frac{w\delta}{\delta+w}$	$\frac{2}{(f \cdot Re)}\left(\frac{w\delta}{\delta+w}\right)^2$	See Fig. 4-17 for $(f \cdot Re)$ values	2,3
3. Annular Channel	t	$\frac{2t^2}{(f \cdot Re)}$	See Fig. 4-18 for $(f \cdot Re)$ values	2,3
4. Rectangular Grooves	W	$.435\left(\frac{\delta}{W}\right)^{3.1}\left(\frac{W}{2\delta+W}\right)^2 \cdot \frac{W^3}{\delta}$	Sharp Corner: $A_w = A_\ell'$; N=No. of grooves ; A_ℓ' = Area Per Groove	4,5,6
5. Circular Grooves	w	$.0221 \frac{d^{2.2}(2\pi-\alpha+\sin\alpha)^{2.1}}{w^{0.2}(2\pi-\alpha)^2}$		4,5,6
6. Triangular Grooves	r_o	------ ------	No empirical values have been developed for triangular grooves	- -
7. Trapezoidal Grooves	w	$0.435 \frac{(w\delta+\delta^2\tan\alpha)^{2.1}}{w^{0.2}\left[\frac{2\delta}{\cos\alpha}(1+\sin\alpha)+w\right]^2}$	Sharp corner: $A_w = A_\ell'$; N=No. of grooves ; A_ℓ' = Area Per Groove	4,5,6
8. Square Wire Mesh	$\frac{W+d}{2}$	$\frac{d^2\varepsilon^3}{122(1-\varepsilon)^3}$		7,8
9. Randomly Packed Spheres	0.41 r	$\frac{(2r)^2\varepsilon^3}{150(1-\varepsilon)^2}$		9,10,11
10. Fibrous Wicks	$\frac{d+\sqrt{32\ K\varepsilon}}{2}$	------ ------	Consult fibrous material suppliers for K and ε values	- -

For laminar flow, which always exists in the liquid phase of a heat pipe, the product (f·Re) is a constant and independent of flow (3) and is only a function of the channel geometry. For cylindrical channels, (f·Re) equals 16 and the permeability is directly proportional to the diameter of the cylinder. For rectangular channels and annuli, (3) (f·Re) can be obtained from Figs. 4-18 and 4-19, respectively.

Although grooves also have well defined geometries, they are open channels characterized by variable flow area and permeability along their length as the meniscus recedes to develop the required capillary pumping. In addition, grooves are also characterized by two effective pumping radii:* one parallel to the flow channel and the other perpendicular to the direction of flow. In rectangular, circular and trapezoidal grooves, as illustrated in Fig. 4-17, the meniscus remains anchored at the groove opening; that is, the meniscus does not recede to the bottom of the groove to develop maximum pumping. For these types of grooves the two effective pumping radii can be determined as follows (4, 5):

$$(r_p)_{\perp} = W \tag{4-7}$$

$$(r_p)_{\parallel} = \frac{2A}{W_p} \tag{4-8}$$

The smaller of the two values determines the capillary pumping limit unless the grooves are sealed at the end in which case $(r_p)_{\perp}$ will govern the capillary pumping limit. Note that sealed grooves can result in a composite pumping effect (see Section 4.4.2). However, this requires that the grooves be fully primed before maximum capillary pumping can be developed (5). A determination of the permeability and effective flow area is a more complex matter requiring integration along the entire length of the groove to account for meniscus recession. A capillary flow factor (N_g) which is defined by Eq. (4-9) has been developed for axial groove geometries (5). Empirical expressions have been developed for N_g using the GAP computer program (6)

$$N_g = \int_{\frac{1}{2}W}^{\infty} \frac{K_x A'_{\ell x}}{R_x^2} \, dR_x \tag{4-9}$$

Where R_x is the effective pumping radius at position x

*The two effective pumping radii should not be confused with the two principal radii of curvature which determine each effective pumping radius.

For grooves with sharp corners at the groove opening

$$N_g = 0.87\left(\frac{A_\ell'}{W^2}\right)^{3.1} \left(\frac{W}{WP}\right)^2 W^3 \qquad (4\text{-}10)$$

For grooves with rounded corners at the groove opening

$$N_g = \left(0.87 - 1.04\,\frac{R_t}{W}\right) \left(\frac{A_\ell'}{W^2}\right)^{\left(3.1 + \frac{2\,R_t}{3\,W}\right)} \left(\frac{W}{WP}\right)^2 W^3 \qquad (4\text{-}11)$$

where A_ℓ' and W_p are the individual groove area and wetted perimeter respectively, associated with a completely filled groove with a flat meniscus. R_t is the radius at the tip of the land (See Fig. 2-6). The permeability (K) can be determined from Eqs. 4-10 and 4-11 as

$$K = \frac{N_g\, r_p}{2\, A_\ell'} \qquad (4\text{-}12)$$

It should be noted that if the rectangular, circular or trapezoidal grooves are open at both ends and nearly closed at the groove opening or covered with porous material such as a wire mesh screen, the effective pumping radius can be obtained from Eq. 4-8, and the permeability can be obtained from Eq. 4-6. If the grooves are sealed at both ends, a composite effect results and the minimum effective pumping radius is that of the groove opening or porous material covering. For triangular and semicircular grooves, R. G. Bressler and P. W. Wyatt (12) performed a numerical evaluation to determine the effective pore radius. Their analytical results, summarized in Table 4-5, agreed well with capillary rise experiments.

A number of variables are introduced in the properties of capillaries made of wire mesh screen, packed spheres and fibrous wicks. These variables include the porosity (ε), packing density, intermeshing in multilayer screens, random sphere and fiber sizes and the effect of tortuosity on flow properties. Because of these variables, properties of these types of capillaries are best established on an experimental basis. Techniques for obtaining experimental properties are discussed in Chapter 8. Table 4-6 summarizes typical data which has been obtained with those techniques.

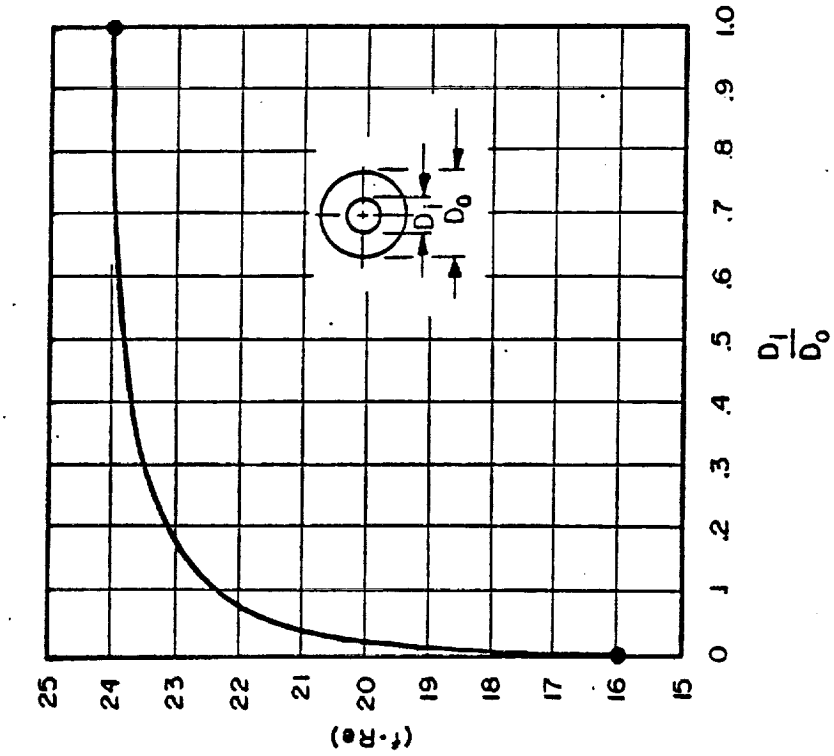

Fig. 4-19. (f·Re) vs. aspect ratio for fully developed laminar flow in circular annuli

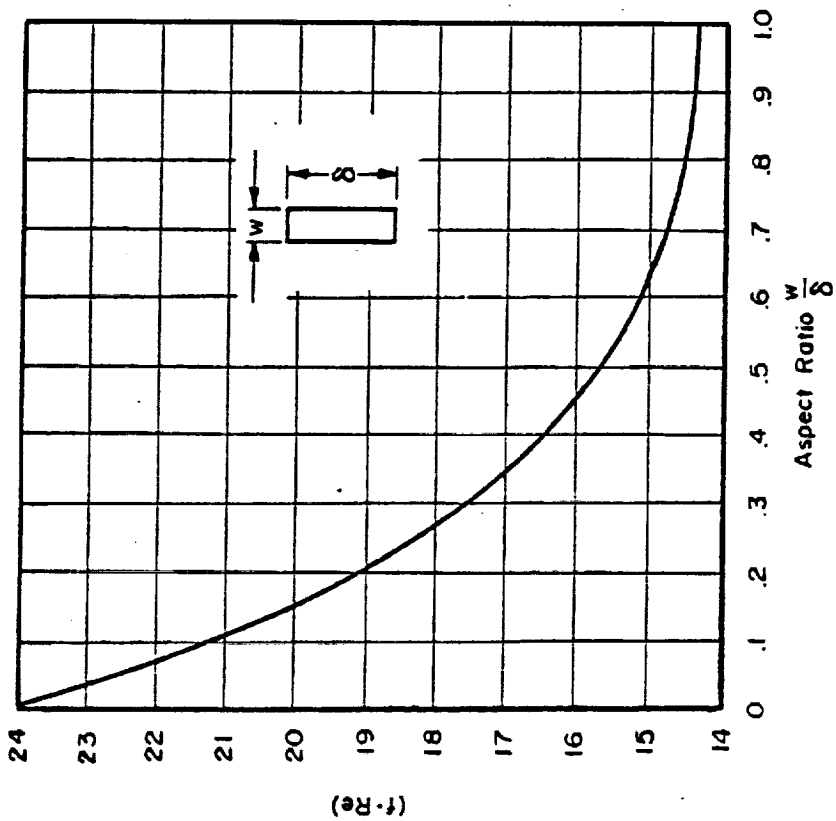

Fig: 4-18. (f·Re) vs. aspect ratio for fully developed laminar flow in rectangular tubes

TABLE 4-6. EXPERIMENTALLY DETERMINED WICK PROPERTIES

No.	Wick Type and Description	Test Liquid	Porosity	$r_p \times 10^6$ m	Method	$K \times 10^{10}$ m^2	Reference
1	Screen, SST, 120 mesh	H_2O		281	R1	3.02	D
2	Screen, SST, 120 mesh, oxddized at 600°C	H_2O		190.9	R1	1.73	D
3	Screen, SST, 200 mesh	H_2O	.733	58	R4	.52	B
4	Screen, SST, 200 mesh	C_6H_6	.733	57	R4		B
5	Screen, SST, 200 mesh	CH_3OH	.733	56	R4		B
6	Screen, SST, 400 mesh	H_2O		29	R3		C
7	Screen, SST, 400 mesh	C_2H_5OH		30	R3		C
8	Screen, SST, 80 x 700, Double Dutch Twill	$(CH_3)_2CHOH$		< 40	R4	.075	J
9	Screen, SST, 165 x 1400, Double Dutch Twill	$(CH_3)_2CHOH$		< 18	R4	.044	J
10	Screen, SST, 200 x 1400, Double Dutch Twill	$(CH_3)_2CHOH$		< 14	R4	.024	J
11	Screen, SST, 250 x 1400, Double Dutch Twill	$(CH_3)_2CHOH$		< 12	R4	.011	J
12	Screen, SST, 325 x 2300, Double Dutch Twill	$(CH_3)_2CHOH$		< 10	R4	.006	J
13	Screen, SST, 375 x 2300, Double Dutch Twill	$(CH_3)_2CHOH$		< 8	R4	.006	J
14	Screen, SST, 450 x 2750, Double Dutch Twill	$(CH_3)_2CHOH$		< 7	R4	.006	J
15	Screen, SST, 670 x 120, Reverse Dutch Twill	$(CH_3)_2CHOH$		< 27	R4		J
16	Screen, SST, 720 x 140, Reverse Dutch Twill	$(CH_3)_2CHOH$		< 21	R4		J
17	Screen, SST, 850 x 155, Reverse Dutch Twill	$(CH_3)_2CHOH$		< 20	R4		J
18	Screen, Nickel, 50 mesh	H_2O		1813	R1	5.81	D

TABLE 4-6. EXPERIMENTALLY DETERMINED WICK PROPERTIES (CONTINUED)

No.	Wick Type and Description	Test Liquid	Porosity	$r_p \times 10^6$ m	Method	$K \times 10^{10}$ m^2	Reference
19	Screen, Nickel, 50 mesh, oxid @ 600°C	H_2O		580.2	R1	6.47	D
20	Screen, Nickel, 50 mesh, sintered	H_2O	.625	305	R1	6.63	A
21	Screen, Nickel, 100 mesh, sintered	H_2O	.679	<131	R1	1.52	A
22	Screen, Nickel, 100 mesh, sintered	H_2O	.678	84	R1		A
23	Screen, Nickel, 200 mesh, sintered	H_2O	.676	64	R1	.77	A
24	Screen, Nickel, 500 mesh	H_2O	.60	12.5	R4		J
25	Screen, Nickel, 1000 mesh	H_2O	.48	13.0	R4		J
26	Screen, Nickel, 1000 mesh	CH_3OH	.48	10.6	R4		J
27	Screen, Nickel, 1500 mesh	H_2O	.36	6.7	R4		J
28	Screen, Nickel, 2000 mesh	H_2O	.22	6.1	R4		H
29	Screen, Nickel, 2000 mesh	CH_3OH	.22	5.3	R4		H
30	Screen, Copper, 60 mesh	H_2O		481	R1	4.20	D
31	Screen, Copper, 60 mesh, oxidized	H_2O		298	R1	2.38	D
32	Screen, Phosphor Bronze, 120 mesh	C_2H_5OH		102	R3		C
33	Screen, Phosphor Bronze, 120 mesh	H_2O		105	R3		C
34	Screen, Phosphor Bronze, 200 mesh	C_2H_5OH		54	R3		C
35	Screen, Phosphor Bronze, 200 mesh	H_2O		60	R3		C
36	Screen, Phosphor Bronze, 250 mesh	C_2H_5OH		51	R3		C

TABLE 4-6. EXPERIMENTALLY DETERMINED WICK PROPERTIES (CONTINUED)

No.	Wick Type and Description	Test Liquid	Porosity	$r_p \times 10^6$ m	Method	$K \times 10^{10}$ m^2	Reference
37	Screen, Phosphor Bronze, 250 mesh	H_2O		48	R3		C
38	Screen, Phosphor Bronze, 270 mesh	C_2H_5OH		41	R3		C
39	Screen, Phosphor Bronze, 270 mesh	H_2O		43	R3		C
40	Screen, Phosphor Bronze, 325 mesh	$C_2 H_5 OH$		32	R3		C
41	Screen, Phosphor Bronze, 325 mesh	H_2O		33	R3		C
42	Felt, Sintered, SST	H_2O	.822	110	R1	11.61	A
43	Felt, Sintered, SST	H_2O	.916	94	R1	5.46	A
44	Felt, Sintered, SST	H_2O	.808	65	R1	1.96	A
45	Felt, 347 SST, C38 (FM 134)	H_2O	.35	49	R1	1.04	L
46	Felt, 347 SST, C38 (FM 123)	H_2O	.35	42.5	R1	.64	L
47	Felt, SST, A-8 (FM 1101, 1106, 1111)	H_2O	.90	26.5	R1	.56	L
48	Felt, SST, A-8 (FM 1102, 1107, 1112)	H_2O	.80	13.5	R1	.087	L
49	Felt, SST, A-8 (FM 1103, 1108)	H_2O	.70	7.5	R1	.028	L
50	Felt, SST, A-8 (FM 1104, 1109)	H_2O	.60	5	R1	.013	L
51	Felt, SST, A-8 (FM 1105, 1110)	H_2O	.40	2.3	R1	.0009	L
52	Felt, 430 SST, B-62 (FM 1305, 1309)	H_2O	.95	260	R1	30.6	L
53	Felt, 430 SST, B-62 (FM 1302, 1306, 1310)	H_2O	.90	191	R1	18.6	L
54	Felt, 430 SST, B-62 (FM 1303, 1307, 1311)	H_2O	.80	120	R1	6.44	L

TABLE 4-6. EXPERIMENTALLY DETERMINED WICK PROPERTIES (CONTINUED)							
No.	Wick Type and Description	Test Liquid	Porosity	$r_p \times 10^6$ m	Method	$K \times 10^{10}$ m^2	Reference
55	Felt, 430 SST, B-62 (FM 1304, 1308, 1312)	H_2O	.60	50	R1	.80	L
56	Felt, Nickel	H_2O	.891	165	R4	5.17	B
57	Felt, Nickel, A30	H_2O	.815	120	R1	.306	D
58	Felt, Nickel, A30 (FM 415)	CH_3OH		55.9	R1	.48	K
59	Felt, Nickel, A-16 (FM 1201, 1205, 1209)	H_2O	.85	40	R1	.88	L
60	Felt, Nickel, A-16 (FM 1205)	H_2O		37.9	R1	1.27	D
61	Felt, Sintered, Nickel	H_2O	.828	< 38	R1		A
62	Felt, Sintered, Nickel	H_2O	.868	< 37	R1	.397	A
63	Felt, Sintered, Nickel	H_2O	.825	< 37	R1	.337	A
64	Felt, Sintered, Nickel	H_2O	.689	< 37	R1	.151	A
65	Felt, Sintered, Nickel	H_2O	.628	< 37	R1		A
66	Felt, Sintered, Nickel	H_2O	.880	<37	R1	.308	A
67	Felt, Sintered, Nickel, A30 (FM 315, 415)	H_2O	.85	37	R1	1.75	L
68	Felt, Sintered, Nickel	H_2O	.709	<36	R1		A
69	Felt, Sintered, Nickel	H_2O	.626	< 35	R1		A
70	Felt, Sintered, Nickel	H_2O	.820	< 32	R1		A
71	Felt, Nickel, A30, oxid @ 600°C	H_2O		32.5	R1		D
72	Felt, Nickel, A16 (FM 1202, 1206, 1210)	H_2O	.80	30	R1	.48	L

TABLE 4-6. EXPERIMENTALLY DETERMINED WICK PROPERTIES (CONTINUED)

No.	Wick Type and Description	Test Liquid	Porosity	$r_p \times 10^6$ m	Method	$K \times 10^{10}$ m^2	Reference
73	Felt, Nickel, A30 (FM 320, 420)	H_2O	.80	25.5	R1	.80	L
74	Felt, Nickel, A16 (FM 1203, 1207, 1211)	H_2O	.70	17	R1	.116	L
75	Felt, Nickel, A16 (FM 1204, 1208, 1212)	H_2O	.60	10.5	R1	.042	L
76	Felt, 347 SS, A30 (FM 627)	H_2O	.55	7	R1	.016	L
77	Felt, Copper	CH_3OH	.895	279	R3		B
78	Felt, Copper	H_2O	.895	229	R4	12.4	B
79	Felt, Copper	C_6H_6	.895	216	R4		B
80	Felt, Copper, FM 1006	H_2O	.80	144	R1	.778	D
81	Felt, Copper, FM 1006, oxid @ 300°C	H_2O	.80	40.6	R1		D
82	Felt, OFHC Copper, A40 (FM 1006)	H_2O	.80	23	R1	.37	L
83	Foam, Nickel, AmPorNik 220-5	CH_3OH	.960	267	R3		B
84	Foam, Nickel, AmPorNik, 220-5	H_2O	.960	229	R4	37.2	B
85	Foam, Nickel, AmPorNik, 220-5	C_6H_6	.960	216	R4		B
86	Foam, Nickel, AmPorNik, 210-5	H_2O	.944	229	R4	27.3	B
87	Foam, Copper, AmPorCop, 210-5	CH_3OH	.945	229	R3		B
88	Foam, Copper, AmPorCop, 210-5	C_6H_6	.945	229	R4		B
89	Foam, Copper, AmPorCop, 210-5	H_2O	.945	216	R4	20.2	B
90	Foam, Copper, AmPorCop, 220-5	H_2O	.912	241	R4	23.2	B

TABLE 4-6. EXPERIMENTALLY DETERMINED WICK PROPERTIES (CONTINUED)

No.	Wick Type and Description	Test Liquid	Porosity	$r_p \times 10^6$ m	Method	$K \times 10^{10}$ m^2	Reference
91	Powder, Sintered, Nickel	H_2O	.696	82	R1		A
92	Powder, Sintered, Nickel	H_2O	.691	69	R1		A
93	Powder, Sintered, Nickel	H_2O	.658	61	R1	2.73	A
94	Powder, Sintered, Nickel	H_2O	.597	58	R1		A
95	Powder, Sintered, Nickel	H_2O		38.7	R1	.07	D
96	Powder, Sintored, Nickel	H_2O	.477	< 31	R1		A
97	Powder, Sintered, Nickel	H_2O	.540	< 36	R1	.808	A
98	Powder, Sintered, Cu	H_2O	.52	9.39	R1	.009	D
99	Deposited Cu		.51			.0234	G
100	Deposited Cu, Bonded		.60			.0255	G
101	Beads, Cu, 20-30 mesh, Sintered	H_2O		175	R1	1.11	K
102	Beads, Monel, 20-30 mesh	H_2O	.40	352	R2		E
103	Beads, Monel, 30-40 mesh	H_2O	.40	252	R2	4.12	E
104	Beads, Monel, 40-50 mesh	H_2O	.40	179	R2	2.31	E
105	Beads, Monel, 50-70 mesh	H_2O	.40	126	R2	1.25	E
106	Beads, Monel, 70-80 mesh	H_2O	.40	96.9	R2	.775	E
107	Beads, Monel, 80-100 mesh	H_2O	.40	81.5	R2	.559	E
108	Beads, Monel, 100-140 mesh	H_2O	.40	63.4	R2	.328	E

TABLE 4-6. EXPERIMENTALLY DETERMINED WICK PROPERTIES (CONTINUED)

No.	Wick Type and Description	Test Liquid	Porosity	$r_p \times 10^6$ m	Method	$K \times 10^{10}$ m^2	Reference
109	Beads, Monel, 140-200 mesh	H_2O	.40	44.5	R2	.110	E
110	SiO_2 Fabric (Refrasil), horizontal	H_2O		16.3	R1	2.37 b	F
111	SiO_2 Fabric (Refrasil), elevated	H_2O		14.6	R1	.0160 b	F
112	Membrane, Nuclepore, 8μ, Polycarbonate	H_2O		7.4	R4		H
113	Membrane, Nuclepore, 8μ, Polycarbonate	CH_3OH		5.0	R4		H
114	Membrane, Nuclepore, 1μ, Polycarbonate	CH_3OH		0.9	R4		H

Notes for Table 4-6

Investigators		Ref. No.
A	Kunz	13
B	Phillips	14
C	Katzoff	15
D	Freggens	16
E	Ferrell	9
F	Farran	17

Investigators		Ref. No.
G	Gould Laboratories	18
H	Dynatherm Corporation	19
J	Kressilk	20
K	Marcus	7
L	Huyck Metals Company	21

Effective Pore Radius Measurement Techniques

R1 Maximum wick height, rising meniscus

R2 Maximum wick height, falling meniscus

R3 Maximum supported column

R4 Air bubble

Permeability was determined by forced flow technique except where noted:

a Gravity flow technique

b Plot of $\frac{dx_a}{dt}$ vs. $\frac{1}{x}$

Empirical expressions developed on the basis of available data are given in Table 4-5. For square wire mesh wicks which are often used in heat pipe design, the spacing between wires (w) is approximately equal to the wire diameter in which case the effective pore radius (r_p) and permeability (K) for this type of wick design can be expressed as (7,8):

$$r_p = d \tag{4-13}$$

$$K = 0.0122\ d^2 \tag{4-14}$$

Where the porosity (ε) used to establish the above permeability is based on an analytical expression developed by Marcus (7) which neglects intermeshing of the wires.

$$\varepsilon = 1 - \frac{\pi S N d}{4} \cong 0.6 \tag{4-15}$$

The dimensionless empirical "Crimping Factor, S" is normally unity if the screen is not tightly wound and the number of wires per inch (N) or mesh size is equal to $\frac{1}{2}$ d for w = d.

4.4.2 Typical Wick Designs

The capillary structures discussed in the preceeding section can be configured in a variety of ways depending on the properties desired for a particular application. Figure 4-20 illustrates some of the more commonly used wick designs, while Table 4-7 presents a "rating" of these wicks in terms of basic performance criteria.

Wick designs are divided into two basic categories: homogeneous and composite. Homogeneous wicks are isotropic structures in which the capillary pumping is derived from effective pore or channel sizes which are uniform throughout the structure. That is, the permeability (K) and the effective pumping radius (r_p) are dependent on the same characteristic property of the wick. Since high capillary pumping is equivalent to possessing small pore radii and low resistance to flow is equivalent to large pore sizes, the design of most homogeneous wicks (non-composite) requires a compromise between these conflicting requirements. Despite the performance limitations imposed by this compromise, homogeneous wick designs are widely used because of their reliability, good start-up under load characteristics, flexibility of application and cost.

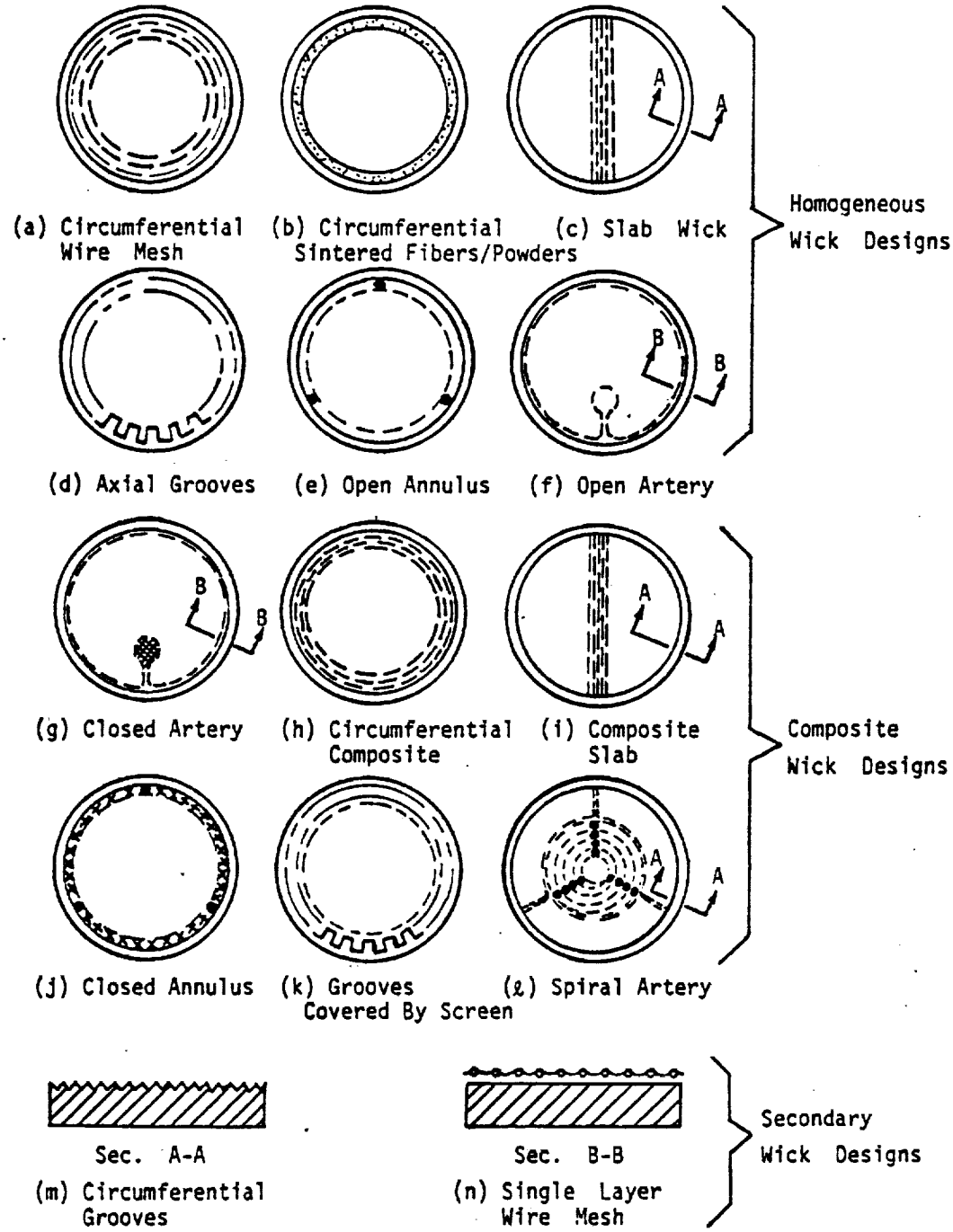

Fig. 4-20. Typical wick designs

TABLE 4-7. WICK SELECTION CRITERIA

	Wick Type	Permeability	Capillary Pumping	Thermal Conductance	Cost Complexity	Reliability	Comments
Homogeneous	a. Circumferential Screen	P-M	G	P	G	G	First Historical Wick
	b. Circumferential Sintered	P-M	G	M	M	G	Screen, Powder, Fiber, Spheres
	c. Slab Wick	P-M	G	G	G	G	With Screw Thread or Single Layer Screen as Circumf. Wick
	d. Axial Grooves	M-G	P	G	M	G	Not Available in All Heat Pipe Materials
	e. Open Annulus	G	P	P	M	G	
	f. Open Artery	G	P	G	M	G	
Composite	g. Closed Artery	G	G	G	P	P	Pedestal, Spiral, or Tunnel Arteries
	h. Circumferential Composite	M	G	M-P	M	P	Conductance Rating Depends on Whether Wick Sintered
	i. Composite Slab	M	G	G	G	P	Not Very Sensitive to "Perfect" Closure of Pumping Wick
	j. Closed Annulus	G	G	P	M-P	P	
	k. Grooves Covered by Screen	M-G	G	G	M-P	P	Not Reduced to Practice
	l. Spiral Artery	M-G	G	G	P	P	

G = Good M = Average P = Poor

The graded-porosity wick (22) is a non-arterial (non-composite) design which tends to offset the competing effects of permeability and pumping and results in optimized fibrous wick designs. With this design the wick porosity is varied such that at every axial location it is only as low as required to insure that the wick remains nearly saturated. Thus the permeability is everywhere as high as possible. The potential increase in capacity over a uniform porosity fibrous wick depends on the particular application, but it can be more than a factor of two greater (22).

Composite wick designs have been investigated for a number of years. Large flow channels in combination with fine capillary structures are used in composite wick designs to independently optimize capillary pumping and permeability. To achieve the resulting high performance, however, the wick structure must be completely "primed". Because vapor or non-condensible gas inclusion or a small saturation pressure differential can prevent complete priming, conventional composite wick designs have proved to be highly unreliable. Techniques to improve priming such as Clapeyron priming (23), meniscus coalescence (24), and jet pump assist (25), have met with various degrees of success as discussed in Section 4.4.2.2. Limited experience with reliable priming techniques, the high cost of such designs, together with operational limitations such as performance during start-up are factors which should be considered in the selection of composite wick designs for any application.

4.4.2.1 Homogeneous Wick Design

Permeability and capillary pumping determine the hydrodynamic heat transport capability of a wick. As stated earlier, a compromise between these two factors is often required in the design of a homogeneous wick. An examination of the equations developed in Chapter 2 for the Heat Transport Capability will show the dependence of this parameter on wick properties. The applicable Eqs. are repeated as:

$$(\dot{Q}L)_{max} = \frac{2 K A_w (1 + n) \cos \theta_c F_\ell N_\ell}{r_p} \qquad (4\text{-}16)$$

where:

$$n = - \frac{r_p D \cos \beta}{2H_\ell \cos \theta_c} + \frac{r_p L \sin \beta}{2H_\ell \cos \theta_c} \qquad (4\text{-}17)$$

$$F_\ell = \frac{1}{1 + \frac{\phi^2}{3}\Psi + \frac{\nu_v}{\nu_\ell}\frac{32\,K}{D^2_{h,v}}\frac{A_w}{A_v}} \qquad (4\text{-}18)$$

with H_ℓ and N_ℓ defined by equations 2-65 and 2-68, respectively.

For all homogeneous wicks except the axial groove, the wick area (A_w) is independent of the capillary properties and, as it can be seen from Table 4-5, the permeability (K) and capillary pumping radius (r_p) can be related by:

$$K \sim r_p^2$$

If vapor losses are neglected ($F_\ell \cong 1$), the dependence on capillary properties can be expressed as follows:

$$(QL)_{max} = \frac{K}{r_p}(1 + n) = r_p\left(1 - \frac{r_p\ h}{2H}\right) \qquad (4\text{-}19)$$

In the absence of gravity ($n = 0$), the wick with the largest practical capillary pore size will yield the best heat transport. For heat pipes which must be operated in gravity for performance verification or as a normal mode of operation, body-forces must be included in the selection of an optimum pore size. Differentiation of Eq. 4-19 yields the following optimum pore size for operation in a 1-g field, ($g = g_o$):

$$(r_p)_{opt} = \frac{H}{h} \qquad (4\text{-}20)$$

For axial grooves, it can be shown that

$$(r_p)_{opt} = (w)_{opt} = \frac{4H}{3h} \qquad (4\text{-}21)$$

Note that, since axial grooves are non-communicating:

$$h = L \sin\beta \qquad (4\text{-}22)$$

where

β = heat pipe elevation angle

and that for all other wicks which communicate with the bottom of the heat pipe:

$$h = L \sin \beta + D \cos \beta \qquad (4\text{-}23)$$

For a 0-g heat pipe application which must be verified in gravity, the optimum pore size should be selected for a test elevation which precludes significant puddle flow contributions. An adverse test elevation of 1.25 mm (0.050 in.) or greater is generally preferred.

Once the required capillary pore size has been identified, the type of wick design suitable for a given application can be selected. Ranges of physical pore sizes, capillary radii and permeabilities for some typical wicks are given in Table 4-8. For reference purposes, the Table also lists the maximum static wicking height $(h)_{max}$ of water at 100°C. The designer is referred to Table 4-5 for the definition of the basic wick properties.

(a) Wire Mesh and Sintered Fibers/Powders Wick Designs

As can be seen from Table 4-8, wicks made of wire mesh screen and sintered fibers or powders can provide fine capillary pore sizes with correspondingly high static wicking heights. On the other hand, these wicks are characterized by low permeability due to the small pore sizes and the relatively tortuous path the liquid must follow. These wicks, therefore, are most suitable for applications where the heat transport capability is not too restrictive and operation against a high elevation is required. Figs. 4-20 a, b, and c, illustrate various typical wire mesh and sintered fibers/powder wick designs. The principle difference between the circumferential and the slab wicks illustrated in Fig. 4-20 is that the circumferential wick offers an ideal vapor flow channel (cylindrical) geometry but requires the heat to be transferred through the wick liquid matrix to the liquid-vapor interface at the evaporator and condenser. This type of wick, therefore, offers minimum vapor flow losses but has low heat transfer coefficients at the evaporator and condenser. The slab wick on the other hand provides efficient heat transfer at the evaporator/condenser but presents higher vapor flow losses. To enhance its heat transfer capability, the slab wick is often used in combination with circumferential grooves or a secondary wick made of a single layer of screen (Fig. 4-20, Sect. A-A & Sect. B-B).

TABLE 4-8. PROPERTIES OF TYPICAL HOMOGENEOUS WICKS

Wick Type	Characteristic Dimension		Effective Capillary Radius		Max. Wicking Height with H_2O at 100°C		Permeability	
	m x 10^{-3}	in x 10^{-3}	m x 10^{-3}	in x 10^{-3}	m x 10^{-3}	inches	m^2 x 10^{-10}	ft^2 x 10^{-12}
30 Mesh Screen	0.50	20	0.43	16.9	29	1.14	25	2.69
100 Mesh Screen	0.14	5.5	0.12	4.7	104	4.1	1.8	0.19
200 Mesh Screen	0.07	2.75	0.063	2.5	197	7.75	0.55	0.059
Sintered Fibers/ Powders	-	-	0.01-0.1	0.4-4.0	1250-125	50-5	0.1-10	0.01-1
Axial Grooves	0.25-1.5	10-60	0.25-1.5	10-60	50-8	2-0.3	35-1250	3.8-135
Open Annulus	0.25-1.5	10-60	0.25-1.5	10-60	50-8	2-0.3	50-2000	5.4-215

With respect to vapor flow losses, the performance of the wick designs illustrated in Figs. 4-20 a, b, and c can be optimized as a function of wick area (A_w) and vapor flow losses (F_ℓ). As can be seen, performance will be limited by liquid flow losses if the wick area is kept small. That is, the performance of the heat pipe goes to zero as the wick area goes to zero. At this point the vapor flow loss factor $F_\ell = 1$. As the wick area is increased, liquid flow losses are reduced but the vapor flow losses are increased. Eventually, the vapor flow loss will dominate and the factor F_ℓ goes to zero as the wick occupies the total cross-sectional area of the heat pipe and the performance goes to zero. Optimum wick area is dependent on a number of factors including the permeability of the wick, the vapor channel(s) geometry and the kinematic viscosity ratio, ν_v/ν_ℓ. Optimum wick design, therefore, is not only dependent on the wick properties but is also dependent on fluid properties as a function of temperature. Figure 4-21 illustrates the optimum performance point which can be obtained with a .00127 m (1/2 inch) diameter heat pipe using ammonia at 273°K and various sizes of wire mesh screens. Optimum operating conditions for both the circumferential wick and the slab wick are illustrated. In determining the optimum wick area, the designer should keep the following points in mind:

(1) Optimization with respect to liquid flow losses is dependent on whether the vapor flow is laminar or turbulent.

(2) Heat pipes are typically required to operate over a temperature range. Optimization should be performed at the low end of the range. (High Vapor Flow losses.)

(3) Fluids for low temperature applications (i.e., cryogenics) tend to have poor liquid transport properties and low kinematic viscosity ratios. Therefore, maximum transport is often achieved with large wick areas.

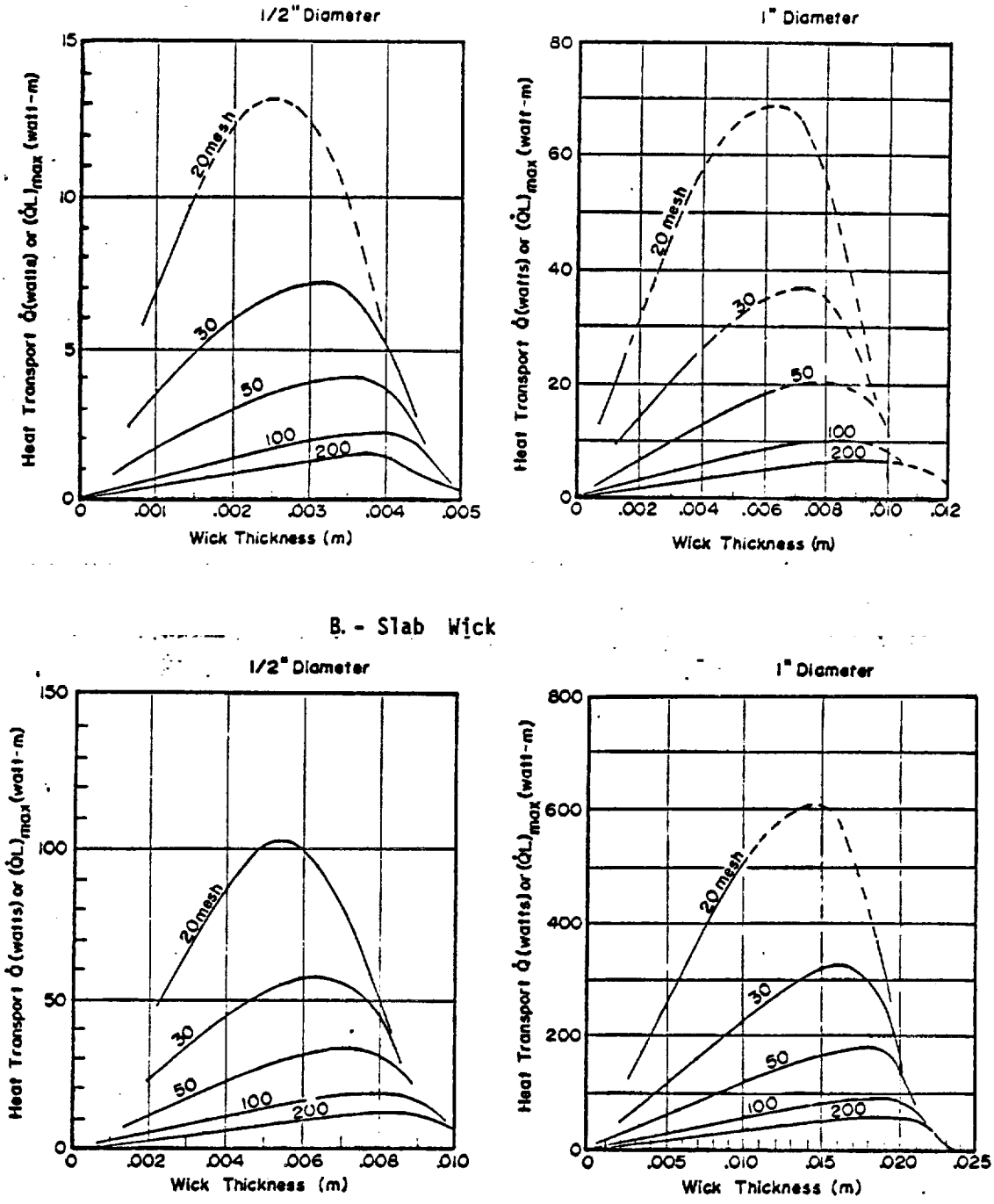

Fig. 4-21. Typical wick area vs. vapor flow optimization...Homogeneous Wicks

(4) Fluids for high temperature applications (i.e., liquid metals) have good liquid transport properties and high kinematic viscosity ratios. Therefore, optimum performance is often achieved with large vapor flow areas.

(5) Other design considerations such as evaporator/condenser heat transfer, pressure containment and fabrication will often influence the design selected resulting in off-optimum performance. For example, a large wick area in a cryogenic heat pipe may result in an excessive pressure containment requirement.

(b) Axially Grooved Wick Designs

For applications where high elevation in gravity is not required and high heat transport performance is desirable, the designer may elect to use wick designs with large open flow channels as illustrated in Fig. 4-20 d, e, & f. The preceeding discussions for optimum pore size determination, wick area optimization, and effect of wick design on thermal conductance also apply to large open flow channel wicks with the exception of axially grooved heat pipes.

The axially grooved wick design differs from other homogeneous wick designs in several important areas. The internal wick configuration consists of a series of parallel flow channels extruded or swaged as an integral part of the tube wall. Each groove is independent of the other and does not communicate with the bottom of the heat pipe. The groove size, therefore, is insensitive to the heat pipe diameter and is dependent only on the heat pipe elevation in a body-force field. Consequently, larger effective capillary sizes can be used in axially grooved designs as compared to other homogeneous wicks; and the performance of an axially grooved heat pipe is only exceeded by the more complex and less reliable composite wick structures. The integral construction also provides high conductance heat transfer paths to the liquid-vapor interface. Axially grooved heat pipes, therefore, can be classified "moderate to high conductance" wick structures.

Several factors should be considered by the designer in the development and evaluation of an axially grooved design. Axial grooves have been successfully produced in a number of materials including aluminum, copper, steel and stainless steel. However, the processes used (extruding and swaging) are limited by the size and the number of grooves that can be produced within a given envelope. Optimization with respect to vapor flow losses, therefore, is often impractical and the designer must optimize his design around fabrication limits. In addition, the axial groove is an open flow channel which is susceptible to liquid-vapor interaction at the groove opening. Finally, the open flow channel allows the liquid meniscus to recede along the length of the heat pipe resulting in a variation in the wick's cross-sectional area (A_w) and permeability (K).

The designer is referred to the results presented in Ref. (4) for an in-depth discussion of axially grooved heat pipe designs, the state-of-the-art of this technology. Extensive analytical modeling for predicting the hydrodynamic behavior including effects of fluid inventory, meniscus recession, liquid-vapor shear interaction and puddle flow effects have been developed in Ref. (6) and are summarized in Chapter 2.

Because of their versatility, simplicity of design, reliability, high heat transport, and high thermal conductance, axially grooved designs have been extensively investigated and developed for aerospace applications. They have been employed in both fixed conductance and thermal control applications including gas controlled variable conductance heat pipes (VCHP) (26), diodes (27), and thermal switches (28). Table 4-9 summarizes the performance of several axially grooved designs which have been developed to date. Their geometries are shown in Fig. 4-22.

TABLE 4-9. TYPICAL AXIALLY GROOVED HEAT PIPE PERFORMANCE

TYPE/FLUID	TEMP. (°K)	o-g HEAT TRANSPORT CAPABILITY (w-m)	STATIC HEIGHT (cm)	FILM COEFFICIENT (w/m^2 C) EVAPORATOR	CONDENSER
SWAGED ALUMINUM					
QAO Geometry					
Ammonia	295	130	1.09	7265	9480
Freon 21	295	28	0.51	1135	1700
Freon 23	295	12	0.46	653	1135
ATS Geometry					
Ammonia	310	145	0.89	5676	8515
Methane	150	18	0.52	1362	--
Nitrogen	80	16	0.30	312	1362
SWAGED COPPER					
LCHPG Geometry					
Water	363	67.6	2.8	--	--
SWAGED STAINLESS STEEL					
Approx. ATS Geometry		Performance Forthcoming			
EXTRUDED ALUMINUM					
ATS Geometry					
Ammonia	273	143	1.6	7000	13600
Methane	125	33.4	1.1	1730	6100
Ethane	200	25	1.3	1370	5900
Lewis Covert Geometry					
Ammonia	293	143	2.51	7300	20500
Methane	120	28	2.13	--	--
Ethane	180	33	2.21	--	--

4.4.2.2 Composite Wick Design

Typical composite wick designs are illustrated in Fig. 4-20. As pointed out earlier, a composite wick is one which uses both small and large capillaries in combination to avoid the compromise between the requirement for small effective pore radii for high capillary pumping and large effective pore radii for high permeability. In the case of arteries or annuli (Fig. 4-20 g, j, & ℓ), the main flow channel is provided by the artery or annulus and the pumping is provided by the fine wire mesh screen which forms the artery or annulus. Composite wicks can also be made by combining coarse and fine wire mesh screen as illustrated in Fig. 4-20 h & i, or by covering the axial grooves with a layer of wire mesh screen. With respect to an axial groove, composite pumping can also be achieved by closing-off the groove opening. The Lewis Covert Groove (Fig. 4-20 f) is such a groove form.

Most of the considerations which are important for homogeneous wick designs also apply to composite wicks. Typical ranges for capillary pumping capability and permeability can be obtained from Table 4-8. The effective capillary radius is that of the fine mesh wick which forms the flow channel and the effective permeability is that of the channel itself. In the case of a wick formed from fine and coarse mesh screen (e.g., composite circumferential and composite slab) the permeability of the coarser screen should be used.

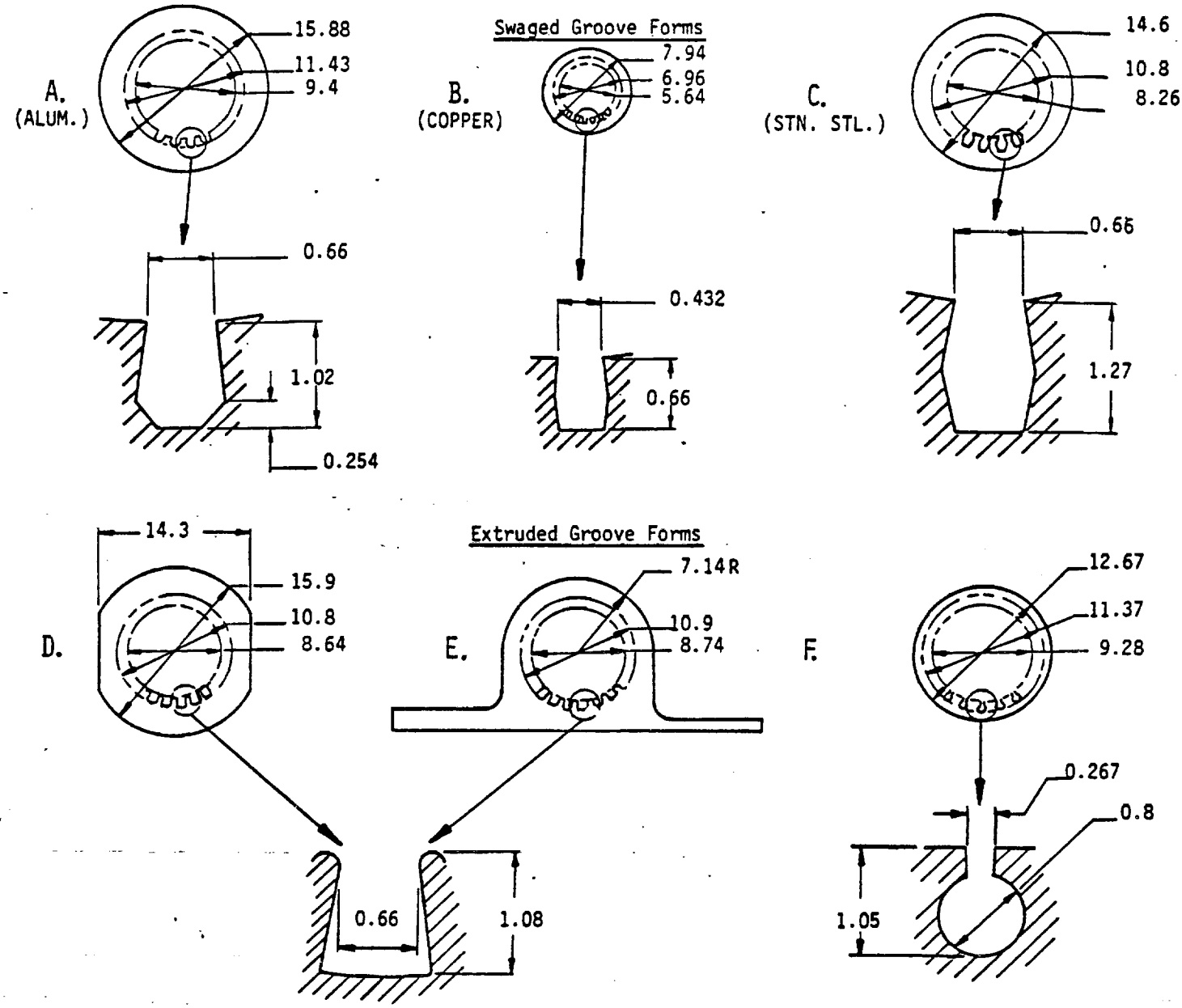

Fig. 4-22. Typical axially grooved heat pipe designs (Dimensions in. mm)

The heat transfer considerations for composite wicks are the same as for homogeneous wicks. The effective heat transfer coefficient is controlled by the thickness of the wick adjacent to the heat input/output surface. As with homogeneous wicks, secondary wicks are often used (Fig. 4-20, Sect. AA & Sect. BB) to minimize the impedance to heat flow in the evaporator and condenser regions. Such secondary wicks also affect the overall heat transport performance of the heat pipe and can become the limiting factor in composite wick designs. Their performance, therefore, should be included in the overall design of a selected wich configuration (see Section 4.4.4).

The composite wick differs from homogeneous wicks in one important aspect--they must be primed. The priming process involves saturating the wick with working fluid either during initial start-up of the heat pipe or after a dry-out. The requirements for priming are:

(1) The capillary pumping of the large flow channel must be sufficient to fill the wick with working fluid at the particular orientation of the heat pipe in a body-force field.

(2) The heat load during priming does not exceed the heat transport capability of the large flow channel.

The self-priming requirement, therefore, establishes an upper limit for the size of the large flow channels, which is similar to the homogeneous wick. In 0-g, the composite wick will always prime as long as the second condition is not violated. But in a 1-g environment, the large flow channels must have a pumping head at least equal to the height of the wick structure. Otherwise, self-priming is impossible in any orientation.

For an annular type composite wick (Fig. 4-20, j) this requirement translates to:

$$\frac{2\sigma \cos\theta}{\delta_{max}} = \rho_\ell \, g \, D_i \qquad (4\text{-}24)$$

where

δ_{max} = the maximum permissible gap

D_i = the internal heat pipe diameter

For a pedestal artery (Fig. 4-20 g), the maximum artery diameter is given by:

$$D_{max} = \frac{1}{2}\left(\sqrt{h^2 + \frac{8\sigma}{\rho_\ell g}} - h\right) \qquad (4\text{-}25)$$

where

h = the height of the pedestal

The maximum theoretical pumping capability of a composite wick can only be realized if the wick is completely filled with liquid. During a partial fill condition, a liquid-vapor interface is located inside the large flow channel. The capillary pumping is thus reduced to a value which corresponds to the effective pore radius of the large flow channel.

This effect is illustrated in Fig. 4-23 for an arterial wick. In Fig. 4-23a, the artery is completely filled with the liquid-vapor interface located in the fine screen, and the maximum capillary pumping corresponds to the pore radius of the screen. In Fig. 4-23b the artery is filled except for a small bubble. The effective pumping radius is now the radius of the bubble. In Fig. 4-23c the bubble has reached its maximum diameter and the effective pumping radius is that of the artery.

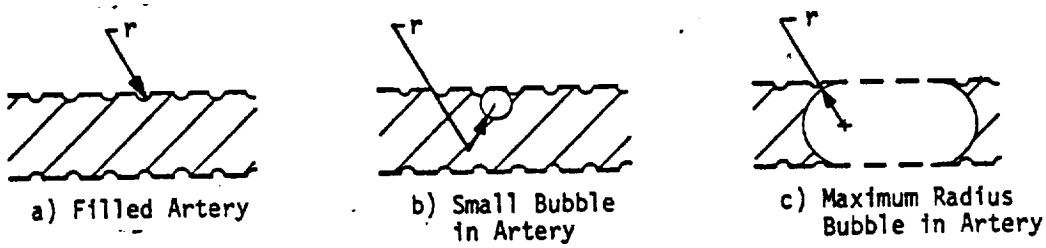

Fig. 4-23. Liquid-vapor interface in arteries

It should be emphasized that the effect of incomplete filling (bubbles) in a composite wick is much more severe than in a homogeneous wick. In the latter, internal voids simply reduce the available liquid flow area but do not affect the capillary pumping. In the composite wick, voids or bubbles will reduce the capillary pumping to a value equal to that of the large flow channel. Incomplete filling can be the result of:

(1) An insufficient amount of working fluid

(2) Nucleation within the composite wick due to excessive local heat fluxes

(3) Entrapment of non-condensible gases.

The formation and stability of voids in composite wicks is not fully understood. Experience has shown that wicks consisting of different mesh size screens are less susceptible to the formation of voids than those with wide open flow channels such as arteries and annuli.

Imperfections in the pumping wick have the same general effect as incomplete filling. The maximum interfacial pressure which the wick can sustain is determined by the largest opening in the pumping wick. Since the maximum interfacial pressure difference exists at the evaporator, imperfections in that region are most damaging to the performance. Close quality control during fabrication of composite wick heat pipes is therefore very important and adds to their cost. Whenever possible, a hydrostatic pressure test should be conducted on the completed wick in order to locate and repair any imperfections.

The unreliable aspects of wick priming have been evaluated by a number of investigators and various techniques to enhance priming have been proposed.

Investigations conducted by Saaski (27) indicate that gas levels in the 10 to 100 parts per million range are sufficient to prevent reliable priming due to blockage by non-condensible gases. Saaski also demonstrated both theoretically and experimentally that the collapse of arterial gas bubble by diffusion, which depends on bubble size and particular conditions, usually takes a long time--often as long as days. Also, it has been demonstrated that under load, conditions can prevail which will cause the expansion of the gas bubbles. Since in practice it is difficult and costly to produce heat pipes with low gas contents and since the introduction of non-condensible gases is necessary in gas controlled variable conductance applications, various priming techniques have been proposed and investigated.

4.4.3 Methods for Priming Composite Wicks

A number of methods for the priming composite wicks have been developed. Pressure priming (Clapeyron priming) (23), Meniscus Coalescence (24), and the Jet Pump Assist (25) are discussed in the next sections.

4.4.3.1 Pressure (Clapeyron) Priming

Although the normal diffusion of non-condensible gas occlusions has been demonstrated as being unsatisfactory to achieve reliable priming of composite wicks, investigations conducted by Saaski indicate that sub-cooling of the condensate can significantly accelerate the loss of non-condensible gas by compressing the gas via the Clapeyron or pressure priming effect. A typical wick design suitable for pressure priming is illustrated in Fig. 4-24. It consists of several layers of fine capillary passages wrapped around a large flow channel (tunnel) wick. The fine capillary passages are sized to self-prime by surface tension even if the tunnel wick is completely drained of liquid. The wick structure is located in the center of the heat pipe envelope and webs are used to connect it with a secondary wick which lines the container wall. When heat is applied to the evaporator, the temperature in the tunnel wick is determined by the temperature of the enclosing liquid contained in the fine capillary passages. Since the liquid leaves the condenser at a sub-cooled temperature relative to the main vapor temperature, the saturation pressure within the tunnel wick is less than the pressure in the main vapor space. This pressure difference can be expressed

by the Clausius-Clapeyron equation which relates temperature and pressure along the saturation line.

$$P_v - P_{v,b} = \frac{P_v \lambda}{R T_v^2} (T_v - T_{v,b}) \qquad (4\text{-}26)$$

where

T_v = Saturation temperature in vapor space

λ = Latent heat

R = Gas constant

$T_{v,b}$ = Saturation temperature in the inclusion

The pressure differential will cause the collapse of any vapor bubbles within the wicks causing the tunnel to be completely filled with liquid or it will compress any non-condensible gas which can significantly accelerate the collapse of the gas inclusion by diffusion. Pressure priming can also provide the necessary driving potential to prime large flow passages which would normally be unable to self-prime in gravity by surface tension. The degree of pressure priming that can be achieved is dependent on the amount of liquid sub-cooling in the condenser and the temperature difference which can be maintained across the wicks. To maintain the high temperature difference across the wick, multiple wraps of fine capillary passages are placed around the tunnel to achieve a high impedance to heat flow. The amount of sub-cooling achieved is dependent on conditions in the condenser. Since heat pipes are typically high conductance devices, significant sub-cooling is not achieved unless significant heat loads are applied. High heat load applications, however, cannot be satisfied until the wick is fully primed. To develop the substantial pressure differential to insure practical pressure priming, heat pipe designs with augmented cooling have been investigated (23). As illustrated in Fig. 4-24, sub-cooling can be achieved by bringing the returning condensate into contact with a secondary heat sink. The vapor phase flow is isolated from this region to insure maximum heat sinking of the liquid.

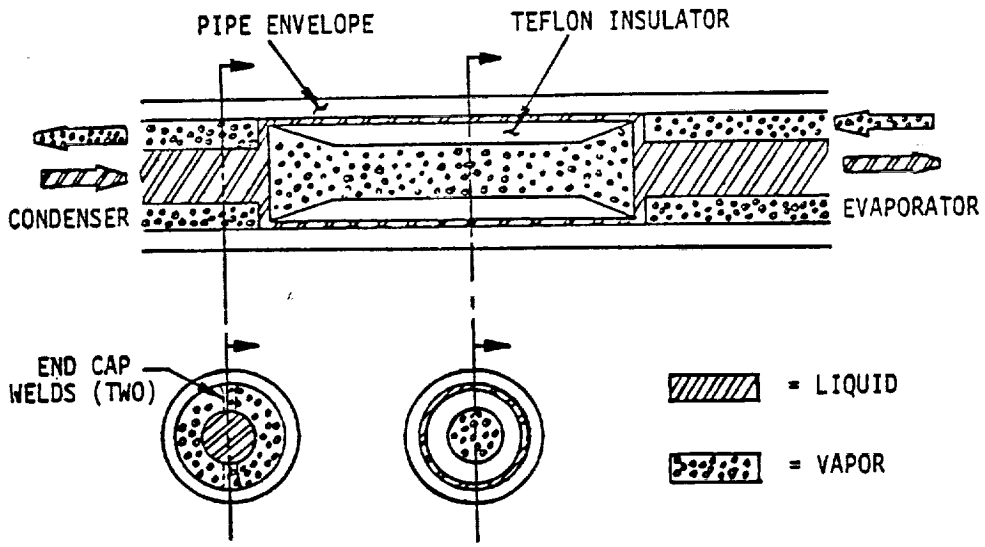

Fig. 4-24. Subcooling section in a pressure-primed wick (23)

4.4.3.2 Meniscus Coalescence

Inclusions are often trapped in a composite wick because the fine capillary structure which forms the larger flow passages will wet or glaze more rapidly than the large flow passages can self-prime. This glazing effect prevents any inclusions from venting and the large flow passages cannot fully self-prime. A method of circumventing the glazing effect is to insert a thin foil into the evaporator end of the wick. This foil contains a pattern of holes to permit venting of gas. If the foil is sized so thin that the menisci coalesce on either side of a liquid plugging the holes (see Fig. 4-25), then the liquid cannot plug the holes in the foil and venting is unimpeded during the priming of the wick (24). The maximum hole size in the priming foil is determined by the capillary pumping required to meet the desired heat pipe performance. This hole diameter in combination with the foil thickness and the diameter of the large flow channel determines the stress level required to achieve meniscus coalescense. Analytical investigations based on the governing equations defined in Fig. 4-25 (24) indicate that the stress level required to achieve meniscus coalescence can be expressed as follows:

$$\bar{s} \geq \frac{2\bar{\delta} - \left(1 - \sqrt{1 - \bar{D}_p^2}\right)}{\left(1-2\bar{\delta}\right)\left(1-\sqrt{1 - \bar{D}_p^2}\right) + 2\bar{\delta}^2} \qquad (4\text{-}27)$$

where:

$\bar{S} = (P_{vs} - P_e)/(4 \sigma \cos \Psi/D_a)$

$\bar{D}_p = D_p \cos \Psi/D_a$

$\bar{\delta} = \delta \cos \Psi/D_a$

D_p = Hole diameter in the priming foil

D_a = Diameter of the artery

δ = Foil thickness

Ψ = Wetting angle

σ = Surface tension

The smallest critical pore diameter $\bar{D}_p$ for which menisci coalescence will occur is given in Fig. 4-25 for given values of foil thickness $\bar{\delta}$ and stress ($\bar{S}$). Note that the above mentioned parameters are dimensionless and that the stress varies from zero to unit. At a value $\bar{S} = 0$, the hole is flooded. In 1-g, this corresponds to the hole just at the surface of a liquid pool. Negative values of $\bar{S}$ correspond to the hole being submerged, and hence theoretically no venting should occur. A value $\bar{S} = 1$ corresponds to the maximum stress that the failed open artery can sustain. Thus if a bubble is entrapped and the stress must be increased greater than $\bar{S} = 1$ for menisci coalescence to occur, when it does occur, the artery will empty of liquid rather than prime.

The value of $\bar{S}$ governs the curvature of the meniscus on the outside of the potential liquid plug in the hole. Thus, for $\bar{S} = 0$ the meniscus is flat, and for $\bar{S} = 1$ the meniscus has the same radius of curvature as the inner meniscus. As a result, for a given hole size $\bar{D}_p$, the required foil thickness for coalescence at $\bar{S} = 0$ is one-half that for $\bar{S} = 1$, which is also apparent in Fig. 4-26.

Several experiments have been conducted to test the theory of menisci coalescence including visual experiments (24), zero gravity tests of two research heat pipes on the sounding-rocket International Heat Pipe Experiment (29), working heat pipes used for the Communications Technology Satellite (30), and a TRW Spacecraft as well as a priming study conducted with a glass heat pipe (31). Results to date indicate good agreement between priming stress factors determined experimentally and the preceding theory. Experience so far indicates that successful priming can be achieved under most but not all conditions.

Entrapment in the condenser zone is one condition under which venting of a non-condensible gas inclusion cannot be accommodated since the condenser end does not have a priming foil. Experiments were conducted with a glass heat pipe (30) to establish the ability to drive the bubble to the evaporator.

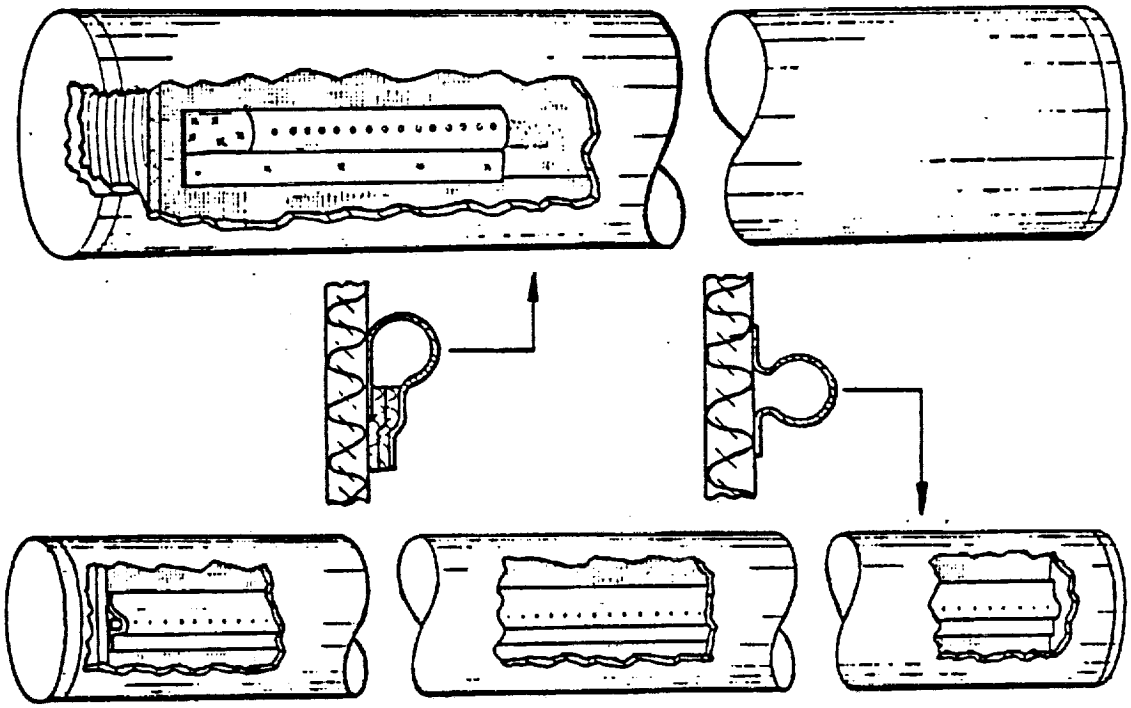

Typical Venting Foil Configurations

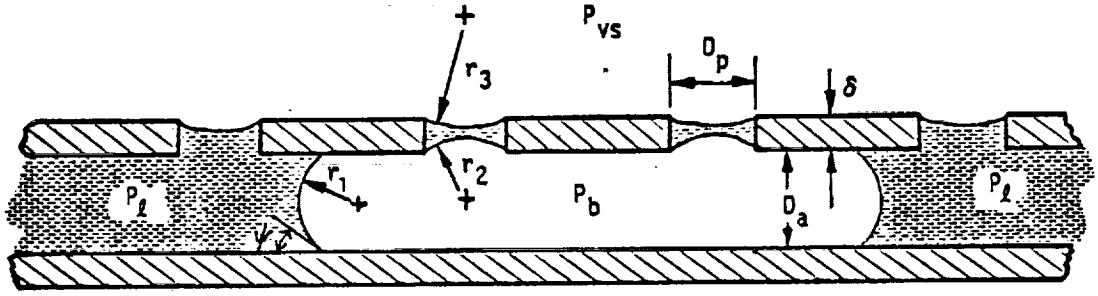

GOVERNING EQUATIONS: $\frac{2\sigma}{r_1} = \frac{2\sigma}{r_2} = P_b - P_\ell$

$$\frac{2\sigma}{r_3} = P_{vs} - P_\ell \qquad r_1 = \frac{D_a}{2\cos\Psi}$$

Fig. 4-25. Menisci coalescence for arterial venting (24)

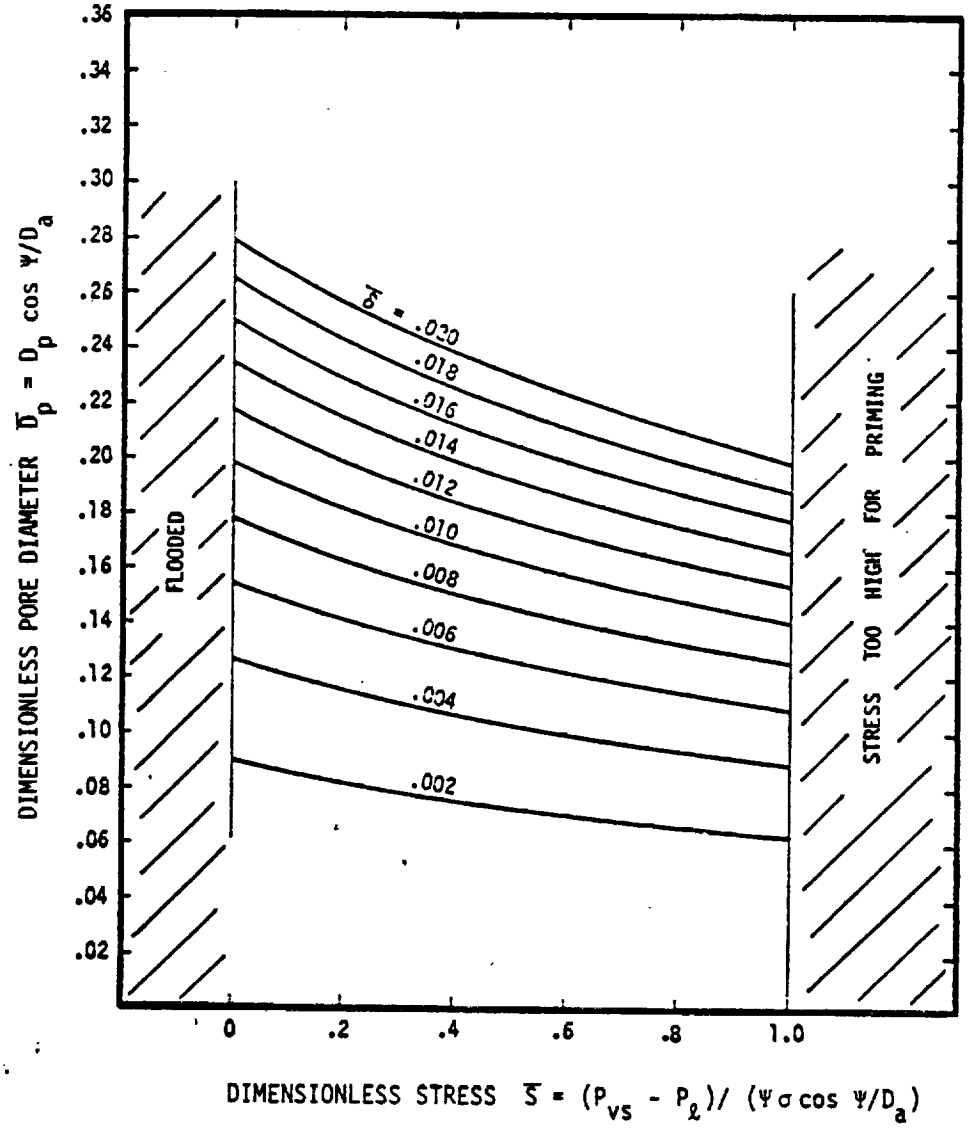

Fig. 4-26. Minimum pore diameter $\bar{D}_p$ vs. stress $\bar{S}$ with the foil thickness as a parameter (24)

Several runs were made for various heat loads and initial bubble sizes and locations. The results indicate that bubble convection was impossible at heat loads and evaporator elevations low enough for priming. Bubbles were observed to convect at heat loads greater than for priming; however, when the bubbles entered the priming foil and vented, the artery would empty of liquid.

As a consequence of these results, for actual heat pipe operation any arterial bubble that might exist would have to be cleared by applying a heat load in excess of the critical priming load, but below the maximum open artery load. Then the load is reduced sufficiently for priming. Another approach is to ignore the existence of any arterial bubble. If a bubble did exist, a burnout would result the first time the heat load was increased above the open artery capacity. Powering down below the critical priming load would result in successful priming because any bubbles would be convected to the evaporator end.

4.4.3.3 Jet Pump Assist

The suction created by a venturi can be utilized to displace and vent vapor or gas inclusions entrapped in a composite wick. Arterial heat pipe designs employing jet pump assist have been investigated by Bienert (25). Reliable operation both with and without a non-condensible gas has been demonstrated with prototype hardware. The concept of the jet pump assisted arterial heat pipe is shown in Fig. 4-27. The jet pump assembly consists of a venturi which separates the vapor in the evaporator from the vapor in the condenser, an injection port at the throat of the venturi, and a suction line which connects the artery with the injection port. During operation, the vapor flowing toward the condenser has to pass through the venturi, and its pressure drops below the saturation pressure in the evaporator. The lowest pressure exists at the throat; most of the pressure drop is recovered in the diverging section of the venturi. Since the artery is connected to the throat, its interior is exposed to the same reduced pressures and vapor and/or gas are pumped from the artery. At the same time, the reduced pressure forces liquid from the condenser into the artery. The pressure difference available for priming is a function of the vapor flow rate (which is synonymous with the heat load) and of the constriction provided by the venturi. Since the jet pump needs a finite vapor flow to generate a pressure difference, the artery must be paralleled by a priming wick. The purpose of this priming wick is to supply liquid to the evaporator before the artery is substantially primed. Sometimes the permeability of the screen from which the artery is formed suffices for this purpose. Occasionally, however, a more substantial priming wick is required.

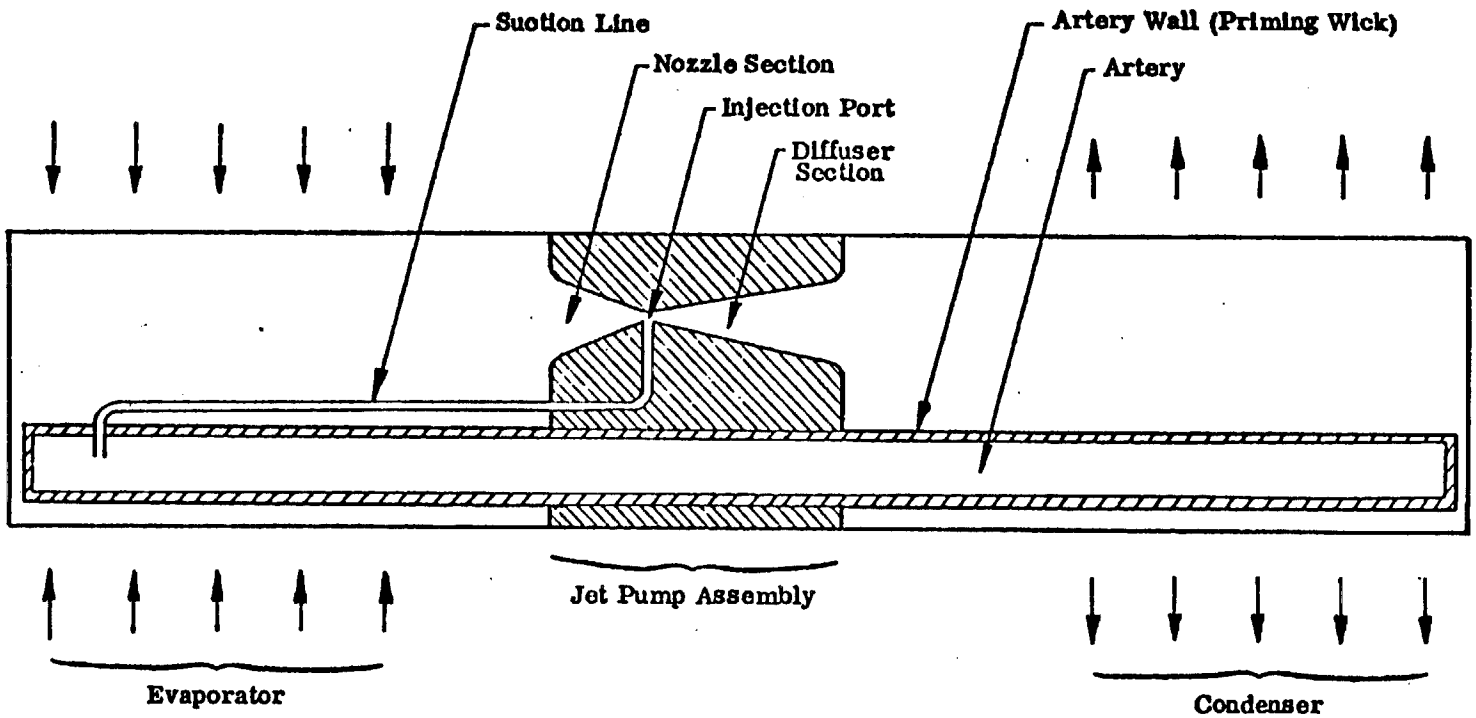

Fig. 4-27. Schematic of jet pump assisted arterial heat pipe (25)

The advantages of the jet pump assist heat pipe are:

(1) No limitations on the artery size since self-priming by surface tension in gravity is not required.

(2) Permits continuous venting of non-condensibles, not only during priming, but as long as vapor flows toward the condenser.

(3) Repriming of the heat pipe can be achieved at a significant fraction of its maximum capacity.

(4) The jet pump assist heat pipe provides stable operation at partially primed conditions.

Some of the disadvantages of the jet pump assist heat pipe are:

(1) Cost and complexity.

(2) Prescribed location of the evaporator/condenser region.

(3) Pressure losses across the venturi which can significantly reduce the performance that can be achieved by capillary pumping.

(4) The need for substantial pumping by the primary wick to provide the necessary priming potential.

4.4.4 Typical Secondary Wick Designs

Secondary wicks are often used in heat pipes to minimize temperature drops at the evaporator and condenser. Such wicks, however, can often significantly affect the performance of the heat pipe especially if they are used in combination with composite wicks. The performance characteristics of secondary wicks, therefore, should be included in the overall evaluation of a heat pipe design.

Figure 4-28 illustrates a typical secondary wick arrangement. Four equally spaced interconnecting bridges are used in the evaporator and condenser sections to interface the centrally located primary wick with the circumferential screw thread grooves on the container wall.

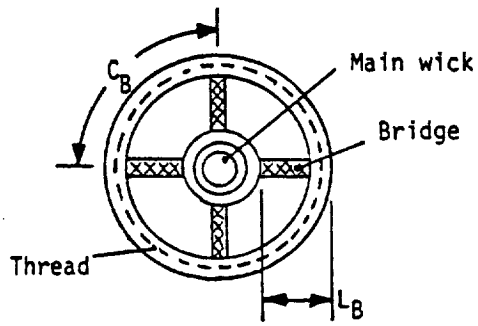

Fig. 4-28. Schematic of a typical secondary wick

In the evaluation of the overall performance of the heat pipe, the hydrodynamic flow and capillary pumping through the individual wick elements must be considered. Each component of the wick system has a characteristic permeability and an effective pumping radius which determine its hydrodynamic heat transport capability. It is seen that the heat transport capability depends on the wick properties as follows:

$$Q \sim \frac{K A}{L} \left(\frac{1}{r_{p1}} - \frac{1}{r_{p2}} \right) \qquad (4\text{-}28)$$

The above equation is in a form which has the appearance of Ohm's law for d.c. circuits and is readily interpreted in terms of a network element resistor of resistance $\frac{L}{K A}$, through which a current Q passes because of the potential difference $\left(\frac{1}{r_{p1}} - \frac{1}{r_{p2}} \right)$. The resistance model of the heat pipe's wick system is shown in Fig. 4-29.

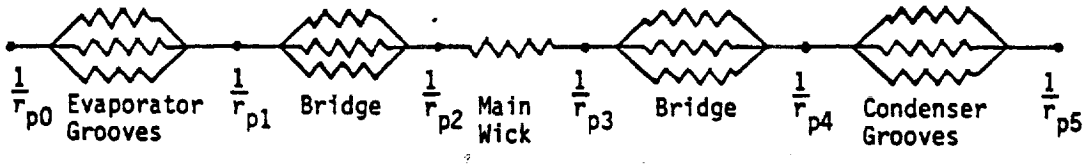

Fig. 4-29. Resistance model for a heat pipe's wick system

The total resistance R of the heat pipe can be expressed as:

$$R = R_{T,e} + R_{B,e} + R_w + R_{B,c} + R_{T,c} \tag{4-29}$$

In the evaporator, $R_{B,e}$ is the equivalent resistance of N_B bridges which can be represented as a system of $N_{B,e}$ resistance in parallel.

$$\frac{1}{R_B} = \sum_{i=1}^{N_B} \frac{1}{R_{B,i}} \tag{4-30}$$

where

$$R_{B,i} = \frac{L_{B,i}}{K_{B,i} \cdot A_{B,i}} \tag{4-31}$$

Since bridges are typically equal resistance paths, then

$$R_{B,e} = \frac{L_B}{N_{B,e} K_B A_B} \tag{4-32}$$

Similarly in the condenser $R_{B,c}$ is given by:

$$R_{B,c} = \frac{L_B}{N_{B,c} K_B A_B} \tag{4-33}$$

In the secondary wick region included between two bridges, heat can flow toward either bridge and the resistance of the region is equivalent to a system of two resistances in parallel. The resistance of each element can be expressed by:

$$R_T = \frac{1}{2} \frac{C_B}{K_T A_T N_T L_e}. \tag{4-34}$$

where for a threaded secondary wick geometry

C_B = the distance between the two bridges

A_T = the cross-section area of the secondary wick

The equivalent resistance of the secondary wick in the evaporator is represented by a system of $2N_B$ resistances R_T in parallel and is given by:

$$R_{T,e} = \frac{R_T}{2N_{B,e}} = \frac{C_{B,e}}{4N_{B,e} K_T A_T N_T L_e} \tag{4-35}$$

Similarly, the equivalent resistance of the secondary wick in the condenser is expressed by:

$$R_{T,c} = \frac{C_{B,c}}{4N_{B,c} K_T A_T N_T L_c} \tag{4-36}$$

The resistance of the main wick is given as:

$$R_w = \frac{L_{eff}}{K_w A_w} \tag{4-37}$$

where

$$L_{eff} = \frac{1}{2} L_e + L_a + \frac{1}{2} L_c$$

The heat transport capability of the heat pipe is defined by the simultaneous solution of the system of individual transport equations. As illustrated in the wick system schematic in Fig. 4-29, the pumping radii of the various wick elements are equal at common interfaces. Additionally, these radii adjust to provide uniform heat transport across each element within the system, therefore:

$$Q = \frac{2N_B}{R_T}\left(\frac{1}{r_{p0}} - \frac{1}{r_{p1}}\right) = \frac{N_B}{R_B}\left(\frac{1}{r_{p1}} - \frac{1}{r_{p2}}\right) = \frac{1}{R_w}\left(\frac{1}{r_{p2}} - \frac{1}{r_{p3}}\right) = \frac{N_B}{R_B}\left(\frac{1}{r_{p3}} - \frac{1}{r_{p4}}\right) = \frac{2N_B}{R_T}\left(\frac{1}{r_{p4}} - \frac{1}{r_{p5}}\right) \tag{4-38}$$

If the maximum heat transport of the wick system requires a pumping radius at the bridge interface (r_{p1}) which is greater than the pore radius of the fine mesh screen used for the bridges and the main wick envelope, the secondary wick is limiting. If the secondary wick is capable of providing the maximum heat pipe transport with a value of (r_{p1}) which is less than the fine mesh pore radius, the main wick is limiting.

4.4.5 Thermal Conductance

As indicated above, thermal conductance is an important factor in the selection of a wick design. The third column in Table 4-9 rates the various wicks in terms of thermal conductance. The primary concern is the heat transfer at the evaporator and condenser since the temperature drop within the vapor is usually negligible. The thermal conductance is not only a property of the wick but also depends directly on the thermal conductivity of the working fluid. With respect to their conductivity, all fluids can be divided into two groups--non-conducting fluids and liquid metals. The range of thermal conductivities for both groups is:

Low Conductivity Fluids: 0.1 - 0.7 W/m-^{o}K (0.06 - 0.04 Btu/Hr-Ft-^{o}F)

Liquid Metals : 10 - 200 W/m-^{o}K (5.8 - 115 Btu/Hr-Ft-^{o}F)

Because the difference in thermal conductivities between low conductivity fluids and liquid metals is more than an order of magnitude, different considerations apply to the two groups. In liquid metal heat pipes, one is seldom concerned with the conductance of the wick itself since the high conductivity of the fluid provides for high heat transfer coefficients even for fairly thick layers of wick. But for heat pipes containing low conductivity fluids, the effective conductance is strongly dependent on the wick design.

A simplified model for the heat transfer process at the evaporator and the condenser assumes that heat is conducted through the heat pipe wall and through the wick/liquid matrix to the liquid-vapor interface where evaporation occurs. More complex models, such as the recession of the liquid-vapor interface into the wick and/or nucleate boiling within the wick, have been proposed but are not sufficiently refined to be used for design purposes.

The conduction model can be used to calculate an effective heat transfer coefficient at the evaporator and condenser which is, (excluding the contribution of the wall):

$$h_{int} = \frac{k_{eff}}{t} \qquad (4\text{-}39)$$

where

k_{eff} = The effective thermal conductivity of the wick liquid matrix

t_w = Wick thickness

From Eq. 4-39 it is evident that high conductance can only be achieved if the thickness of the wick adjacent to the evaporation and condensation surfaces is kept at a minimum. This requirement has led to the development of "high conductance" wick structures in which the main transport wick is removed from the wall and only a thin secondary wick is used for circumferential distribution of the working fluid. Examples of such high conductance wicks are: the porous slab and the arterial wick, in both the conventional and the composite configuration.

The effective thermal conductivity of the wick/liquid matrix is bracketed by the series and the parallel path conduction models (Section 2.8) which is repeated here for easy reference:

$$K_w = \frac{K_s K_\ell}{\varepsilon K_s + (1 - \varepsilon) K_\ell} \qquad \text{(Series Paths)} \qquad (4\text{-}40)$$

$$K_w = (1 - \varepsilon K_s) + \varepsilon K_\ell \qquad \text{(Parallel Paths)} \qquad (4\text{-}41)$$

As a general rule, the series path conduction model will apply for wicks which are only in mechanical contact; e.g., wraps of screen, packed particles, fibers, or spheres. Sintered wicks, on the other hand, will have an effective conductivity which is better approximated using the parallel path model. Typical heat transfer coefficients for heat pipes containing non-conduction working fluids are summarized in Table 4-10.

The effective conductance of grooves, which are integral parts of the heat pipe envelope, are not described by either of the above models.

For axial grooves, Kamotani (32) suggests the following:

$$h_e = \frac{N K_\ell}{2\pi R_v} \frac{1}{.0701 + \frac{K_\ell}{K_w}\frac{\delta}{t_f}} \qquad \text{(Evaporator)} \qquad (4\text{-}42)$$

$$h_c = \frac{N K_\ell}{2\pi R_v} \frac{1}{.0221 + \frac{K_\ell}{K_w}\frac{\delta}{t_f}} \qquad \text{(Condenser)} \qquad (4\text{-}43)$$

where:

K_ℓ = Liquid thermal conductivity

K_w = Thermal conductivity of pipe wall

N = Number of grooves

δ = Groove depth

$\bar{t}_f$ = Average land thickness

TABLE 4-10. TYPICAL HEAT TRANSFER COEFFICIENTS FOR HEAT PIPES

	Wall Material/Type	Heat Transfer Coefficients		Comments
		$W/m^2-{}^oK$	$Btu/Hr-Ft^2-{}^oF$	
Heat Pipe Envelope	Aluminum	173,000	100,000	0.89×10^{-3}m (0.035 in) wall
	Copper	440,000	250,000	0.89×10^{-3}m (0.035 in) wall
	Stainless 316	24,000	14,000	0.89×10^{-3}m (0.035 in) wall
	Molybdenum	154,000	89,000	0.89×10^{-3}m (0.035 in) wall
Wicks	Multilayer Screen	600-1000	100-170	10^{-3}m (0.040 in) Thick SST Wick - Non-Conducting Fluid
	Sintered Wick	4700-6700	830-1180	2.25×10^{-3}m (0.09 in) Circular Wick - Water (10)
	Secondary Wick (Single Layer)	3000-9000	350-1600	200 Mesh Screen Non-Conducting Fluid
	Grooves	3000-15000	500-2500	Aluminum Wall 20-200 Grooves/inch

4.4.6 Wick Fabrication

One final important criterion (last column, Table 4-7) for selecting a wick is its fabricability and the corresponding cost to manufacture. This criterion is highly subjective since its importance depends a great deal on the application. For example, in a heat pipe which is intended to protect a vital component of an expensive spacecraft, cost will be of secondary importance when judged against performance and reliability. On the other hand, heat pipes which are designed for mass production must contain wicks which can be manufactured at low cost.

As a general rule, those wicks which are simple to install and do not require precise process control to manufacture are usually the least expensive. Multiple wraps of screen, layers of fibrous material, or slabs of porous material fall into this category. Wicks which are individually assembled such as arteries, annuli, etc., are high cost wicks. Sintered wicks are medium cost wicks, and their cost will depend to a large extent on the available process. They are expensive in small quantities but can be much less expensive when mass produced. The cost of grooved tubing is determined by the material and the groove geometry. Grooves can be extruded or swaged rather inexpensively in aluminum, copper and other ductile materials. Grooved aluminum tubing is moderately expensive in small quantities because of prorated die costs, while in large quantities it can be produced inexpensively.

For axially grooved tubing, experience to date indicates that the extrusion process is the best method for producing aluminum tubing. Well defined groove forms and good dimensional control have been achieved. Mounting flanges can be extruded as an integral part of the tubing which can simplify interfacing in many applications. In addition, the ability to produce complex groove forms has been demonstrated by the NASA Lewis Covert Groove extrusion which should lead to higher performance and greatly reduce sensitivity to 1-g testing. For the intermediate to high temperature range, however, axially grooved tubing of materials such as copper and its alloys, stainless steel, carbon steels and super alloys are required, and the swaging process is the only known process which can effectively be used today to produce axially grooved tubing in these materials on a cost effective basis.

4.5 CONTAINER DESIGN

The heat pipe container is a leak tight enclosure which isolates the working fluid from the outside environment, mechanically retains the wick structure in position and provides the necessary interface with the heat source and heat sink. A variety of shapes, sizes, and configurations have been developed for different applications including flat plates, rectangular shapes, conical and annular geometries. The tubular geometry made of tubing or pipe materials is the most common configuration employed in heat pipe designs and the following section addresses itself primarily to this cross-section. The design considerations discussed, however, are basic and can be applied to the design of any shape or geometry. The basic container design considerations are as follows:

(1) Structural integrity and leak tight containment of the working fluid

(2) Compatibility with the working fluid and the external environment

(3) External interfacing with the heat source(s) and heat sink(s)

(4) Internal size and geometry suitable for liquid and vapor flow requirement

(5) Fabrication considerations including machining, forming, cleaning, welding and charging

(6) Heat transfer consideration as it applies to the external interface, conduction through the container wall and the evaporator/condensation processes within the heat pipe

The size and internal geometry of the container is dependent on the requirements of the selected wick structure, the vapor flow area requirement, heat transfer considerations, external interface requirements and leak tight pressure containment of the working fluids. Design considerations with respect to container material selection, pressure retention and external interface are discussed in the next sections.

4.5.1 Material Selection

The material selected for the construction of the heat pipe container must be compatible with the working fluid and the external environment. In addition, the material must provide sufficient strength for the retention of the vapor pressure, good thermal conductivity and it must provide satisfactory fabrication properties.

Since leak tight pressure retention of the working fluid is paramount to reliable, long-term operation of the heat pipe, the material selected must provide adequate strength, it must be non-porous to prevent diffusion of gases or working fluid vapor and it must be easily sealed. The strength properties of typical heat pipe container materials are summarized in Fig. 4-30 (33). Joining (welding, brazing, etc.) characteristics are summarized in Table 4-11. For applications where the container must retain substantial internal pressure and where personnel safety is critical, such as heat pipes shipped via commercial carriers, it is recommended (34) that the ASME Boiler and Pressure Vessel Code, 1965 (35) be the principal source of material properties and allowable stresses for use in the structural analysis and design of heat pipes. Additional information can be obtained from sources such as MIL-HDBK-5B (36) the American Society Metals Handbook (37) and the Mechanical Engineers' Handbook (38).

The ASME code specifies that the maximum allowable stress at any temperature be one-quarter of the material's ultimate tensile strength F_{tu}, at that temperature. Material properties and allowable stresses for the two most commonly used heat pipe materials (6061-T6 aluminum alloy and 304 stainless steel) are given in Table 4-12. These values were excerpted from the ASME Code; similar tables can be constructed for other ductile materials listed in MIL-HDBK-5B for military or aerospace applications. For reference purposes, maximum allowable stresses as a function of temperature for various materials are given in Fig. 4-30.

Allowable stresses for welded tubing are also given in Table 4-12. The ASME Code specifies that welds of the type which would be used on heat pipes shall be double-welded (i.e., both sides), fully radiographed butt joints. The allowable stresses in Table 4-12 refer to this type of weld. The code permits the use of single-welded, fully radiographed butt joints if they can be shown to be of the same quality as the double-welded joints. Since the quality of single-welded joints in thinner gauge materials can be shown to have the same quality as the double-welded (and since double welding is completely impractical on small-diameter tubes), single-welded, fully radiographed butt joints discussed in Section 4.5.2.3 are considered to have a strength equal to that of a double-welded joint.

Normally, the temperature drop through a heat pipe wall is negligible even if low conductivity materials are used because the conductance path (wall thickness) is often very small. However, if thick walls are required for pressure retention and if the application consists of concentrated local heat loads, a high thermal conductivity material may be

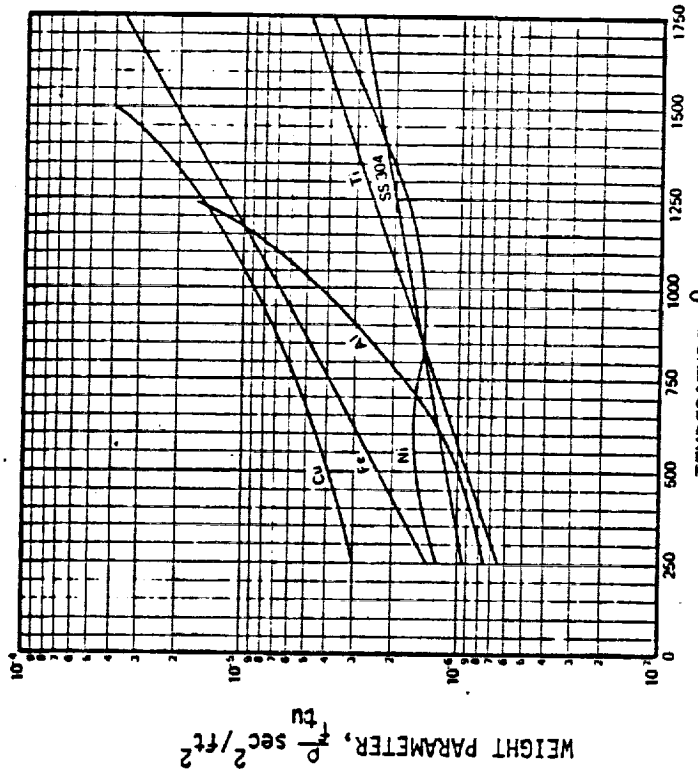

Fig. 4-31. Material weight parameter versus temperature for several heat pipe materials (1 sec^2/ft^2 = 10.76 sec^2/m^2; 1 ^{0}R = 0.5556^{0}K) (33)

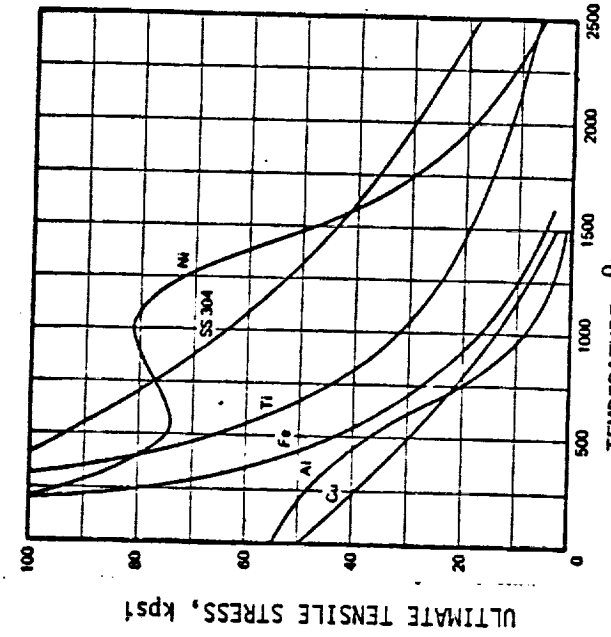

Fig. 4-30. Ultimate tensile strength of several solid materials, (1^0 R=0.5556 ^{0}K, 1 kpsi = 6.895 x 10^6 N/m^2) (33)

TABLE 4-11. CONTAINER MATERIAL FABRICATION PROPERTIES

MATERIAL	MACHINABILITY	WELDING	JOINING	FORMING
6063 Aluminum	Good	Good	Poor	Good
6061 Aluminum	Good	Good	Poor	Good
304 Stainless Steel	Fair	Good	Good	Poor
316 Stainless Steel	Fair	Good	Good	Poor
A-178 Carbon Steel	Good	Good	Good	Fair
Copper (CDA-101)	Fair	Good	Good	Fair/Good

TABLE 4-12. MAXIMUM ALLOWABLE STRESSES (34)

	Ultimate tensile strength, F_{tu} at 100°F	Tensile yield strength, F_{ty} at 100°F	Maximum allowable stress at temperature, ksi				Modulus of elasticity, E	Coefficient of thermal expansion
			100°F	150°F	200°F	400°F		
Aluminum drawn tube (seamless)[a]								
• 6061 -T6	42 ksi	35 ksi	10.5	10.2	9.9	—	10.5×10^6 psi	13.0×10^{-6} in./°F
• 6061 -T6 welded[b]	24	(14)[d]	6.0	5.9	5.7	—		
• 6063 -T6	33	28	8.25	7.8	7.5	—		
• 6063 -T6 welded[b]	17	(11)[d]	4.25	4.20	4.0	—		
Aluminum seamless pipe and extruded tube[a]								
• 6061 -T6	38 ksi	35 ksi	9.5	9.2	9.0	—	10.5×10^6 psi	13.0×10^{-6} in./°F
• 6061 -T6 welded[b]	24	(14)[d]	6.0	5.9	5.7	—		
• 6063 -T6	30	25	7.5	7.1	6.8	—		
• 6063 -T6 welded[b]	17	(11)[d]	4.25	4.2	4.0	—		
High alloy steel[c] seamless pipe and tube								
• TP 304 (18-8)	75 ksi	35	18.75	17.85	17.00	15.45	29×10^6 psi	8.5×10^{-6} in./°F
• TP 304L (18-8)	70	35	17.50	17.25	17.00	15.00		

[a] Excerpted from Table UNF-23 of Section VIII, ASME Unfired Pressure Vessels (ref. 22)

[b] These allowables apply to doubled welded, fully radiographed butt joints as per the ASME code. Refer to discussion in materials section.

[c] Excerpted from Table UHA-23 of Section VIII

[d] From reference 29

preferred. Fig. 4-32 summarizes typical thermal conductivities of various metals as a function of temperature. Note that the thermal conductivity of various metals is affected differently by temperature and that the most significant change in properties occurs in the cryogenic temperature range. Other material properties such as weight to strength ratio (weight parameter) and density are given in Figs. 4-31 and 4-34, respectively.

Fabrication of the container must be considered in the selection of the materials. Joining (welding, brazing, etc.), machining, forming, extruding, sintering, and cleaning are typical processes employed in the manufacturing of the heat pipe. The relative workability of typical heat pipe container materials is given in Table 4-11. For certain heat pipe designs, such as axially grooved tubing, fabrication is the dominant factor affecting the performance that can be realized. The extrusion process is typically used to form axial grooves in aluminum alloys and swaging has been successfully employed in forming grooves in aluminum alloys, copper and its alloys, stainless steels, carbon steels and super alloys.

4.5.2 Structural Considerations

The primary structural considerations which must be evaluated in the heat pipe container design are its ability to withstand internal pressure and temperature, and external (induced) loads. The internal pressure of the heat pipe is dependent on the maximum temperature during processing, handling, storage, shipping, or during its operational lifetime. This maximum temperature also determines the strength of the container material. In addition to the stresses associated with the internal pressure, the heat pipe may also be subjected to externally induced environmental loads including pressure loads, acceleration, vibration and shock. The externally induced loads can occur during shipment, handling, and operation or may be caused by such factors as differential expansion loads due to mounting restraints within the system. From the structural analysis view point, the externally induced loads are equivalent to axial and bending stresses which the heat pipe must be able to sustain in combination with internally induced pressure loads.

A comprehensive analysis by a cognizant stress engineer should be performed to insure proper heat pipe structural design. Methods which can be applied to the preliminary structural design of heat pipes have been developed in the "Heat Pipe Manufacturing Study" (34). Recommended structural analysis procedures applicable to strength calculations for heat pipes developed in this study are summarized in the following sections.

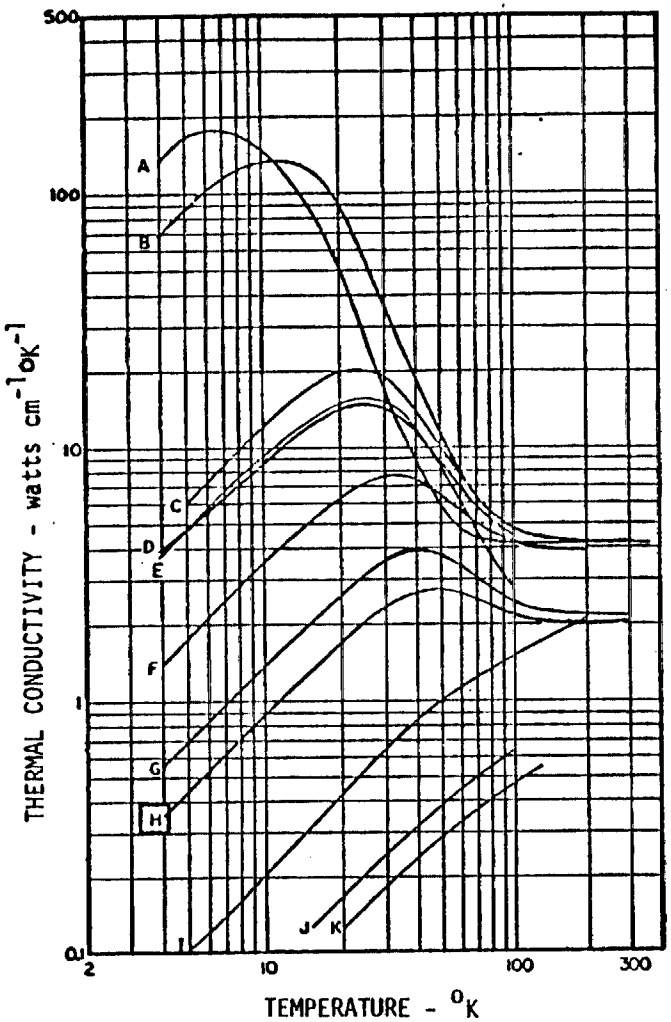

Low-temperature thermal conductivities of some materials having relatively high conductivities. A, silver 99.999% pure (39); B, high purity copper (42); C, coalesced copper (42); D, copper, electrolytic tough pitch (42); E, aluminum single crystal (43); F, free-machining tellurium copper (42); G, aluminum, 1100 F (43); H, aluminum, 6063-T5 (43); I, copper, phosphorous deoxidized (42); J, aluminum, 2024-T4 (43); K, free-machining leaded brass (42).

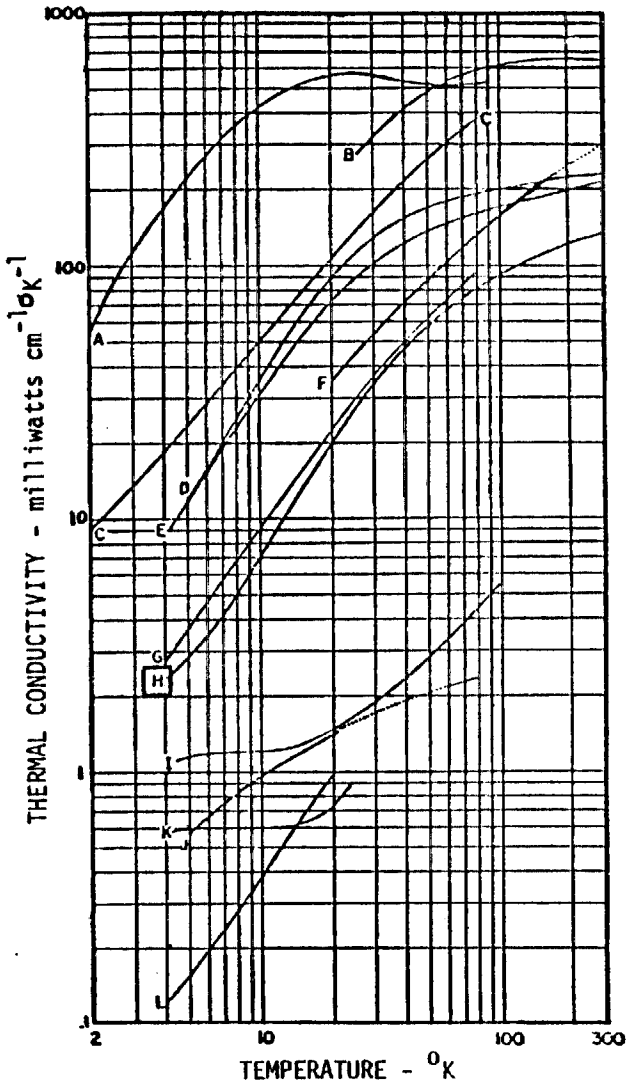

Low-temperature conductivities of some solids with relatively low conductivities. A, 50-50 lead-tin solder (44); B, steel, SAE 101 (39); C, beryllium copper (44); D, constantan (39); E, Monel*(39); I, fused quartz (39); J, polytern fluoroethylene (Teflon*) (41); K, polymethylmethacrylate (perspon) (39); L, nylon (44).

Fig. 4-32. Thermal conductivity of various metals at low temperatures

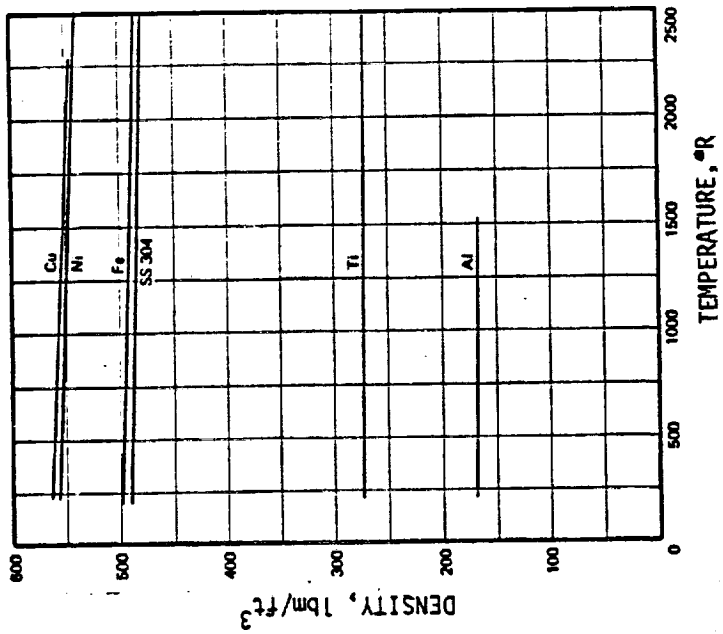

Fig. 4-34. Density of several solid materials, (1 deg R-0.556 deg K, 1 lbm/ft^3 = 16.02 kg/m^3) (33)

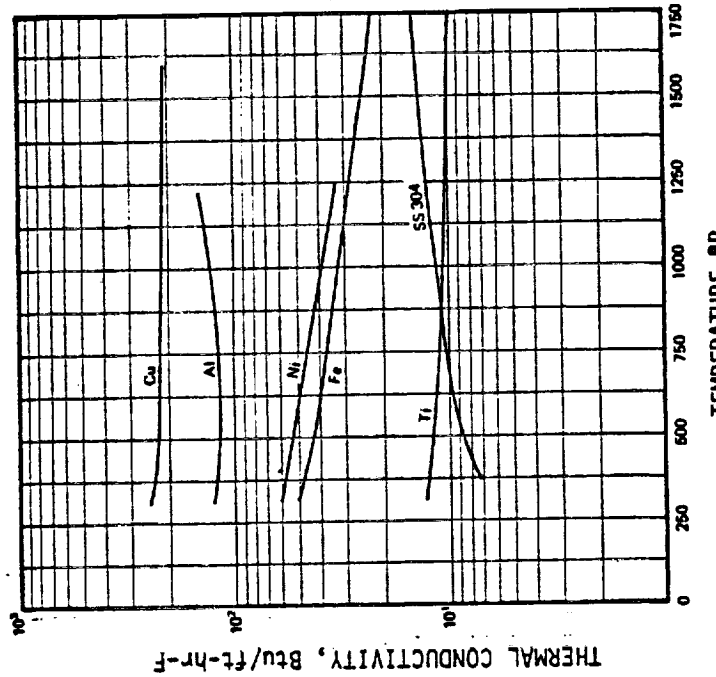

Fig. 4-33. Thermal conductivity of several solid materials, (1 deg R = 0.556 deg K, 1 Btu/ft-hr-F = 1.730 W/m-K) (33)

4.5.2.1 Pressure Containment

As a ground rule, the design approach for tubes subject to internal pressurization follows that of the ASME Boiler and Pressure Vessel Code, 1965 - Section VIII, "Unfired Pressure Vessels" (35). The code is recommended as a design guide on the basis of its general acceptance in commercial and governmental areas of pressure vessel application.

As per this reference, a factor of safety of 4 on ultimate strength is used. Although some NASA criteria do specify lower factors of safety, it is recommended that the higher safety factor be used because of certain heat pipe characteristics which are different from the usual aerospace structures. First, heat pipes are handled and transported in the charged condition, and Federal regulations (39, 40) require that pressurized container shipped by commercial transportation conform to the ASME Code. Second, heat pipes are generally not "high technology" items and consequently, extensive structural analysis, design verification testing, and manufacturing quality assurance are not performed, as is the case with the typical aerospace structure. The ASME code also provides a method for experimentally determining the allowable operating pressure when the strength is difficult to calculate (as, for example, pinched-off fill tubes).

4.5.2.2 Tubular Container Design

The ASME Pressure vessel code limits the maximum operating pressure in a vessel to the pressure at which the most critical part reaches one quarter of the material's ultimate tensile strength, F_{tu}. The vessel can have different operating pressures at different temperatures. Each vessel must also be tested (proof pressure) to 1.5 times this maximum operating pressure without observable deformation or leaks. In addition, the code lists formulae for use in calculating allowable pressures and stresses. These relations are modifications to the thick-walled (Lame) solution for cylinders and spheres (41). The thick-walled solutions are listed in Table 4-13, and then reduced to the simplified thin-walled formulae which are sufficiently accurate for the geometries usually encountered in heat pipes, although they are somewhat different than those listed in the code. In these equations, the dimensions resulting in the minimum net section should be used including allowances for corrosion, threading or grooving and manufacturing tolerances. Figure 4-35 contains typical container design requirements for 6061 and 6063 aluminum and 304 stainless steel based on the hoop stress. Allowances for corrosion, threading, grooving and manufacturing tolerances are not included in these curves. The curves can be used to quickly determine required tube size when the maximum operating pressure is known.

TABLE 4-13. HOOP AND AXIAL STRESSES

Internal Pressure Hoop Stress

$$f_{\substack{hoop \\ max}} = p(R_2^2 + R_1^2)/(R_2^2 - R_1^2) \qquad \text{(Thick-walled cylinder)} \qquad (4\text{-}44)$$

$$f_{hoop} = \frac{pR}{t} \qquad \text{(Thin-walled cylinder)} \qquad (4\text{-}45)$$

$$R = 1/2\ (R_2 + R_1) \qquad (R_2/R_1 < 1.25)$$

$$t = R_2 - R_1$$

Internal Pressure Axial Stress

$$f_{axial} = \frac{pR}{2t} \qquad \text{(Thin-walled cylinder)} \qquad (4\text{-}46)$$

Transition Section

The hoop and axial stresses due to internal pressures in a thin-walled conical shell (e.g., a reducer) are given by the relations:

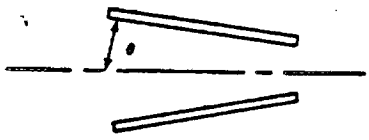

$$f_{hoop} = pR/t \cos\theta \qquad (4\text{-}47)$$

$$f_{axial} = pR/2t \cos\theta \qquad \text{(Conical shell)} \qquad (4\text{-}48)$$

Stress Due to Bends in a Tube

Between 10% of the yield and 20% of the ultimate strength

Stress Due to End Caps

	MAXIMUM BENDING STRESSES	f_{bend}	
⊃	CYLINDER ATTACHED TO A HEMISPHERE	0.03 pR/2t	(4-49)
)	CYLINDER ATTACHED TO A 2/1 ELLIPSE	1.18 pR/2t	(4-50)
▯	RIGID END CAP	3.10 pR/2t	(4-51)

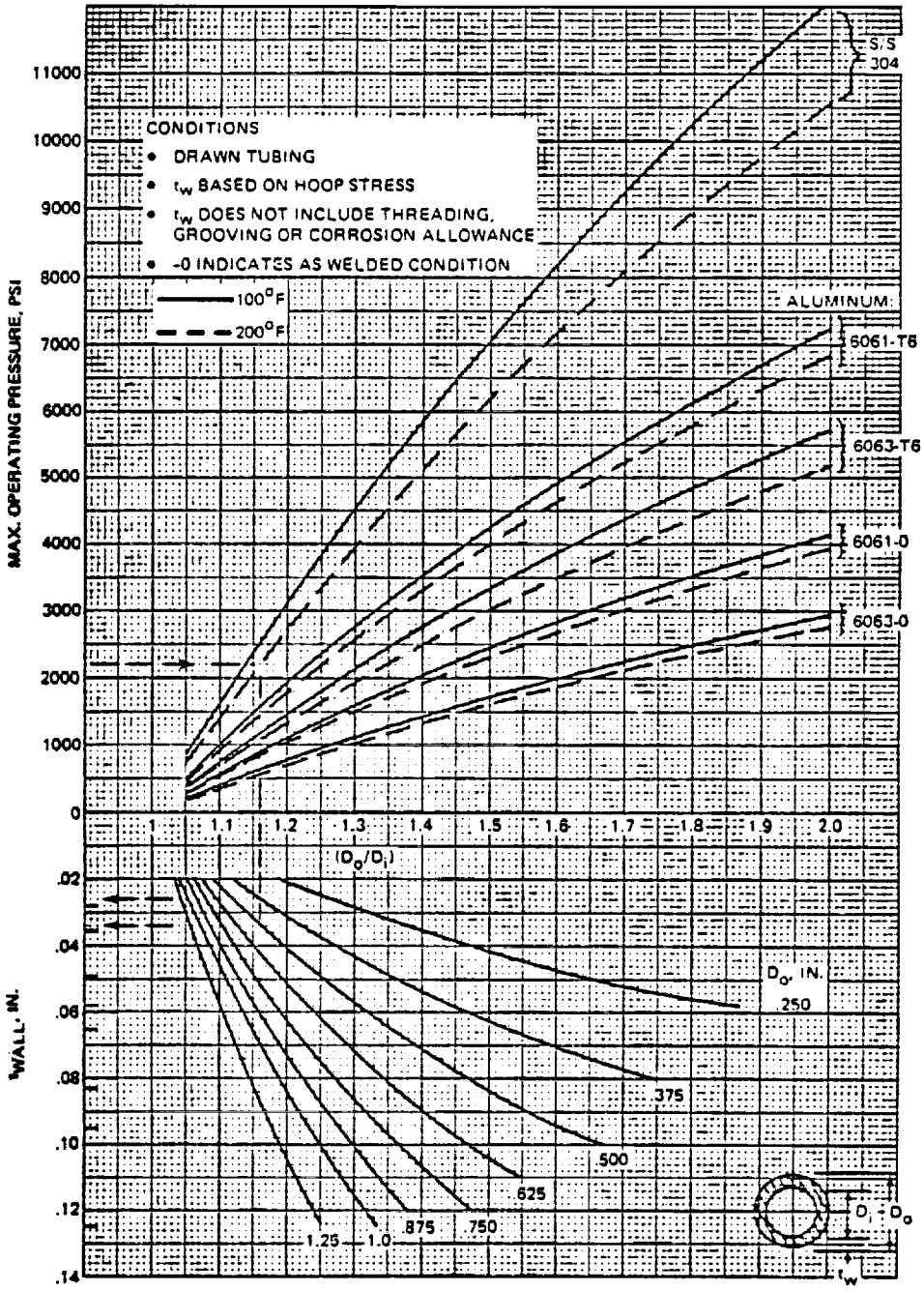

Fig. 4-35. Heat pipe envelope design curves (34)

In addition to the familiar hoop stress and axial stress, various localized axial stresses due to bends, end caps, saddles, restrained thermal expansion and dynamic (vibration) loading should be included in the structural analysis. Table 4-14 summarizes the various stress combinations that must be checked to determine the maximum operating stress in a heat pipe. The checkmarks in each column indicate the stresses that are additive for a particular situation. Although the major contributors are given, the Table is not all inclusive and it is conceivable that other combinations can occur that are not listed.

TABLE 4-14. STRESS CHECKLIST (34)

Stress	Reference section	Possible stress combinations					Design criteria
Hoop	5.2.4.1	✓					• f_{max} = largest of the possible combinations
Axial	5.2.4.1		✓	✓	✓	✓	• $f_{max} \leq 1/4\ F_{tu}$
Bends	5.2.4.3		✓				
End caps	5.2.4.4			✓			
Saddles	5.2.4.5				✓		
Thermal expansion	5.2.4.6				✓		
Dynamic loading	5.2.4.7					✓	

Localized axial stresses due to bends and end caps can be estimated using the expressions summarized in Table 4-13. It is suggested in Ref.34 that 10% of the yield strength and 22% of the ultimate strength of the material be used to obtain a conservative estimate of the residual bending stresses in thin-walled tubes. The actual residual stress lies somewhere between these two values and acts in the axial direction. The foregoing criterion assumes a smooth-walled tube. In actual practice, the tube may be threaded or grooved and higher than average local strain could be developed in the thinner sections. In such cases, it is recommended that bend samples be made to determine the minimum bend radius and the proper bending speed. Table 4-15, extracted from Military Standard MS33611 (ASG), can be used as a guide to establish allowable bend radii.

The presence of a cap at the pipe end restrains the radial expansion which occurs in the pipe wall away from the ends. This restraint results in local bending stresses which are maximum at the restraint and die out with increasing distance away from the restraint. The maximum bending stresses for various types of end restraints are determined in Ref. 34, and are summarized in Table 4-13. These local bending stresses are additive to the basic pressure vessel axial stresses. This sum should be less than $F_{tu}/4$ for the design criteria to be satisfied. Also, the end cap region is an area of the pipe where "as welded" material properties must be used unless subsequent heat treatment is done after welding.

TABLE 4-15. TUBE BEND RADII

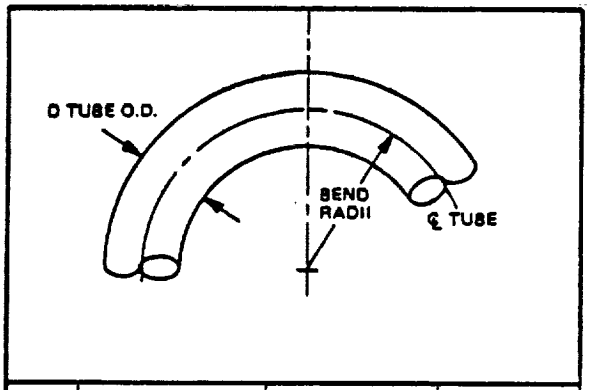

TUBE O.D.	SPECIAL BEND RADII SEE NOTE[a]		RECOMMENDED BEND RADII SEE NOTE[b]		ADDITIONAL RADII SEE NOTE[c]
	1-1/2D	2D	3D	4D	6D
1/8	0.188	0.250	0.375	0.500	0.750
3/16	0.281	0.375	0.563	0.750	1.125
1/4	0.375	0.500	0.750	1.000	1.500
5/16	0.469	0.625	0.938	1.250	1.875
3/8	0.563	0.750	1.125	1.500	2.250
7/16	0.656	0.875	1.312	1.750	2.625
1/2	0.750	1.000	1.500	2.000	3.000
5/8	0.938	1.250	1.875	2.500	3.750
3/4	1.125	1.500	2.250	3.000	4.500
7/8	1.3125	1.750	2.625	3.500	5.250
1	1.500	2.000	3.000	4.000	6.000
1-1/8	1.688	2.250	3.375	4.500	6.750
1-1/4	1.875	2.500	3.750	5.000	7.500
1-3/8	2.063	2.750	4.125	5.500	8.250
1-1/2	2.250	3.000	4.500	6.000	9.000
1-5/8	2.438	3.250	4.875	6.500	9.750
1-3/4	2.625	3.500	5.250	7.000	10.500
1-7/8	2.813	3.750	5.625	7.500	11.250
2	3.000	4.000	6.000	8.000	12.000
2-1/4	3.375	4.500	6.750	9.000	13.500
2-1/2	3.750	5.000	7.500	10.000	15.000
3	4.500	6.000	9.000	12.000	18.000

NOTES:

(a) Use of special bends (1-1/2D to 2D) in fluid systems with working pressures of 1500 psi or greater require the approval of the procuring service. Flatness, wrinkle and scratch requirements shall be as specified in Notes (d) and (e).

(b) Recommended bends (3D and 4D) require no approval and shall be used wherever possible. Flatness, wrinkle and scratch requirements shall be as specified in Notes (d) and (e).

(c) Additional bends (6D) shall be used only where fabrication or design difficulties preclude the use of recommended bends. Applications do not require specific approval and are limited only by the flatness, wrinkle and scratch requirements provided in Notes (d) and (e).

(d) Flatness limitations

(1) Flatness in the area of a tube bend shall be defined by the formula:

$$\text{Flatness} = \frac{\text{Max OD} - \text{Min OD}}{\text{Nominal OD}} \times 100 \text{ percent}$$

(2) Tube flatness for fluid systems with working pressures of 1000 psi or greater shall not exceed 5 percent

(3) Tube flatness for fluid systems with working pressures less than 1000 psi shall not exceed 10 percent

(e) Wrinkles and scratches:

(1) For fluid systems with working pressures 500 psi or greater, there shall be no wrinkles or kinks deeper than 1 percent of tube OD and no scratches deeper than 5 percent of the nominal wall thickness.

(2) For fluid systems with working pressures of less than 500 psi there shall be no wrinkles or kinks deeper than 2 percent of tube OD and no scratches deeper than 10 percent the nominal wall thickness.

Bend radii for tube diameters other than those specified may be established by multiplying the tube outside diameter by the appropriate numerical prefix noted in the table for the class bend desired.

Present bending dies may be used until such time as tools must by replaced.

[Ref: Mil-STD MS 33611 (ASG)]

Analyses to determine localized axial stresses due to saddles, restrained thermal expansion and dynamic loads are rather complicated and should be performed by a cognizant stress engineer. Analytical methods suitable to heat pipe designs can be found in Ref. 34.

4.5.2.3 End Cap Design

The ASME Code, 1965, describes two configurations, designated here as Type I and Type II, for welded flat circular heads that are recommended for heat pipe use. Design details are given in Fig. 4-36. The wall thickness, t_s, is the minimum net section after all allowances for corrosion, threading, or grooving have been made.

For these designs, the minimum required end cap thickness (t_{ec}) is specified in the ASME code as:

$$t = D\sqrt{4\,Cp_m/F_{tu}} \qquad (4\text{-}52)$$

where:

C = A factor obtained from Fig. 4-36

D = 2R is the average diameter of the pipe

p_m = internal pipe pressure

Figures 4-37 and 4-38 show typical variations in required thickness, t_s, with internal pipe pressure, p_m, for 6061-T6 aluminum and 304 stainless steel, respectively. These curves assume a value of 0.5 for the factor C, which gives conservative results.

4.5.2.4 Fill Tube Design

The design of fill tubes is similar to that of tubes and end caps with the exception of the fill tube pinch-off itself. A typical fill tube design is shown in Fig. 4-39.

Since this is a region of the heat pipe for which strength cannot be calculated with satisfactory accuracy, the maximum operating pressure should be determined experimentally (see Section 4.5.2.5).

In practice, the fill tube dimensions are determined by how tight a mechanical seal or crimp can be achieved prior to welding. A large inside diameter with a narrow wall will have good pump-down characteristics, but poor crimping properties - cracks are easily developed when the material is deformed. Too narrow an opening with a thick wall will have poor pump-down characteristics.

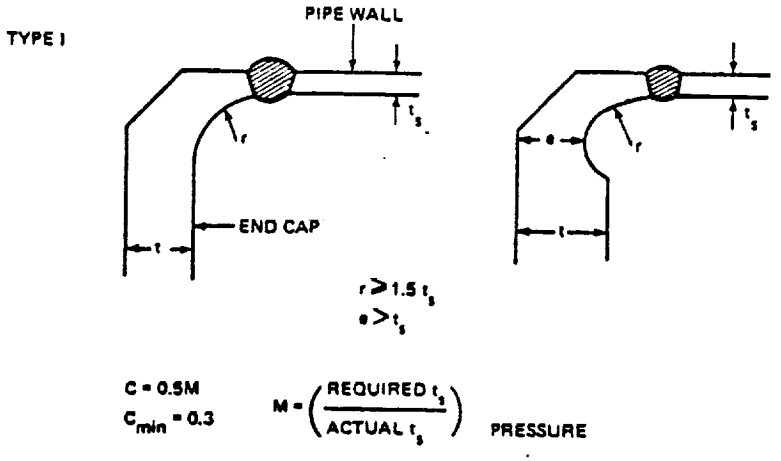

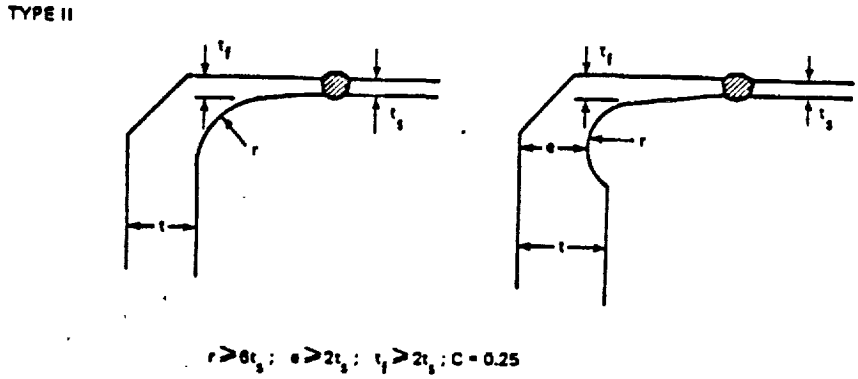

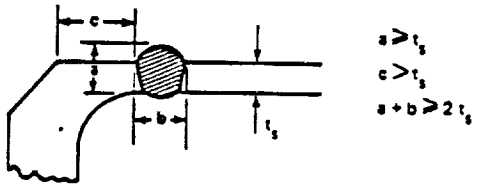

Acceptable Post Weld Detail

Fig. 4-36. End cap design detail (34)

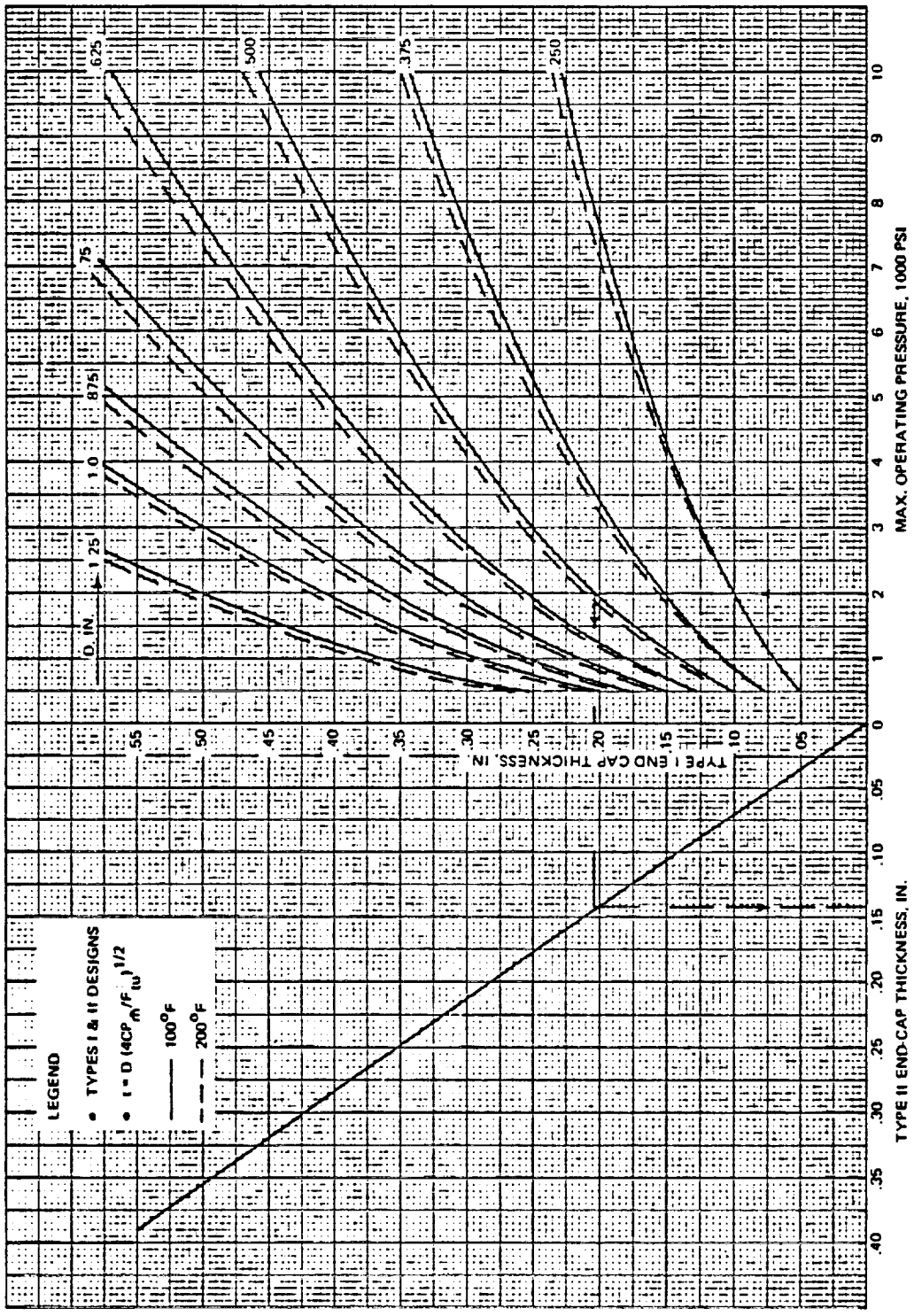

Fig. 4-37. End cap design curves, 6061-T6 aluminum (as welded) (34)

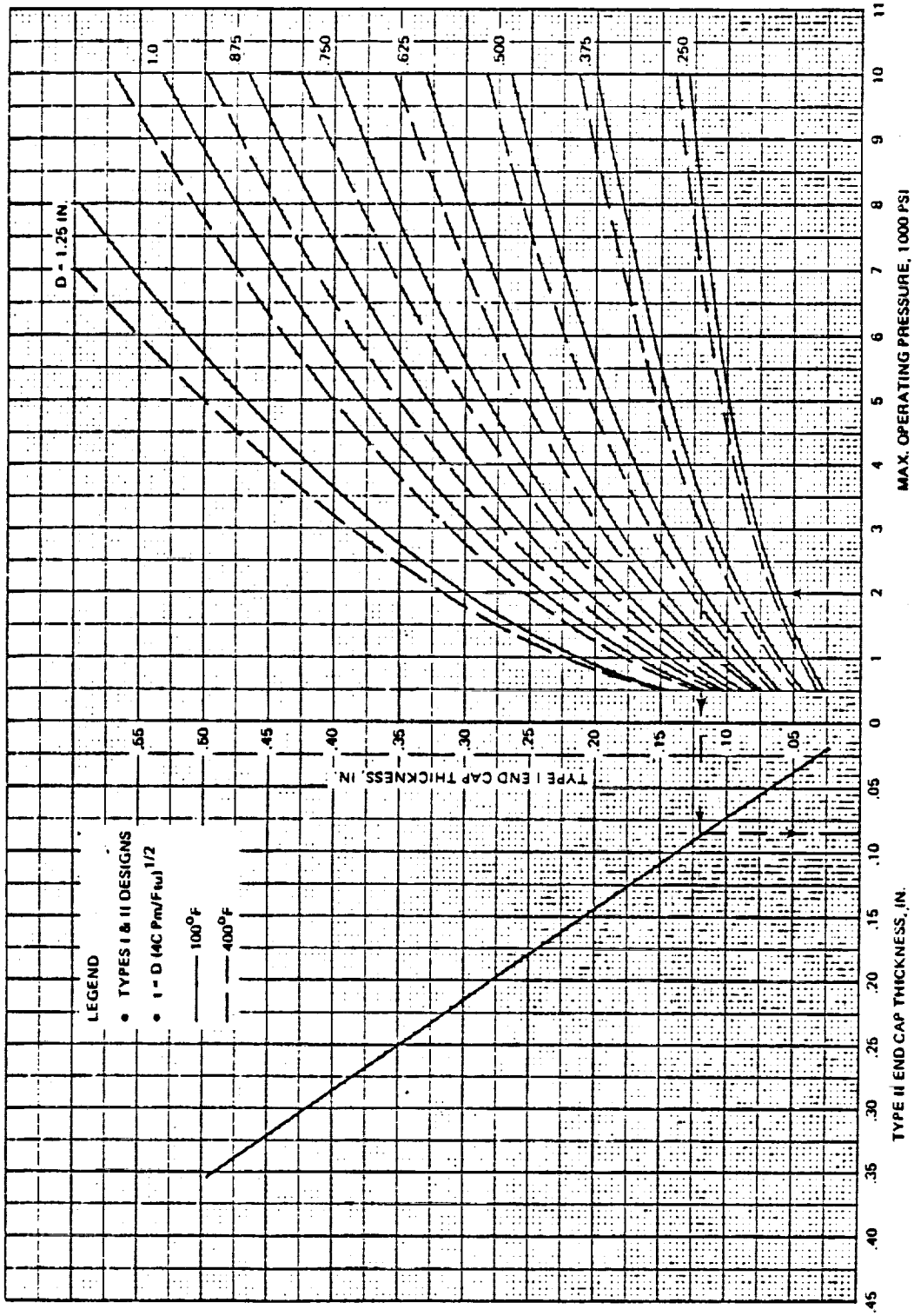

Fig. 4-38. End cap design curves, 304 stainless steel (as welded) (34)

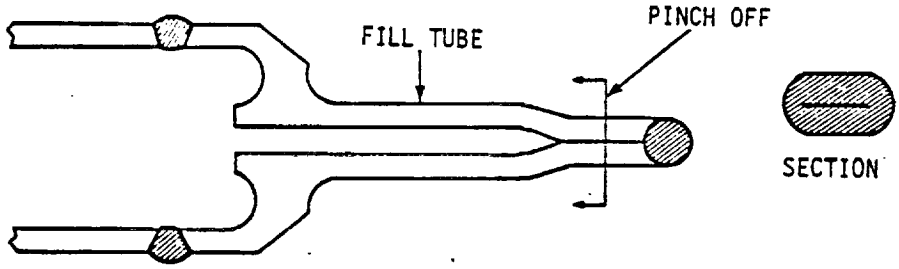

Fig. 4-39. Typical fill tube design (34)

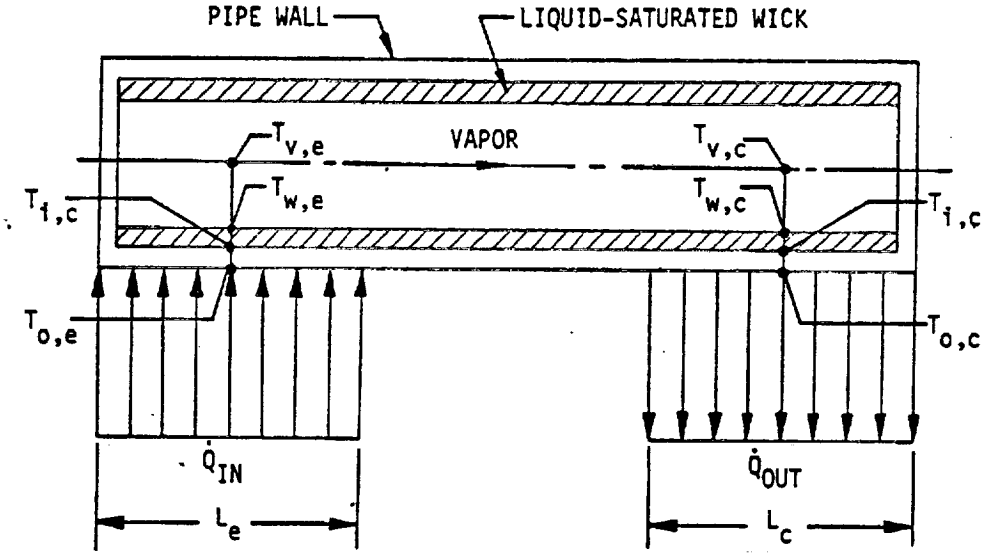

Fig. 4-40. Sketch of heat flow through a heat pipe

One fill-tube geometry that has been favored by a number of heat pipe fabricators uses a 3/16 to 1/4 in. (0.476 cm to 0.635 cm) o.d. tube with a 1/16 in. (0.159 cm) i.d. hole. It produces reasonable pump-down times (≈ 1/2 hr.) and repeatable crimp closures, in both stainless steel and aluminum. Burst test samples with aliminum charge tubes have given 3100 psi (2.137×10^7 newt/m^2) for a fully annealed condition and 7500 psi (5.171×10^7 newt/m^2) for -T6 tubes that were heated to 600°F (316°C) for 1 min. and air cooled to room temperature prior to pinch off.

4.5.2.5 Experimental Pressure Containment Verification

The ASME Code also provides a means of experimentally determining the maximum operating pressure of vessels for which the strength cannot be calculated with a satisfactory assurance of accuracy. These tests cannot, however, be used to obtain a higher value of maximum operating pressure than would be obtained for a vessel for which the strength can be calculated. There are two types of tests which can be used - a proof test, and a burst test. If the material yield strength, F_{ty}, is less than 0.625 of the material ultimate strength, F_{tu}, a burst test must be performed.

The maximum operating pressure can be obtained from the results of a single destructive burst test by the relation:

$$p_m = p_B F_{tu}/5F_a \qquad (4\text{-}53)$$

where:

p_m = maximum operating pressure

p_B = actual burst pressure

F_a = average tensile strength of four test specimens taken from the part after failure or from the same billet as the test specimen; or the maximum tensile strength in the material specification

F_{tu} = material tensile ultimate strength

The maximum operating pressure can be obtained non-destructively from the results of a proof test by the relation:

$$p_m = p_p F_{ty}/2F_{ay} \qquad (4\text{-}54)$$